Towards an astrochronological framework for the lower Paleoproterozoic Kuruman and Brockman Iron Formations

Margriet L. Lantink[1,2]*, Joshua H. F. L. Davies[3,4], Rick Hennekam[5], David McB Martin[6], Paul R. D. Mason[1], Gert-Jan Reichart[1,5] and Frederik J. Hilgen[1]

[1] Department of Earth Sciences, Utrecht University, the Netherlands; [2] Department of Geoscience, University of Wisconsin-Madison, WI, Unites States; [3] Sciences de la Terre et de l'atmosphère, Université du Québec à Montréal, QC, Canada; [4] Department of Earth Sciences, University of Geneva, Switzerland; [5] Department of Ocean Systems, Royal Netherlands Institute of Sea Research (NIOZ), the Netherlands; [6] Department of Mines, Industry Regulation and Safety, Geological Survey of Western Australia, Perth, WA, Australia

*Corresponding author (lantink@wisc.edu)

Keywords: Milankovitch cycles, astronomical climate forcing, banded iron formations, Precambrian, astrochronology, geochronology

<u>This PDF includes</u>:

Main manuscript

Figures 1-14

Supplementary Information

Abstract

Recent evidence for astronomical-induced cycles in banded iron formations (BIFs) hints at the intriguing possibility of developing astrochronological, i.e. precise time-stratigraphic, frameworks for the earliest Proterozoic as also reconstructed for parts of the Mesozoic and Paleozoic. The ca 2.47-Ga Kuruman Iron Formation (Griqualand West Basin, South Africa) and Dales Gorge Member of the Brockman Iron Formation (Hamersley Basin, Western Australia) are of special interest in this regard, given their inferred temporal overlap and similar long-period eccentricity imprint. This suggests that these two BIFs may be correlated on the basis of their large-scale cycle patterns and using additional radio-isotopic age constraints.

To examine the possibility of establishing such a framework, we generated and analysed several high-resolution proxy records from both drill-core and outcrop, combined with chemical abrasion ID-TIMS U–Pb dating of presumed volcanically sourced zircon. Time-series analysis of these records yields a variety of spectral peaks, of which a prominent ~5 m and ~16 m cycle can be linked to the basic stratigraphic alternations and bundling. New and improved U–Pb ages of the Dales Gorge Member and Kuruman Iron Formation, respectively, indicate a comparable average sedimentation rate of 10–12 m/Myr for both BIF units. Based on this rate, we attribute the ~5 m cycle to the long 405-kyr eccentricity cycle. More tentatively, we interpret the ~16 m cycle as the very long 2.4-Myr eccentricity cycle, having a reduced period of ~1.3 Myr due to chaotic behaviour in the solar system. Other identified cycles (~580 kyr, ~700 kyr and ~1.8 Myr) might be explained in terms of weaker eccentricity components and/or as harmonics and combination tones of these cycles.

An initial attempt to establish cyclostratigraphic correlations between the Kuruman Iron Formation and Dales Gorge Member solely based on their characteristic cycle patterns proved unsuccessful, which may be due to a difference in stratigraphic recording of the astronomical signal between their different depositional environments. Next, we used the U–Pb ages to first constrain correlations at the scale of the ~16 m cycle, followed by a correlation of the basic ~5 m cycles. The resultant framework remains problematic and debatable at the individual 405 kyr cycle-level, and should merely be considered as a starting point for future studies. Particularly, our findings highlight the need for further investigations into how Milankovitch forcing influenced BIF sedimentation and paleoenvironmental conditions at a time when the Earth and solar system behaved fundamentally different from today.

1. Introduction

Astronomical age models based on the calibration of sedimentary cycles to astronomical target curves of precession, obliquity, eccentricity and/or insolation have now been constructed for the entire Cenozoic (Gradstein et al., 2020; Hinnov, 2018; Hinnov and Hilgen, 2012). Due to their high resolution, these age models or astrochronologies have been key to solving fundamental research questions concerning the astronomical origin and pacing ('Milankovitch forcing') of e.g. ice ages and hyperthermals, and associated nonlinear feedbacks within Earth's climate system (Hays et al., 1976; Hilgen, 1991; Imbrie et al., 1984; Sexton et al., 2011; Westerhold et al., 2020; Zachos et al., 2010). In addition, the development of very long, tuned paleoclimate records has enabled us to differentiate the contribution of the Milankovitch 'Grand cycles' – which have periodicities in the order of millions of years – from other forcing mechanisms such as tectonics and volcanism that operate on the same time scale (Boulila et al., 2012; Martinez and Dera, 2015; Olsen et al., 2019). Similar astrochronologies have also been developed for parts of the Mesozoic (e.g. Batenburg et al., 2012; Sprovieri et al., 2013; Ikeda and Tada, 2014; Huang, 2018; Olsen et al., 2019) and Paleozoic (e.g. Wu et al., 2013; Fang et al., 2015; Sinnesael et al., 2021), yet these are essentially relative, that is, providing astronomical duration but not age, due to the absence of a reliable astronomical solution prior to ~50 Ma. Instead, these 'floating' or radio-isotopically anchored age models are based on identification of the long 405-kyr eccentricity cycle, the only cycle whose period is regarded as stable in deep time (Laskar et al., 2004; 2011) while being of sufficiently large amplitude to be typically expressed in sedimentary sequences.

Recently, the expression of the 405 kyr cycle was detected in ancient marine deposits at ca 2.47 Ga (Lantink et al., 2019; de Oliveira Carvalho Rodrigues et al., 2019), in so-called banded iron formations (BIFs), deposited in the prelude to the Great Oxidation Event (GOE; Bekker et al., 2004; Holland, 2002). This raises the question whether a similar integrated stratigraphic framework and astrochronology may be developed for these BIFs, namely the Kuruman Iron Formation (IF) in South Africa and the Dales Gorge Member of the Brockman IF in NW Australia. It is generally assumed that these lithostratigraphic units were deposited near-synchronously, and possibly even within the same basin, based on similarities in the succession of lithofacies and SHRIMP U–Pb zircon ages (Button, 1976; Cheney, 1996; Martin et al., 1998; Nelson et al., 1999; Pickard, 2003; Trendall, 1968; Trendall et al., 2004). Establishing a cyclostratigraphic framework would, for the first time, allow their relative timing to be determined much more precisely, and as such, be of important value for reconstructions of paleogeography and basin evolution (Beukes and Gutzmer, 2008; Knoll and Beukes, 2009) as well as environmental redox changes during this critical period of Earth history (e.g. Anbar et al., 2007; Kendall et al., 2010; Gumsley et al., 2017).

Here we combine cyclostratigraphic analysis and chemical abrasion isotope dilution thermal ionization mass spectrometry (CA-ID-TIMS) U–Pb dating of zircon found within the Kuruman and Dales Gorge Member BIFs to examine their potential for high-resolution (405 kyr cycle-scale) correlations using the inferred eccentricity-related cycle patterns. We begin our investigation with a number of new, high-resolution proxy records from both stratigraphic units, i.e., bulk iron-manganese ratio (Fe/Mn) data from X-ray fluorescence (XRF) core scanning and magnetic susceptibility data from the Kuruman IF, and verticality logs and ferric oxide and carbonate abundance data from the Brockman IF. These records are subjected to detailed cyclostratigraphic study focusing on the regular metre-scale alternations, building upon and refining the results of Lantink et al. (2019) and de Oliveira Rodriguez et al. (2019). Next, we present new and improved U–Pb ages obtained from zircon found within shale rich layers in the Dales Gorge Member as well as the Kuruman BIF, and discuss the possible Milankovitch origin of observed cycles in the depth domain. We then examine possible cyclostratigraphic correlations between the two BIF units, starting from their characteristic cycle patterns as expressed in the weathering profile. Finally, we discuss the implications of our correlation exercise and the resulting astrochronologic framework for how the different BIF depositional environments responded to the astronomical forcing.

2. Geological setting and stratigraphy

The largest BIF successions of the Precambrian rock archive were deposited during the transition from the Archean to Proterozoic between approximately 2.6 – 2.4 Ga. These iron- and silica-rich, largely chemical sedimentary deposits are exceptionally well-preserved in the Griqualand West Basin in South Africa and the Hamersley Basin in NW Australia, each of which extend over several hundred kilometres on the Kaapvaal and Pilbara cratons, respectively (Fig. 1). In both areas, the BIF-hosting Ghaap (SA) and Hamersley (WA) Groups show remarkable similarity in age and corresponding succession of lithofacies, from relatively shallow-marine (platform) carbonates, carbonaceous and black shales to deeper-marine iron formations of the Kuruman and Brockman IFs, respectively. In particular in the Griqualand West Basin, such a shelf-to-basin facies transition is also well preserved in a lateral sense, from the central Ghaap plateau area to Prieska in the south (Fig. 2; Fig. S1) (Beukes and Gutzmer, 2008; Beukes, 1980, 1983; Knoll and Beukes, 2009). The strong lithostratigraphic correlation between the Ghaap and

Hamersley sequences, combined with paleomagnetic support for a Pilbara-Kaapvaal supercraton around that time, suggests that deposition may have occurred in a single large marine depository and/or in (partly) connected basins (Beukes and Gutzmer, 2008; Cheney, 1996; Martin et al. 1998) at low paleolatitude (de Kock et al., 2009; Gumsley et al., 2017).

The stratigraphy of the Kuruman IF as visible in outcrop (Fig. 3a) is characterised by a pattern of regular alternations in the weathering profile at a basic thickness scale of ~5 m, and a larger-scale bundling of around ~16–22 m. This characteristic pattern was laterally correlated over 250 km, from Kuruman Kop to Prieska (Fig. 1) in Lantink et al. (2019). The alternations partly correspond to the 'stilpnomelane lutite – BIF macrocycles' of Beukes (1978, 1980) described from drill-core (Fig. S1 and S2), who originally proposed a volcanic-biogenic origin. Based on evidence from high-precision U–Pb dating, Lantink et al. (2019) attributed the alternations to the long (405 kyr) and very long-period (now ~2.4 Myr) eccentricity cycle of the Earth's orbit, and suggested a low-latitude climatic, possibly monsoonal, influence. A similar cycle hierarchy and same Milankovitch origin was proposed for the metre-scale BIF vs. 'shale' (S) macrobanding as manifested in the weathering profile of the Dales Gorge Member (Fig. 2b; Lantink et al., 2019). Of these, seventeen macroband alternations have been formally defined and are known to correlate within the entire Hamersley region (Fig. S1) (Harmsworth et al., 1990; Trendall and Blockley, 1970). Based on sequence stratigraphic analysis, Krapež et al. (2003) and Pickard et al. (2004) have interpreted the S macrobands – 'S' being defined as shale with subordinate cherts and carbonate (Trendall, 1965) – as distal density currents linked to periods of eustatic sea level fall. In line with a dominant eccentricity and thus low-latitude climate control, Lantink et al. (2019; 2023) suggested the shales to record periods of increased runoff and organic carbon productivity caused by an intensification of the monsoon.

3. Materials and methods

3.1 Studied sections/cores

For our cyclostratigraphic study of the Kuruman IF and Dales Gorge Member, new proxy records needed to be generated and/or were used from a number of selected drill-cores and sections in the field. For the analysis of the Kuruman IF, high-resolution lithological, geochemical and well-log data were acquired from the new UUBH-1 core drilled near section Whitebank (Figs. 1 and 3a). The rationale behind the UUBH-1 drilling project was to provide a stratigraphically accurate, detailed record of the Kuruman IF cyclostratigraphy to complement the more basic logs of the alternations in the weathering profile and lithology in Lantink et al. (2019). For the investigation of the Dales Gorge Member, drone-based 'verticality' profiles were generated from its outcrops within the Hamersley Range at two different locations, namely at Mount Bruce, and at a section ~5 km west of Mount Jack (Fig. 1 and Fig. 3b). These field sections were selected for their representative pattern of the distinct metre-scale alternations in relief and relative distance from each other (~80 km). In addition, we used existing high-resolution mineral abundance data from two drill-cores, DG47A (47A) and DD98SGP001 (SGP001), obtained from hyperspectral scanning and made available by the Geological Survey of Western Australia (GSWA). Core 47A forms the basis of the Dales Gorge Member type section, published as a photograph composite by Trendall and Blockley (1968); this core was also analysed in the cyclostratigraphic study of de Oliveira Carvalho Rodrigues et al. (2019) based on a grayscale scan. The SGP001 core was drilled at the Silvergrass area located ~150 km to the west of hole 47A and intersects the Joffre Member, Whaleback Shale Member and the upper part of the Dales Gorge Member.

3.2 Kuruman proxy records from the new UUBH-1 core

3.2.1. Drilling and on-site logging

The UUBH-1 core was drilled ~15 km west of Kuruman town at Fairholt farm (27° 28′ 44.4′ S, 23° 19′ 13.0′ E), using NQ diamond casing and orientation drilling (~10° off vertical to the NE, perpendicular to an overall stratigraphic dip of 7° SW) from September to November 2017. Retrieved core material was carefully checked on a daily basis to ensure the correct stratigraphic order was maintained during drilling. In addition, a schematic lithological log was made (Fig. S2) according to the same lithological facies ranking as explained in Lantink et al. (2019), i.e., 0 = stilpnomelane lutite, 1 = siderite, 2 = siderite-magnetite, 3 = magnetite-siderite, 4 = magnetite-chert 'zebra facies', 5 = magnetite. A complete succession of the Kuruman IF, from the lower Griquatown IF into the upper Gamohaan Formation, was intersected between 51.31 m and 327.15 m depth with only a minor (~1.3 m) interval of core loss. Downhole geophysical logging was carried out after completion of the drilling and yielded magnetic susceptibility, natural gamma ray and density logs. The core was subsequently cut in half at the University of Johannesburg. One archive half was kept in South Africa, and the other half was shipped to The Netherlands.

3.2.2 XRF core scanning and calibration

To obtain a high-resolution chemical record of the Kuruman and upper Gamohaan Formations, X-ray fluorescence (XRF) core scanning was carried out with the Avaatech core scanner at the Royal Netherlands institute of Sea Research (NIOZ) on Texel. Prior to the analyses, the stratigraphic order of the core was again carefully checked by comparison to the original drill-site photos. In case of shattered lithology, true stratigraphic thicknesses were also estimated from the photos and/or drill-core metre marks. Individual 1 m core segments were placed into split plastic tubes and were supported from underneath with foam to create a stable and even surface. The XRF analyses were carried out with a 12 x 10 mm slit dimension and 1 cm step size, on cleaned surfaces covered with a 4-µm SPEXCerti Ultralene foil to prevent any cross contamination. Calcite veins were circumvented by changing the y direction of the detector, i.e., by moving it more towards the sides of the core scanning surface). Tube energy settings, primary beam filters and measurement time were optimised for minor and trace elements while maintaining a dead time between 20 to 40 % (see Table S1 for applied settings). Spectral data were processed using bAxil spectrum analysis software developed by Brightspec. Eight external reference standards (GSR-4, GSR-6, GSD-10, JSd-1, JSd-3, MESS 3, SARM 2, and SARM 3; see Hennekam et al., 2019) were scanned every two weeks and indicated a constant performance (i.e., no statistical difference between concentrations in standards and intensities measured) of the XRF core scanner during the entire duration of the experiment of circa two months.

To convert the raw core scanner data (intensities) to element concentrations, a large subset of discrete samples was selected and prepared for bulk-rock quantitative wavelength dispersive XRF analysis. About 100 samples of ~10 cm thickness and spaced at 1 metre intervals were powdered and homogenized using a Retsch tungsten carbide jaw crusher and Herzog mill. Approximately 0.6 g of dry rock powder was fused into glass beads at 1,200 °C and analysed with an ARL Perform'X sequential XRF spectrometer at Utrecht University. For the calibration we used the multivariate log-ratio approach of Weltje et al. (2015) as implemented within the AvaaXelerate software package of Bloemsma (2015). This resulted in a much cleaner (i.e., less noisy) pattern for many of the elements of interest – in particular Fe, Mn and Al – and high R^2 values in the corresponding cross-plots with the bulk-rock XRF reference values (Fig. S3).

3.2.3 XRF-core scanning depth scale

Individually scanned core segments were combined into a single XRF-core-scanning composite record by precisely determining the overlap between successive intervals. For this purpose we used the high-resolution photos that were taken from every interval when placed inside the scanner (Fig. S4). To enable comparison to the well log data, this composite depth record was subsequently recalibrated by matching the positions of the distinct shale layers within the XRF-core-scanning records (peaks in Zr, Al, K etc.) to the depths of their corresponding peaks in the downhole natural gamma signal. This yielded a stratigraphically accurate natural gamma log-corrected depth scale, which is presented in the main figures and was used for time series analysis. No further stratigraphic dip corrections were made because of the very minor (~3°) offset from drilling perpendicular to the bedding, yielding a thickness change of only 0.15 %.

3.3 Dales Gorge Member field logs and core proxy records

3.3.1 3-D outcrop models and verticality profiles

Since the hill exposures of the Dales Gorge Member turned out to be too steep for manual logging of the basic lithology and weathering profile, 3-D photogrammetry models were constructed for the Mt Bruce and Mt Jack locations using an unmanned aerial vehicle (UAV) (Fig. 4). To limit the model size but at the same time maintain enough stratigraphic detail, we concentrated for the Mt Bruce section on two narrower subsections located on its north-eastern face, namely 'Mt Bruce West' and 'Mt Bruce East', that were representative for the upper and lower part of the Dales Gorge Member stratigraphy, respectively. The same was done for section Mt Jack, which was studied at a 'Mt Jack East' and 'Mt Jack West' subsection. Photographs were taken manually by a 20-megapixel camera mounted on a multirotor UAV (DJI Mavic 2 Pro), which was flown parallel to the outcrop surface and provided approximately 70 % horizontal overlap between successive photos. Each outcrop area was photographed from different heights and camera angles (at 0, 45 and 90°) to provide complete coverage and to aid alignment during processing.

To ensure correct stratigraphic thicknesses were maintained in the photogrammetric model, one to three ground control points (GCPs) were placed at the base and top of each subsection (apart from at Mt Jack West) and surveyed using an Emlid Reach RS+ GNSS receiver ('rover'). Raw GNSS measurements of the rover and a second Emlid receiver ('base station') were processed using the post-processing package RTKLIB and provided centimetre accuracy of the GCP locations relative to the base station. GCP positions were then used to optimise camera positions during the digital 3-D model building as done in Agisoft Metashape, yielding less than 0.1 % error in the z direction (Fig. S5).

High-resolution dense point clouds were subsequently imported into the visualisation and interpretation software Cloudcompare. After applying a stratigraphic dip correction (using 'matrix transformation'), a simple log was made from the individual thicknesses of alternating high- versus low-relief intervals (using 'point picking'). In addition, a quantitative record of the outcrop's verticality (using 'compute geometrical features') was extracted along representative sections/slices, by compressing and averaging the computed verticality point cloud in the y/x relative to z direction. Individual verticality records and corresponding logs were subsequently combined into a single Mt Bruce and Mt Jack composite (Fig. S6).

3.3.2 Hylogger records cores 47A and SGP001

To complement our analysis of the Dales Gorge Member outcrop data, we used existing mineral reflectance data from cores 47A and SGP001. The mineral reflectance data had been previously collected and made available by the GSWA, using the Hylogger spectral scanner at the Perth Core library (Hancock and Huntington, 2010). From this dataset, the pattern of total ferric oxide mineral abundance, i.e., hematite and goethite, as well as total carbonate abundance, turned out to particularly well reflect the characteristic macroband pattern of the Dales Gorge upon initial inspection in 'The Spectral Geologist' (TSG) visualization programme during our visit to the core library. With thanks to the GSWA, these proxy records were subsequently extracted at a 1 cm depth resolution using the TSG software – from the visible near-infrared and short-wave plus thermal infrared range, respectively – for our cyclostratigraphic purposes. Note that the ferric oxide and carbonate abundances constitute relative weight percentage (wt %) and should be regarded in a purely qualitative way, since only a subset of minerals i.e. those present in the TSG software library are included in the determination of the total wt %, while minerals not visible in the targeted spectral range, as well as aspectral minerals such as magnetite, are excluded. Importantly, we further applied several corrections to the 47A depth record, as careful inspection of the original Trendall and Blockley (1968) photographs revealed that several pieces of core had been turned upside down or were in the wrong position during acquisition of the Hylogger data.

3.4 Time-series analysis

We combined visual inspection with time-series analysis of selected proxy records to investigate the presence and expression of large-scale (> metre-thick) cycles in the stratigraphy of the studied Kuruman and Brockman IF sections. For the analysis of the Kuruman IF we focused on the (log-transformed) iron-manganese ratio as derived from XRF core scanning of core UUBH-1 and on the magnetic susceptibility record as derived from downhole geophysical logging (see also Section 4.1). For the Dales Gorge Member we used the composite verticality records of the Mt Bruce and Mt Jack sections and the (log-transformed) ferric oxide and carbonate abundance records of core 47A as derived from the Hylogger dataset.

Time-series analysis of all proxy records, including record preparation, spectral analysis, statistical hypothesis testing and bandpass filtering, was performed using the Acycle package of Li et al. (2019) and Astrochron package of Meyers (2014). Acycle was used to detrend records by subtracting a 35 % locally weighted scatter-plot smoothing (LOWESS) curve, after which initial spectral analysis was carried out using the Lomb-Scargle method (Lomb, 1976; Scargle, 1982) on original depth series. Astrochron was subsequently used to conduct multi-taper method spectral analysis (Thomson, 1982) on linearly interpolated series (resampled at 10 cm) and using a time-bandwidth product of 3. Calculation of 90, 95 and 99 % autoregressive noise confidence levels was based on the locally-weighted regression spectral background estimation (LOWSPEC) method of Meyers (2012). Gaussian bandpass filtering (in Acycle) was used to isolate individual power spectral components of interest for visual comparison with the original proxy record in the stratigraphic (depth) domain.

3.5 CA-ID-TIMS zircon dating

To obtain accurate and precise U–Pb zircon ages for the Dales Gorge Member, several of the shale macrobands as exposed in the gorges of the Karijini National Park were sampled for zircon extraction. The two shale samples used in this study are DS1 and DS9, which come from the Wittenoom Gorge type outcrop section as illustrated in Figure 4 of Trendall and Blockley (1970) and represent repeats of samples previously collected by A.F. Trendall (e.g., Trendall et al., 2004). The DS1 sample was collected over the entire width of the upper stilpnomelane-rich shale and corresponds to an approximate height of 13.9 m in the 47A type section core (this core has a stratigraphic height scale instead of depth scale). The DS9 sample comes from the upper stilpnomelane-rich shale band of this macroband interval, corresponding to a height of 64.9 m in core 47A.

In an attempt to generate additional and more precise age constraints from the Kuruman IF, quarter core samples were taken from the stilpnomelane-rich shales at 110.75 m, 130.44 m and 212.38 m depth in UUBH-1, corresponding to the lutite 4, 3 and 2 intervals which had previously been dated in Lantink et al. (2019) using material from the other half core left in Johannesburg. All samples were subsequently processed for zircon extraction. Following separation of euhedral zircon crystals, the grains were chemical abraded (Mattinson 2005; Widmann et al. 2019) to remove the effect of decay-damage-related Pb loss and dated using ID-TIMS techniques identical to those outlined in Lantink et al. (2019).

Depositional rate modelling was conducted using the R package Bchron (Haslett and Parnell, 2008) with concordant weighted mean $^{207}Pb/^{206}Pb$ ages or single grain $^{207}Pb/^{206}Pb$ ages depending on how many concordant analysis were found in each sample. For the lower Brockman IF, a third recently derived CA-ID-TIMS age from a shale close to the base of the Joffre Member at 371.2 m depth in core SGP001 (Lantink et al., 2022) was included in the calculation of the depositional rate, together with the new ages from DS1 and DS9. For this purpose, a single depth scale for these three samples had to be created which we did by correlating the Hylogger patterns of the SGP001 and 47A cores. This yielded a corresponding virtual depth of 495.2 m for DS9 and 546.2 m for DS1 below the 371.2 m shale in SGP001. A slightly updated depositional rate model was established for the Kuruman IF based on additional concordant zircon analyses obtained for the shales at 110 m and 212 m depth in core UUBH-1.

4. Results

4.1 Cyclostratigraphic analysis of the Kuruman Iron Formation

For our cyclostratigraphic study of the Kuruman IF we focus on two key proxies – that is, the iron-manganese ratio (Fe/Mn) and magnetic susceptibility (MS) signal – which were selected from the XRF core scanning and geophysical logging data set, respectively, as obtained from the UUBH-1 core (Dataset S1). We chose these two proxies because overall, they proved to most accurately reflect the characteristic cycle pattern of the Kuruman IF as described from outcrop (Lantink et al., 2019). Note, however, that the inverse of manganese (1/Mn), and ratio of iron over aluminium (Fe/Al) (Fig. S7), show an almost identical pattern to the Fe/Mn record, and that this pattern is also reflected in our lithofacies rank series (Fig. S2). Variations in Fe/Mn (or 1/Mn) are considered mainly a proxy for relative changes in carbonate concentration, given that Mn in the Kuruman IF is primarily bound to the carbonate mineral fraction (ankerite, siderite) (Oonk et al., 2017). Variations in Fe/Al are considered a proxy for variations in detrital silicate fraction, while the MS signal is largely controlled by abundance of magnetite (Cowan and Cooper, 2009). Below, we will first describe how the characteristic cycle pattern of the Kuruman IF was recognised in the selected UUBH-1 core proxies and compares to the original field logs of Lantink et al. (2019), before proceeding to a more detailed examination of the cyclostratigraphy using time series analysis.

4.1.1 Visual identification

The Fe/Mn and MS records of core UUBH-1 show distinct regular alternations throughout the stratigraphy of the Kuruman IF (100–302 m depth) and upper Gamohaan Formation (302–327 m depth) that, upon initial inspection, seem to occur on two principle thickness scales. First, large amplitude swings can be distinguished at a thickness scale of about 5 m, which are particularly evident in the log(Fe/Mn) record, and below a depth of ~170 m (Fig. 5). The maxima of this basic ~5 m-scale alternation correspond to intervals which are relatively rich in iron oxides, hereafter referred to as 'BIF', while the minima represent intervals relatively rich in iron carbonate and shale. These alternations, in turn, are grouped into larger-scale bundles composed one to three more pronounced ~5 m-scale maxima, occurring at an approximate 15 to 20 m spacing.

The more pronounced ~5 m-scale BIF intervals and bundles expressed in the normal Fe/Mn record can be readily identified as the characteristic cycle pattern observed in the Kuruman IF weathering profile by Lantink et al. (2019), when compared to the original field logs of Whitebank and Woodstock (Fig. 5). The strongest and thickest Fe/Mn peaks – i.e., the three maxima at 260–275 m depth; followed by two maxima at 240–250 m; followed by a single pronounced interval at 215 m; and then four alternations from 180–200 m with an anomalously thick and prominent zone at 200 m – bear a remarkable resemblance to the characteristic sequence of indurated BIF intervals labelled as cycles 2abc, 3ab, 4b and 5abcd. Recognising this link, the identification of the other previously defined BIF intervals – i.e., 1abc at the base of the Kuruman IF; 2d and 4a; and 6abc, 7a, 7bc and 8a in the upper part – becomes relatively straightforward. One notable exception is BIF 6a, which is rather poorly developed in the Fe/Mn record around 170 m depth, but nevertheless manifested in the MS record (Fig. 5), and to a moderate degree in the Fe/Al record (Fig. S7).

When we correlate this characteristic pattern of pronounced BIFs between the core and field logs (see thick correlation lines in Fig. 5), additional more subtle Fe/Mn maxima at a regular ~4 to 5 m spacing can be distinguished in the relatively iron oxide-poor intervals separating bundles 1 to 6. These weaker ~5 m-scale 'BIF' intervals – which we indicate with 1a.0, 1d, 2e, 3c, 3d, 3e, 4c, 4d, 5a.2, 5e and 6a.2 – are only partially expressed in the (logs of the) weathering profile at Woodstock and Whitebank. Given their clear manifestation in the core data, however, we can now add them to the original Lantink et al. (2019) cycle numbering and our correlations between the field logs and core UUBH-1 (see thinner horizontal lines in Fig. 5).

Taking a second, closer look at our established field-to-core framework reveals that, due to a different expression of several of the 'weaker' BIF intervals, the core proxy records exhibit a somewhat deviating bundling pattern than the general pattern observed in outcrop. For example, in both the Fe/Mn and MS records, 'BIF' 1d is substantially more pronounced than in the weathering profile logs, which results in a much less clear definition of bundles 1 and 2; note, incidentally, the distinct semi-5 m-scale variability present in this lower part of the Kuruman IF. In addition, 'BIF' intervals 3d and 3e are slightly more pronounced in the log(Fe/Mn) record than in the field and much more pronounced in the MS signal, pointing to the presence of an additional 'BIF' bundle in between 3 and 4. Note also, however, that the MS record shows a notoriously different bundling pattern than the log(Fe/Mn) record around this stratigraphic interval, with 3a and 3b seemingly forming part of two separate bundles.

4.1.2 Spectral analysis and bandpass filtering

To examine this apparently more complex bundling pattern of the Kuruman IF in more detail, we switch to time series analysis. In Fig. 6, the results of Lomb-Scargle (L-S) and multi-taper method (MTM) spectral analysis are presented for the log(Fe/Mn) and MS records, showing high concentration of power around three low-frequency bands, namely at ~4.5–6.5 m, ~14–25 m and ~30–50 m. More specifically, the log(Fe/Mn) MTM spectrum shows a dominant peak at 15.8 m and strong peaks at 5.6 m, 22.8 m and 46 m, exceeding both the 99 % LOWSPEC significance level and 90 % harmonic F-test confidence level (Fig. 6). For the MS record we find essentially the same results, except that a strong 22.8 m and 46 m peak are absent in its corresponding MTM spectrum. Instead, additional significant peaks (satisfying both the required LOWSPEC and harmonic confidence levels; Meyers, 2014), are observed at 8.8 m and 11.4 m, as well as around 87 m.

Next, we use bandpass filtering to extract these main low-frequency cycles from the log(Fe/Mn) and MS records. For extracting the ~4.5–6.5 m components, we applied a wide (Gaussian) filter bandwidth centred around 5.3 m which, as expected, picks up each of the previously identified abc-alternations (Fig. 5). Furthermore, an additional filtered ~5 m cycle is identified in the relatively thick interval between 5a.2 and 5b ('5a.3') in the filtered log(Fe/Mn) record, but this cycle is not picked up in the filtered MS record. For extracting the ~14–25 m components we applied a narrow filtering around 15.6 m and 22.7 m to the log(Fe/Mn) record, as well as a broad filtering around 18.2 m (Fig. 5). As shown in Fig. 5, each of the previously identified bundles, including the weak 3c to 3e in between bundles no. 3 and 4, are followed by the filtered ~16 m cycle, which furthermore places additional cycles in between bundles no. 1 and 2 (i.e., around 1d) and around bundles no. 5 and 6 (i.e., around 5a, 5c, 6a and 6c). These '~16 m-scale' bundles are also picked up by the broad ~18 m filter, which identified 1d to 2a, 3d to 3e, and 6a as relatively weak additional ~16 m cycles. In contrast, the filtered ~23 m cycle only follows the more pronounced BIF bundles 1 to 5a, coinciding with distinct ~18 m filter maxima, and shows minima around 1d, 3d or 3e, and 6a, coinciding with weak ~18 m filter maxima. Thus, two simultaneously occurring cycles with periodicities of ~16 m and ~23 m appear to determine (largely) the characteristic bundling of ~5 m-scale BIF intervals in this main part of the Kuruman IF stratigraphy (i.e., below 170 m core depth).

These results overlap with but also differ from Lantink et al. (2019), where similar MTM power spectra were generated for weathering profile logs, with dominant periodicities around ~4.3–6.3 m and ~16 m–22 m. However, in that study, the ~16 m and ~22 m components were attributed to a single cycle resulting from an upward change (decrease) in depositional rate, as a stronger amplitude was observed for the ~22 m cycle in the lower part of the Kuruman IF versus a stronger ~16 m cycle amplitude in the upper part from 4ab upwards. This interpretation was supported by a similar parallel shift in the dominant wavelength associated with the basic abc-alternations from ~6 m to ~4.5 m. However, no such a distinct trend is observed here in the amplitude or thickness of the filtered ~5 m cycle in the log(Fe/Mn) and MS records, nor do we see any changes in the amplitude of the filtered ~16 m or ~23 m cycles, between 170 m to 320 m core depth.

Extraction of the ~47 m cycle from the log(Fe/Mn) record reveals a link with the phasing of the ~16 m and ~23 m cycles (Fig. 5). When the filtered ~16 and ~23m cycles are in phase, corresponding to a maximum in the amplitude of the broadly filtered ~18 m cycle, this coincides (roughly) with a maximum in the filtered ~47 m cycle. Conversely, minima in the filtered ~47 m cycle correspond to an out-of-phase relationship between the filtered ~16 m and ~23 m cycles, i.e., during ~23 m cycle maxima that coincide with a minimum in the ~16 m cycle (and minimum amplitude of the broadly filtered ~18 m cycle).

Lastly, we apply bandpass filtering to the MS record for extracting the moderately strong ~9 m, ~11.5 m and ~87 m cycles present in its corresponding MTM spectrum. As visible in Fig. 5, the filtered ~9 m curve exhibits largest amplitude around bundle 6, placing successive maxima around 6a, 6b, 6c and 6d, which are also partially followed by the ~11.5 m filter. Lower in the stratigraphy, the filtered 11.5 m cycle also picks up BIF intervals 5a and 5a.2, the relatively thick 4b, and the slightly more pronounced 2a and 2c relative to 2b. Both the filtered ~9 m and ~11.5 m cycles exhibit a minimum around the pronounced MS minimum in between 3a and 3b. This minimum is further recognised as a minimum in the filtered ~16 m MS cycle; note that in the filtered ~16 m log(Fe/Mn) signal this minimum is placed above 3b. The filtered ~87 m MS signal shows successive maxima at bundle 2 and in between bundles 5 and 6, thus seemingly arising from the relatively thick carbonaceous shaley intervals surrounding BIF bundle 4.

4.2 Cyclostratigraphic analysis of the Dales Gorge Member

4.2.1 Visual identification

The cyclostratigraphy of the Dales Gorge Member as reflected in the logs and verticality profiles of the Mt Bruce and Mt Jack sections (Fig. 7) shows clear similarities but also differences with the Kuruman IF. In the first place, regular metre-scale alternations are visible between well-exposed ridges or cliffs and more weathered, low-relief intervals, which occur at a basic thickness scale of about ~5–7 m in the lower two-third part of the stratigraphy. The alternations are associated with the formal 'BIF–S macrobanding' of Harmsworth et al. (1990) and Trendall and Blockley (1968) and have been labelled accordingly (Fig. 7). However, they are not completely the same, as our 'S intervals' are relatively thicker given that they are based on relief and not lithology. Still, the relative thickness proportion of 'BIF' versus 'S' in the Dales Gorge Member is generally larger than in the Kuruman IF, which creates a more staircase-like weathering profile with steeper slopes.

In the second place, a regular ~15–20 m-scale variability is visible, most clearly in the interval from DB1-DB12, which is manifested by the occurrence of relatively thicker S macrobands, i.e., DS4, 6, 9 and 11. However, the number of BIF–S alternations in each bundle is less than the characteristic three to four BIF intervals per large-scale bundle observed for the Kuruman IF, with instead alternating groups of either three or two BIF macrobands (namely DB1 to 3, DB4 and 5, DB6 to 8, and DB9 and 10). In the bundles comprising just two BIF–S macroband alternations, one of the two BIF intervals is ~1.5 times thicker than its neighbour and occurs adjacent to a thicker (~3–5 m) S interval.

A seemingly different bundling pattern is observed in the lowermost (DB0) and upper third (DB12 to 16) of the Dales Gorge Member (Fig. 7). These intervals are characterised by a larger absolute as well as relative proportion of BIF versus S intervals in terms of stratigraphic thickness, with BIF macrobands that are at least 1.5 to more than 2 times thicker than in the 'basic' BIF–S alternations in the central part of the Dales Gorge Member. The very thick (~12–13 m) DB0 at the base seems to represent a single BIF bundle on its own, while also showing some affinity with the next BIF above (DB1), due to its more pronounced upper part and the relatively thin shale DS1 (compared to DS4, DS6 etc.) separating it from

DB1. Similarly, the four ~5 m-scale ‘cherty BIF’-S alternations of the Colonial Chert Member below DB0 do not show any obvious grouping, although the upper two beds are slightly more pronounced and demonstrate some affinity with DB0 due to the relatively thin interstitial S interval CS6. Above DB12, the separation of DB13 to 15 from DB16 to 16a by the thicker S interval DS16 looks as a continuation of the two-three-two BIF grouping, but it occurs at a much larger thickness scale of ~25–30 m instead of ~16 m. In addition, DB12 and DB13 show a slight affinity towards each other due to the relatively thin DS13 and the more pronounced and thicker lower part of DB13.

Further insight into the internal structure of the thicker BIF macrobands can be gained if we look more closely at the verticality profiles and their correlative Hylogger mineral records from cores 47A and SGP001 (Fig. 8). Particularly in the ferric oxide abundance record, a clear subdivision is noticeable in several of the thicker BIF intervals, indicating that they consist of a merged (partially) double ~5 m-scale BIF–S alternation. This is particularly evident in DB12, whose ferric oxide signal reveals two distinct ~5 m-scale maxima and a pronounced minimum halfway in between, indicating a weakly developed S layer at that position. In this way, DB12 looks somewhat analogous to the double BIF macrobands DB16 and 16A, which are also separated by a very weak shale S16A, although their individual BIF–S alternations are significantly thicker (~7 m in 47A and SGP001; 8–9 m at Mt Bruce) than those in DB12. Double alternations are further noticeable in DB13, DB15, DB9 and to some extent in DB4. For DB13 and 15, the subdivision as seen in the verticality and ferric oxide profiles is more asymmetric, with a second upper ‘BIF’ maximum that is relatively thinner (~3–4 m).

At comparable thickness scale, thin slightly more prominent beds or ferric oxide maxima can be distinguished in the thicker S macrobands, suggesting the presence of an additional BIF–S alternation in these intervals. This is particularly obvious for the faint maximum in the Mt Jack verticality profile around DS6, which occurs at the same ~5 m scale as DB6 to 8 above. However, the thinner (1.5–2 m) spacing of the two conspicuous ‘BIF’ beds in DS11 seems to indicate variability at the sub-macroband level, as also seen in between CB4 and CB6 of the Mt Jack log. In general, this sub- or semi-5 m-scale variability is more strongly developed in the carbonate record of core 47A (Fig. 8) such as around DS1 to DB1 and DB4. Note further that the positions of the carbonate minima associated with the ~5 m-scale BIF–S variability are generally offset from those in the ferric oxide record, as can for instance be seen from the more symmetric subdivision of DB15 and DB16 to 16A (Fig. 8).

4.2.2 Spectral analysis and bandpass filtering

Spectral analysis was carried out on all four Dales Gorge Member proxies to independently test for cyclicity associated with the observed metre-scale BIF–S alternations and bundling. The resultant MTM spectrum of the Mt Jack verticality record shows dominant power concentration around 7 m, in addition to strong peaks at 3.5 m, 5.4 m and 9 m, each exceeding the 99 % LOWSPEC and 90 % harmonic confidence level (Fig. 9). The L-S and MTM spectra of the Mt Bruce record look essentially the same as for the Mt Jack record, apart from that all periodicities (except the 7 m cycle) are ~10 % thicker, and an additional ~18 m and 29 m peak are recognised as significant peaks (reaching 90–95 % LOWSPEC confidence). A very similar L-S spectrum is also found for the 47A ferric oxide record, but in this case the main periodicities are ~10 % thinner compared to those in the Mt Jack spectrum (i.e., the 5.4 m peak has become 4.9 m). In addition, significant peaks are identified around 20–25 m, ~42 m, and at 10.4 m, 11.3 m and 12.9 m in the equivalent MTM spectrum, but note that not all of these peaks correspond to a harmonic F-test peak (Fig. 9B) and the spectrum is relatively noisy. In contrast, the MTM spectrum of the 47A carbonate record shows a much cleaner pattern of well isolated peaks at 3.1 m, 5 m, 8.3 m and 15.4 m which does not show any significant cycles in the 10–13 m range or around 7 m.

For all four Dales Gorge Member proxies, bandpass filtering was again used for isolating the most prominent cyclical components, and whose filter outputs are subsequently compared to the original records (Fig. 7 and 8). First of all, extraction of the very strong ~7 m cycle from the verticality and ferric oxide records shows that it follows the individual BIF–S macroband alternations 1 to 11. In particular, the filtered ~7 m cycle shows a good match with the relatively (~1.5 times) thicker BIF macrobands DB1 to 3, DB4 and DB9. The filtered ~5 m cycle, on the other hand, tracks only the thinner BIF–S alternations 5, 6 to 8, 10 and 11, as well as the four cherty BIF–S alternations of the Colonial Chert Member. Thus, the combination of a ~7 m and ~5 m cycle seems responsible for the basic BIF–S alternations characteristic of the lower two-third part of the Dales Gorge Member. In addition, the ~5 m filtering places an additional cycle in each of the thicker S intervals (DS6 and 11) or at the transition from thick S to thicker (~7 m) BIF intervals (DS4 to DB4 and DS9 to DB9). The maxima of these filtered extra ~5 m cycles coincide with minima in the filtered ~7 m cycle in these intervals, suggesting the weak development of, indeed, an additional ~5 m-scale BIF in the thicker S macrobands, which is suppressed or overwhelmed by a stronger ~7 m cycle. The inference of a ~5 m cycle fitting within each of these thicker S macrobands is consistent with cyclostratigraphic evidence for a somewhat lower sedimentation rate in the shaley facies compared to BIF facies (Lantink et al., 2023).

Besides the ~5 m and ~7 m cycles, bandpass filtering around ~9 m reveals a correspondence to the even (~2 times) thicker BIF–S alternations as characteristic of the upper third of the Dales Gorge

Member stratigraphy, as well as DB9. In particular, the filtered ~9 m cycle follows the thicker and more pronounced lower parts of DB13 and DB15. In addition, the ~9 m filtering picks up the double BIF macroband DB12, placing a maximum in the middle that counteracts the minimum in the filtered ~5 m cycle at that position (but note that the minima in the filtered ~9 m cycle correspond to the upper and lower edge of DB12 instead of to DS12 and 13). In the ferric oxide record, the prominent parts of DB13 to 15 are also picked up by the filtered ~7 m cycle; note that the very low filter amplitude in the Mt Bruce and Mt Jack records is likely because of the significantly larger thickness of their upper BIF–S macrobands. Moreover, the thick and double BIF interval DB16 to 16A is identified as a double (filtered) ~9 m cycle, as well as ~7 m cycle, while being identified as three (filtered) ~5 m cycles.

Filtering of the strong ~16 m cycle shows that, as for the Kuruman IF, this cycle follows the characteristic bundling of two or three BIF–S alternations in the majority of the Dales Gorge Member stratigraphy. In Figs. 7 and 8, both the filtered ~16–18 m cycle (using a narrow filter bandwidth) and ~18–20 m cycle (using a broad filter bandwidth) track each of the thicker S macrobands defining the bundles, including DS13. Note also that all of these thicker S intervals are typically associated with minima in the filtered ~9 m cycle, and as noted earlier, the ~7 m cycle, while being associated with maxima in the filtered ~5 m cycle. In the basal part of the Dales Gorge Member, however, the ~16 m filtering does not follow the characteristic group of three BIF macrobands DB1 to 3: here, the filtered ~16 m cycle minimum is situated higher, around DS2 instead of DS1, while the next filtered ~16 m maximum below is placed around the top part of DB0. This appears to explain the apparent merging or affinity of DB1 with DB0. Secondly, the very thick bundle DB13 to 15 higher up in the stratigraphy is identified as a double rather than single ~16 m cycle.

This thicker bundle in the upper part of the Dales Gorge Member appears to be related instead to the lower-power cycles in the ~20–29 m range (Fig. 8). As visible in Figs. 7 and 8, their correspondingly filtered curves identify bundle DB13 to 15 (as well as DB11–12 and DB16–16A) as a single cycle and generally exhibit largest amplitude in this upper interval. More specifically, the ~27–29 m cycle present in the Mt Bruce and Mt Jack spectra seems the consequence of the relatively thicker upper macrobands in these two sections compared to in core 47A, where this cycle has a shorter mean wavelength of ~20–22 m according to the spectral analysis (Fig. 9). In the carbonate abundance record of core 47A, the filtered ~22 m cycle shows a relatively large amplitude, especially in the lower and middle part of the Dales Gorge Member, indicating that DS1, DB4 and DB8 are successive (filtered) ~22 m cycle minima (Fig. 8). In the ferric oxide record, the expression of the ~22 m cycle is more subtle, revealed by amplitude variations of the broadly filtered ~18–20 m cycle (~16 m-scale bundling) (Fig. 8). As for the

Kuruman IF, filtering of the ~42–43 m cycle indicates a link with the ~16 m and ~22 m cycles: maxima in the filtered ~43 m cycle (shown for the Mt Jack record; Fig. 7) coincide roughly with maxima in the amplitude of the broadly filtered ~18–20 m cycle, which in turn correspond with a combined maximum in the narrowly filtered ~16 m and 22 m cycles that reinforce each other.

To extract the weaker ~10–13 m spectral components (Fig. 9) from the 47A ferric oxide record, a broad filtering was applied around 11.5 m. The resultantly filtered ~11.5 m cycle shows a clear correspondence with the alternatingly strong-weak-strong BIF pattern of DB1 to 3 and DB13 to 15, as well as with the upper, more pronounced part of DB0, and with the double DB12 (Fig. 8).

Lastly, we applied a bandpass filter to the Mt Jack verticality and 47A carbonate records for extracting the strong ~3–3.5 m components (Fig. 8; Fig. S8) present in their corresponding power spectra (Fig. 9). Comparison of the filtered ~3.5 m cycle in the Mt Jack record shows a consistent 2:1 hierarchy with the filtered ~7 m cycle, with maxima in the filtered ~3.5 m cycle occurring systematically at the transition from S to BIF interval. This suggests that the ~3.5 m cycle in this record represents largely, but not exclusively (Fig. S8), a harmonic resulting from the somewhat ‘rectangular’ shape of the BIF–S alternations (i.e. the larger thickness proportion of the BIF relative to S intervals). In contrast, the filtering results for the carbonate record (Fig. 8) indicate the presence of a real ~3.1 m cycle that is manifested as a splitting of the thicker (~7 m-scale) BIF–S alternations.

4.3 U–Pb ages and sedimentation rate

Concordant high-precision U–Pb TIMS results were obtained from the targeted stilpnomelane-rich shale intervals of the Dales Gorge Member (DS1 and DS9 upper), as well as from the Kuruman IF, allowing for a more robust assessment of their relative timing than was hitherto possible based on available U–Pb SHRIMP ages of the Dales Gorge Member (Nelson et al., 1999; Trendall et al., 2004; Wingate et al., 2021a, 2021b). The calculated $^{207}Pb/^{206}Pb$ ages derived from shale DS1 and DS9 upper are 2482.1 ± 1.9 Ma (2σ) and 2477.8 ± 0.9 Ma, respectively (Fig. 10) corresponding to 13.9 m and 64.9 m height in the 47A core. These ages constrain the depositional time frame of the Dales Gorge Member to the lower circa three quarters of the Kuruman IF, whose onset is estimated at 2484.6 ± 0.34 Ma, reflecting the previously acquired TIMS U–Pb age for the basal Klein Naute Shale of Lantink et al. (2019). Our TIMS ages for DS1 and DS9 are also consistent with but more precise than recent SHRIMP analyses from a larger population of zircon from the same samples (Wingate et al., 2021a, 2021b). In addition, revised $^{207}Pb/^{206}Pb$ ages were calculated for the shales at 212 m and 110 m depth in core UUBH-1 (lutites 2 and

4 of Lantink et al., 2019) from adding new concordant zircon analyses to the weighted mean age of each sample. This yielded slightly older and significantly more precise ages of 2476.9 ± 0.9 Ma and 2464.8 ± 0.77 Ma, respectively (Fig. 10), compared to the initial results of Lantink et al. (2019).

Importantly, our new U–Pb ages indicate an identical accumulation rate for the Dales Gorge Member and Kuruman IF. An average accumulation rate of 12 (+20 and -10) m/Myr is estimated for the Dales Gorge and overlying Whaleback Shale Members (Fig. 11), which includes a third, recently established TIMS U–Pb age from a shale at 371 m depth in core SGP001 of 2469.1 ± 0.65 Ma (Lantink et al., 2022). Likewise, our updated depositional rate model for the Kuruman IF suggests an average accumulation rate of 10–12 ± 10 m/Myr for the time interval corresponding to the Dales Gorge Member, which decreases slightly with increasing stratigraphic height. Thus the U–Pb geochronology appears to be consistent with a common or shared origin for the in thickness-matching cycles of Kuruman IF and Dales Gorge Member described in Sections 4.1 and 4.2.

5. Time calibration of the observed cycles and possible origin

The goal of this study was to examine the possibility of a correlation between the Kuruman IF and Dales Gorge Member based on their inferred long-period eccentricity related cycle pattern. As such, we must first turn to the question of whether such a Milankovitch control is a plausible explanation.

5.1 Astronomical interpretation of the basic alternations and bundling

As previously discussed in Lantink et al. (2019), we find it difficult to imagine a phenomenon other than astronomical forcing that can explain the periodic nature, hierarchical stacking (i.e. bundling) and vast lateral continuity of the observed metre-scale alternations in the Kuruman IF and Dales Gorge Member. The lateral continuity of the alternations in the Kuruman IF spans at least 250 km (Lantink et al., 2019). Similarly for the Dales Gorge Member, a lateral continuity of ~150 km of the characteristic BIF–S macroband pattern is indicated by the four localities targeted in the current study (Fig. 1 and 4). However, this continuity may in fact be extended to almost 500 km knowing that the classical BIF–S macroband pattern of the Dales Gorge Member can be laterally traced over the full W-E extent of the Hamersley Basin (Harmsworth et al., 1990; Trendall and Blockley, 1970).

For the Kuruman IF, independent support from U–Pb dating was already provided in Lantink et al. (2019) for the hypothesis that the main ~5 m-scale iron oxide (‘BIF’) vs carbonate-shale cyclicity represents the stratigraphic expression of the long 405 kyr eccentricity cycle (see also Section 2). Our updated, slightly higher sedimentation rate established here for the lower half of the UUBH-1 core (Fig. 9) seems in even better agreement with this interpretation. When assuming a sedimentation rate of 12 m/Myr, we obtain a period of 467 kyr for the main 5.6 m peak, and a period of 400 kyr for the weaker but also significant peak around 4.8 m, as present in the log(Fe/Mn) MTM spectrum (Fig. 6). Note that the average wavelength of the 405 kyr-related cycle in the Kuruman IF is estimated to be closer to 4.8 m than to 5.6 m, since a mean thickness of 5.1 m is obtained when counting the number of (filtered) ~5 m-scale alternations in the interval from 1a to 5d (i.e., 23 cycles in 117 m of stratigraphy). This implies that the 5.6 m periodicity as derived from spectral analysis is biased towards longer wavelengths, probably due to relatively thicker and more prominent alternations in the BIF-dominated intervals which contribute more to the amplitude of the power spectrum than the relatively thinner alternations in the carbonate- and shale-dominated intervals.

For the equivalent BIF vs S cyclicity in the Dales Gorge Member, the sedimentation rate of 12 m/Myr for core 47A (Fig. 9) yields a period of 408 kyr if the average 4.9 m wavelength (peak) in the ferric iron record is selected (MTM spectrum; Fig. 8). Again, the calculated period based on the U–Pb-derived sedimentation rate is remarkably close to that of the 405-kyr eccentricity cycle. Thus, as for the Kuruman IF, the cyclostratigraphic and U–Pb dating results are in mutual support of a long eccentricity origin for the ~5 m-scale cyclicity in the Dales Gorge Member.

This interpretation is different from that of de Oliveira Rodrigues et al. (2019), who also suggested a link between the BIF–S macrobanding and the 405 kyr eccentricity cycle in their ‘Timescale 1’, but reported a cycle thickness of 8 m, as opposed to ~5 m, based on analysis of a grayscale scan of the Dales Gorge Member type section core. In addition, our results for the Dales Gorge Member question the recent study of Zhou et al. (2022), who applied the Bayesian inversion method of Meyers and Malinverno (2018) to a 2 m-thick section (of DB12) from the same grayscale record, but assumed a maximum sedimentation rate ‘prior’ that was lower than the average rate reported in Lantink et al. (2019) and as confirmed by this study. As a consequence, Zhou et al. (2022) obtained an estimated total duration of 1.2 Myr for the studied interval by interpreting Calamina cyclothem variability of ~10–15 cm thickness – a likely candidate for the expression of climatic precession (Lantink et al., 2019; 2022; 2023) – as short (~100 kyr) eccentricity. This implies that the precession frequency, Earth-Moon distance and length-of-day estimated by Zhou et al. (2022) are likely based on a fundamentally incorrect Milankovitch interpretation.

Second, in line with 'Hypothesis 2', it was argued in Lantink et al. (2019) that the very long ~2.4 Myr eccentricity cycle is a most logical candidate for the apparent '~16–22 m' cycle responsible for the bundling of the ~5 m cycles in the Kuruman IF. The ~2.4 Myr eccentricity cycle is the strongest eccentricity component after the 405 kyr and short (~100 kyr) eccentricity cycles (e.g. Laskar et al., 2004), and is also denoted as the 'Mars-Earth' $g_4 - g_3$ cycle, where g terms refer to the fundamental frequency of the rotation of the orbits of Mars (4) and Earth (3) on their respective orbital planes. Given the prominent expression of the 405 kyr cycle in the Kuruman IF weathering profile, it was therefore argued that a similarly strong imprint of the $g_4 - g_3$ eccentricity cycle would be expected, in case of a nonlinear response and associated power transfer from the domain of climatic precession (the inferred primary insolation driver) to its longer-period amplitude modulating cycles of eccentricity. The observed 1:3 to 1:4 ratio between the inferred 405 kyr- and ($g_4 - g_3$)-related cycles was attributed to a reduction in the period of $g_4 - g_3$ to ~1.2 – 1.6 Myr due to chaotic diffusion (Lantink et al., 2019), as also observed in the Mesozoic (e.g. Olsen and Kent, 1999; Ma et al., 2017).

Unlike the $g_4 - g_3$ cycle, the period of the 405 kyr ($g_2 - g_5$) cycle – arising from the secular orbital motions of Venus and Jupiter – is considered relatively stable over the history of the solar system (e.g. Hoang et al., 2021; Laskar et al., 2004, 2011; Laskar, 1993). Accordingly, this cycle can be used for time calibration of other (longer-period) cycles. Lantink et al. (2019) related the 4.5–6.1 m cycle as seen in the evolutive harmonic spectrum of the Whitebank section to the stable 405 kyr eccentricity cycle to obtain a period between 1.4 and 1.6 Myr for the single larger-scale cycle associated with the bundling. However, based on our more detailed cyclostratigraphic account of the Kuruman IF and Dales Gorge Member (Sections 4.1.2 and 4.2.2), now at least two cycles appear to be involved in the bundling in both stratigraphic units, of which the dominant cycle has a period of ~16 m. Therefore, it currently seems most logical to attribute this ~16 m cycle to $g_4 - g_3$. Using the established mean thickness of the 405 kyr-related cyclicity in both successions, the ~16 m cycle converts to a mean period of ~1.3 Myr (Table 1), i.e., shorter than initially estimated by Lantink et al. (2019). More precisely, we estimate a period of 1.27 ± 0.05 Myr for the Kuruman IF, based on counting between 21 and 23 (interpreted) 405 kyr-related cycles and 7 filtered ~16 m cycles in the interval from BIF 1a to 5c.

5.2 Milankovitch origin of other long-period cycles?

Given our Milankovitch interpretation for the basic ~5 m and ~16 m cycle, what could be the origin of other long-wavelength cycles involved in the characteristic bundling pattern of the Kuruman IF and

Dales Gorge Member? In particular, an explanation is needed for the origin of the ~23 m cycle that is additionally involved in the characteristic large-scale bundling and most clearly developed in the Kuruman IF weathering profile, and for the strong the ~7 m and ~9 m cycles that are thought to be responsible for the characteristic 'merging' of BIF intervals, mainly in the Dales Gorge Member. From an eccentricity perspective, the most logical candidate for the ~9 m cycle would, given its time-calibrated period of ~700 kyr (Table 1), be the present-day 690 kyr ($g_2 - g_1$) eccentricity term. However, the amplitude of the ~9 m cycle in the studied Dales Gorge Member records is much larger than would be expected for the $g_2 - g_1$ cycle, particularly when compared to the amplitude of $g_2 - g_5$ (Table 1; Laskar et al., 2004).

Of comparable amplitude to $g_2 - g_1$ is the eccentricity term $(g_2 - g_5) - (g_4 - g_3)$, which occurs as the upper side band of the 405 kyr cycle in eccentricity power spectra (see for example Fig. 4 in Laskar, 2020). In the La2004 solution (Laskar et al., 2004), the $(g_2 - g_5) - (g_4 - g_3)$ cycle has a period of 490 kyr, but this period becomes ~590 kyr when we adjust for a 1.3 Myr period of $g_4 - g_3$. This period approximates the time-calibrated period of the strong ~7 m cycle (i.e., 560 kyr) in the Dales Gorge Member as identified from the verticality and ferric oxide records (Table 1). Despite its relative weakness, the $(g_2 - g_5) - (g_4 - g_3)$ cycle has been previously detected in paleoclimate archives (Olsen et al., 2019). Nonetheless an explanation is needed for why such a relatively weak eccentricity term, resulting from the combination of four *g*-frequencies, would be so dominantly manifested as a cycle in the stratigraphy of the Dales Gorge Member.

Even more puzzling is the origin of the ~23 m cycle from the point of view of our Milankovitch hypothesis. Looking at the eccentricity spectrum of La2004 for 0–33 Ma (Fig. 4 of Laskar, 2020), there is no obvious candidate which matches the estimated ~1.8 Myr period of this cycle and is of sufficiently large amplitude. An alternative hypothesis that we therefore need to consider is that instead of the ~16 m cycle, the ~23 m cycle represents $g_4 - g_3$ (also reduced in period due to chaotic diffusion). In that case, the ~16 m cycle could reflect the ~1.2 Myr Earth-Mars obliquity amplitude modulation term $s_3 - s_4$ (s terms referring to the precession of the orbit's ascending nodes). This obliquity cycle is dynamically linked to the $g_4 - g_3$ cycle in the secular resonance theta (θ) currently manifested as $\theta = (s_3 - s_4) - 2(g_4 - g_3)$ (Laskar, 1990) i.e., exhibiting a 2:1 frequency ratio. (The ~16 m and ~23 m cycles observed here, with a frequency ratio of approximately 3:2, would imply a different resonance state.) A stronger stratigraphic expression of $s_3 - s_4$ than $g_4 - g_3$, however, seems less likely given the evidence for a long (405 kyr) eccentricity imprint, implying a dominant precession control on insolation, and the low paleolatitude position indicated by paleomagnetic data from the Ongeluk Formation at ca 2.43 Ga

(Gumsley et al., 2017). A third astronomical scenario we may consider is that both the ~1.3 Myr and ~1.8 Myr cycles are related to eccentricity, and both are an expression of chaotic orbital behaviour. For instance, the ~1.3 Myr cycle might reflect a shift from the present-day ~1 Myr ($g_1 - g_5$) cycle towards lower frequencies, as can be observed in some eccentricity solutions (Charbonnier et al., 2023; Laskar et al., 2004).

However, a more systematic evaluation of astronomical solutions is needed first to investigate how pronounced and persistent these chaotic changes in the frequency and amplitude of the $g_1 - g_5$ and $g_4 - g_3$ (and $s_3 - s_4$) cycle may have been. Moreover, the relatively weak ~11.5 m cycle as expressed in certain intervals of the Kuruman IF and Dales Gorge Member may be a more logical candidate for $g_1 - g_5$ (Table 1), also given that both a ~980 kyr and ~1.3 Myr cycle have been tentatively identified in the Joffre Member of the Brockman IF higher up in the stratigraphy (Lantink et al., 2022).

5.3 Indirect terms resulting from nonlinear response?

Given the absence of an obvious astronomical explanation for the ~23 m cycle, and the anomalously large amplitude of the ~7 m and ~9 m cycles, the question arises whether we can explain these cycles in a different way. It has been well-established for the younger part of the geological record that harmonics and combination tones of the primary astronomical signal can develop as a result of a nonlinear response by the climate system (e.g. Crowley et al., 1992; Imbrie et al., 1993; Le Treut and Ghil, 1983; Ruddiman et al., 1989; Short et al., 1991) and/or depositional system (e.g. Herbert, 1994; von Dobeneck and Schmieder, 1999; Weedon, 2003; Westphal et al., 2004). In fact, such a nonlinear response is rather the rule than the exception. While the responsible nonlinear dynamics are often poorly understood, harmonic cycles may result from distortion or resonant amplification of a single orbital cycle, while combination tones (‘intermodulation frequencies’) arise from nonlinear coupling (interactions) of two or more primary cycles (Le Treut and Gill, 1983; Herbert, 1994; von Dobeneck and Schmieder, 1999). A well-known example is the occurrence of an ~80 kyr, double obliquity cycle in Pleistocene climate-sensitive proxy records (Huybers, 2006; Huybers and Wunsch 2005; Marino et al., 2009; Raymo and Nisancioglu, 2003; Ruddiman et al., 1989).

Such nonlinear effects were likely playing a role as well during deposition of the Kuruman and Brockman IFs, as is indicated by for instance the ~2–2.5 m variability in the lower part of the Kuruman IF, the Colonial Chert Member and the Dales Gorge Member (Section 4.1.1 and 4.2.1), which appears to reflect a semi-405 kyr cycle and/or double ~100 kyr cycle; the 3–3.5 m cyclicity in the Dales Gorge

Member, which may represent a semi-7 m cycle (Fig. S8); and a ~46 m cycle, which likely represents a difference tone of the ~16 m and ~23 m cycle.

It is therefore not unlikely that the ~23 m cycle also represents some kind of harmonic or combination term induced by nonlinear response within the climate and/or depositional system. Based on its period, the ~23 m cycle could represent a double ~11.5 m cycle (possibly related to $g_1 – g_5$). Likewise, we can formulate an alternative explanation for the origin of the strong ~7 m cycle in the Dales Gorge Member, that is, as a non-orbital difference term of the ~5 m ($g_2 – g_5$-related) and ~16 m (possibly $g_4 – g_3$-related) cycle. The ~9 m cycle could represent a difference tone of the ~5 m ($g_2 – g_5$) and ~11.5 m ($g_1 – g_5$) cycle, and/or a harmonic of the ~16 m ($g_4 – g_3$) cycle (Table 1). We further note that the presence or absence of a ~7 m, ~9 m and ~23 m cycle is rather proxy- and location-specific, which may be an additional indication for a nonlinear origin of the cycles related to the depositional system (see also Section 7.1.1).

Lastly, we note that the astronomical cycles are themselves combination tones, originating from combinations of Earth’s axial precession frequency (p) and the fundamental planetary frequencies (g and s). More specifically, the main eccentricity cycles can be written as a combination of two g_i frequencies of the inner planets plus Jupiter (with i = 1 to 5) or in fact, of their corresponding climatic precession terms $p + g_i$. These frequencies can in turn be combined to form higher-order eccentricity terms which become progressively weaker. By definition, the relatively weak $(g_2 – g_5) – (g_4 – g_3)$ eccentricity term is thus a difference tone of the $g_2 – g_5$ and $g_4 – g_3$. In addition, the $g_2 – g_1$ cycle represents a difference cycle of the fundamental frequencies g_2 and g_1, but can also be written as the combination of $g_2 – g_5$ and $g_1 – g_5$. Thus, instead of representing harmonics and/or combination tones arising purely from nonlinear response of the climate and/or depositional system, the ~7 m and ~9 m cycles could alternatively, or additionally, result from amplitude distortion of the primary eccentricity terms $(g_2 – g_5) – (g_4 – g_3)$ and $(g_2 – g_1)$. The same explanation may be invoked for the ~2–2.5 m variability, which could originate from amplitude distortion of the weak ~200 kyr eccentricity terms $-2g_2 – 2g_5$, as also identified in paleoclimate records from the Paleogene (Hilgen et al., 2020). The 3–3.5 m cycle could possibly be related to the very weak ~280 kyr eccentricity term arising from $(g_2 – g_5) + (g_1 – g_5)$ (Table 1).

In summary, much uncertainty remains concerning the astronomical origin – linear or nonlinear – or otherwise, of several cyclic components involved in the characteristic cycle patterns of the Kuruman IF and Dales Gorge Member, most notably, the ~7 m, ~9 m and ~23 m cycles. Nonetheless, we consider the cyclostratigraphic and U–Pb evidence presented in Section 4 sufficiently convincing in support of the Milankovitch interpretation of Lantink et al. (2019) for their main hierarchy of two cycles, namely i) a ~5 m cycle defining (largely) the basic 'BIF' versus 'S' alternations related to the 405 kyr eccentricity cycle; and ii) a ~16 m cycle dominantly responsible for the bundling of several BIF intervals (associated with the ~5 m cycle), which may reflect the expression of the Mars-Earth eccentricity cycle with a period of ~1.3 Myr. Therefore, we consider it justified to proceed to establish a cyclostratigraphic correlation between the Kuruman IF and Dales Gorge Member, focusing on the expression and scale of the ~5 m and ~16 m cycles.

6. Establishing of a 405 kyr-scale cycle framework

6.1 Correlation option I: based on the characteristic weathering profile pattern

Cyclostratigraphic correlations between outcrops of the Kuruman IF in the Griqualand West Basin have previously been established over 250 km on the basis of the characteristic pattern in the succession of prominent BIF bundles as seen in weathering profile (i.e., 2abc, 3ab, 4(a)b, and the double (~16 m-scale) bundle 5abcd, see Lantink et al., 2019). Likewise, the correlation between the weathering profile logs and the new UUBH-1 core proxy records based on identification of this characteristic pattern proved relatively straightforward in the present study (Section 4.1). Similarly, the distinctive cycle pattern seen in outcrops and cores of the Dales Gorge Member has been used for detailed correlations across the Hamersley Basin over many hundreds of kilometres. Thus, adopting the same visual approach seems a promising starting strategy for establishing the intended high-resolution correlations between the Kuruman IF and the Dales Gorge Member. To establish these correlations, we will use the log(Fe/Mn) record of the Kuruman IF, which is generally more representative for its weathering profile than the MS record. For the Dales Gorge Member, we will use the log(ferric oxide) record of core 47A as representative proxy, because the cycle thicknesses in that record are more similar to those in the Kuruman IF than the verticality profiles of Mt Jack and Mt Bruce.

As a starting point for our correlation, we choose bundle 2abc, the characteristic group of three prominent BIF intervals seen in the Kuruman IF weathering profile (Lantink et al., 2019). Looking at the outcrop pictures of the Dales Gorge Member (Fig. 3 and 4), and the verticality and log(ferric oxide) records (Fig. 7 and 8), the three well-defined alternations of roughly equal thickness DB6 to 8 bear most resemblance to 2abc, and were correlated accordingly (Fig. S12). Subsequently, the most logical correlation, when focusing on the more pronounced and/or thicker BIF intervals, is to correlate 3ab to DB9 and 10, 4ab to DB11 and 12 (where 4b corresponds to the lower part of DB12), and the very prominent bundle 5abcd to DB13–15, interpreting DB13 and DB15 each as a double ~5 m cycle. Additional support for this correlation may be the striking resemblance of interval 4b–5d with DB12 to 15 as expressed in the carbonate abundance record of core 47A (Fig. 8). To complete our scheme, we must correlate the lower bundle 1abc in the Kuruman IF to DB4 and 5, and 6ab to the very prominent DB16 and 16A at the top of the Dales Gorge Member.

However, starting from this initial correlation option I, we encounter two critical inconsistencies regarding our cyclostratigraphic and U–Pb zircon dating results. Firstly, there are no correlative ~5 m-scale BIF–S alternations in the Dales Gorge Member for the three weaker BIFs 3c to 3e in the extra ~16 m-scale bundle in between 3 and 4 of the Kuruman IF. As a consequence, 3c, 3d and 3e need to be correlated to DS11, implying a condensed interval. To avoid this condensed interval (or alternatively a hiatus), the correlations of the cycles above 3b can be shifted upwards by two ~5 m cycles in the Dales Gorge Member, however, this revision results in a loss of fit between the cycle patterns in the two units (Fig. 12).

Secondly, correlation option I is not compatible with the U–Pb geochronology, especially when considering the ages of DS9 in the Dales Gorge Member and the shale at 212 m in core UUBH-1 of the Kuruman IF. The 2σ age uncertainties associated with these ages allow for a maximum difference of 2.8 Myr between the two dated stratigraphic levels. This is in direct conflict with the at least eight ~5 m or 405 kyr eccentricity-related cycles identified in this interval in the Kuruman IF, implying a duration of 3.2 Myr (Fig. 12). This implies that the Dales Gorge Member needs to be shifted upwards relative to the Kuruman IF by at least one (filtered) ~16 m cycle to make the cyclostratigraphic correlations consistent with the U–Pb results.

6.2 Correlation option IIa: most consistent with the U–Pb geochronology and characteristic pattern

We therefore explore a second, alternative correlation between the Kuruman IF and Dales Gorge Member that is both consistent with the U–Pb dates and the characteristic cycle patterns (succession of prominent BIF bundles) by shifting the Dales Gorge Member two (filtered) ~16 m cycles upwards. In this way, the 212 m shale and DS9 are placed within two or three ~5 m cycles from each other, which is consistent with their mean U–Pb age difference of 1.2 Myr. From a cyclostratigraphic point of view, this two-bundle shift is required to correlate 2abc to the other group of three pronounced, roughly equal BIF macrobands in the Dales Gorge Member, namely DB1 to 3. For the remainder of the stratigraphy, we proceed by first correlating at the ~16 m bundle level, followed by linking the more prominent ~5 m-scale BIF intervals of each bundle. Accordingly, 3ab correspond to DB4 and 5, 4b to DB9 and 5a to DB12. For the upper part, we shift the Dales Gorge Member upwards by only one filtered ~16 m cycle in order for the correlation to make more sense in terms of pattern resemblance, by linking the characteristic group of three prominent BIF intervals 5bcd to DB13–15, and 6a to DB16 (Fig. 13).

Although this second correlation (option IIa) initially did not seem most logical in terms of resemblance in characteristic pattern, similarities in the expression and/or the number of prominent BIF intervals per correlated bundle are still largely maintained and are in some cases even improved. In particular, the correlation of 2abc to DB1–3, instead of to DB6–8 (as was the case for option I), makes sense from the perspective of the UUBH-1 proxy records (as opposed to weathering profile expression), in which 2a forms part of bundle 2abc as well as showing affinity with the distinct 1d below (Fig. 5). This pattern looks similar to the characteristic merging of DB1 with the top of DB0 in the Dales Gorge Member; both features are related to the somewhat higher stratigraphic position of a ~16 m-scale cycle maximum (i.e., around 1d and the top of DB0, respectively; see narrow ~16 m filter output in Fig. 5). In addition, 2a and 2c are slightly more pronounced than 2b, as are DB1 and DB3, which in both cases is related to the expression of the ~11.5 m cycle in this interval. Moreover, higher up in the stratigraphy, the resemblance of 4d followed by the very prominent, double 5a with DB11 to 12 (according to option II) is improved and appears more logical than with DS12 to DB13 (according to option I).

However, at the individual ~5 m- and ~16 m-cycle level, we also encounter several misfits if we stick to our strategy of linking the most prominent BIF intervals. In the middle section, the result of correlating 3ab to DB4 and 5 is that an additional ~5 m cycle is required in DS4, on top of an already-inferred extra cycle, as well as one additional ~5 m cycle in between 4c and 4d. In addition, this correlation implies that the top of DB9 correlates to the interval in between 4a and 4b in the Kuruman IF. Higher up in the stratigraphy, the consequence of linking 5b to the lower, more pronounced part of DB13 is that it requires the absence of an additional ~5 m cycle above 5a.2 (‘5a.3’), but again the addition of a ~5 m cycle in between 5b and 5c, if we assume that DB13 represents a double ~5 m cycle. In addition, correlation IIa implies the absence of a second ~5 m cycle for the upper part of DB15.

Furthermore, with correlation IIa we have thus far treated bundle DB13–15 as a single ~16 m bundle, in contradiction to what is suggested by the double (filtered) ~16 m maximum around this interval. The issue is that it is still unclear whether the depositional rate of the Dales Gorge Member increased in this upper part of the stratigraphy, in which case DB13 to 15 could reflect a single ~16 m bundle equivalent to DB1 to 3; or whether the depositional rate has stayed relatively constant, in which case the overall thicker (≥ 7 m) BIF macrobands in this upper part are due to a weaker expression of the ~5 m cycle. A further complicating factor is the uncertainty in the period of the 16 m-scale cycle interpreted as $g_4 - g_3$, which is inherently unstable. Resolving these uncertainties ultimately requires a more detailed investigation into the expression of sub-405 kyr eccentricity-related Milankovitch cyclicity in this interval, which is beyond the scope of the present study. However, some clues may already be derived from the carbonate abundance record of core 47A, which shows a continuation of the ~5 m cycle in most of the upper third part of the Dales Gorge Member (Fig. 8), suggesting that sedimentation rates did not differ significantly from the lower two-third.

6.3 Correlation option IIb: most consistent with the ~5 m and ~16 m filtering

The discrepancies of correlation IIa with respect to the postulated number of (filtered) ~5 m and ~16 m cycles in the Dales Gorge Member can be largely resolved when considering a third, modified correlation II (option IIb) that attaches more importance to the ~5 m and ~16 m filtering of the Kuruman IF and Dales Gorge Member, than to the resemblance in cycle pattern. This results in a modified correlation option IIb, in which the cycles in the 2e to 4c interval of the Kuruman IF are shifted upwards by one (filtered) ~5 m cycle with respect to the Dales Gorge Member (Fig. 14). In that case, no extra ~5 m cycles need to be assumed in DS4 and 4c–d. However, this means that the very prominent BIF intervals 3b and 4b in the Kuruman IF are now correlated to shale DS6 and to the less prominent BIF macroband DB10, respectively, in the Dales Gorge Member. Also, the weak BIF 2e is now correlated to the prominent DB4.

Similarly, shifting the correlations above double BIF 5a in the Kuruman IF to DB12 in the Dales Gorge Member by two (filtered) ~5 m cycles upwards, resolves the need for an additional ~5 m cycle between 5b and 5c, and is compatible with a second ~5 m cycle in the top of DB15. However, as a consequence, 5c is now correlated to the less prominent upper part of DB13, the weak 5e to the prominent lower part of DB15, and the less prominent 6c to the very prominent DB16A. In this way, we have arrived at a correlation that is based on a maximum alignment of the filtered ~5 m and ~16 m cycles between the Kuruman IF and Dales Gorge Member (Fig. 14) by abandoning our previous strategy of trying to achieve the best possible pattern fit.

The resultant mismatch in stratigraphic expression of some correlated ~5 m-scale ‘BIF’ and ‘S’ intervals seems difficult to reconcile at first. However, this pattern misfit can be potentially explained by taking the marked differences in the cyclostratigraphy of the Kuruman IF and Dales Gorge Member into account, which seem to partly underlie the problems that we encounter in establishing the correlations (Section 7.1). These differences specifically pertain to the presence of a relatively strong ~23 m cycle in the Kuruman IF compared to ~16 m cycle, and a very strong ~7 m and ~9 m cycle (and moderately strong ~11.5 m) in Dales Gorge Member. As a result there are intervals in the stratigraphy where a ~5 m-scale 'BIF' is reinforced by a maximum in the ~23 m cycle in the Kuruman IF, while in the supposedly time-equivalent interval in the Dales Gorge Member this 'BIF' is suppressed by minima in the ~7 m and 9 m (and ~11.5 m) cycles, or vice versa. For instance, we observe that the weak BIF 2e in the Kuruman IF corresponds to a minimum in the ~23 m cycle (Fig. 5; Fig. S9), while its counterpart DB4 in the Dales Gorge Member (according to option IIb) corresponds to maxima in the ~7 m and ~9 m cycles (Fig. 7 and 8; Fig. S9). Conversely, the prominent BIF 3b in the Kuruman corresponds to a maximum in the ~23 m cycle, which counteracts the minimum in the ~16 m cycle in this interval (see also the MS record in Fig. 5), while the correlated DS6 in the Dales Gorge Member corresponds to minima in the ~7 m and ~9 m cycles, reinforcing the ~16 m-scale (shale) minimum. Similar explanations may be formulated for the pattern mismatch in the correlation of 4b to DB10 and 5c to DB13 upper, albeit less convincingly (Fig. S9). Furthermore, it remains strange why the very weak 5e would correlate to the prominent lower part of DB15, and the moderately strong 6a to the weaker upper part of DB15 (Fig. 14).

Further discussion points concerning option IIb are the implied absence of an extra 405 kyr-related cycle in between 5a.2 and 5b, and the implied extra 405 kyr-related cycle in between 4a and 4b. Concerning the 5a.2 to 5b interval, the absence of a relatively thin cycle '5a.3' may not be unrealistic, given also that the ~5 m filtering of the MS record does not pick up an additional ~5 m cycle maximum. This is also true for the interval between 4a and 4b, where the existence of an additional 'hidden' 405 kyr-related cycle seems not unrealistic given its relatively large thickness. Moreover, the addition of a 405 kyr-related cycle would increase the total number of 405 kyr-related cycles between the well-dated Klein Naute Shale and the shale at 212 m depth to 18 or 19 cycles (interpreting 1a.0 as one to two ~5 m cycles). The assumption of nineteen 405 kyr-related cycles between these two dated horizons would imply a duration of 7.7 Myr, which is identical to the mean U–Pb age difference of 7.7 Myr.

Finally, we note that correlation IIb seems less consistent with the U–Pb geochronology and the number of filtered ~16 m cycles in the uncorrelated upper part of the Kuruman IF and Whaleback Shale-Joffre Members above the Dales Gorge Member. There is only one filtered ~16 m cycle recognised between 6c and the shale in between 7a and 7b, which has a calculated mean age of 2468.2 ± 1.5 Ma, in contrast to three (filtered) ~16 m cycles in between DB16A and the shale at the Whaleback Shale–Joffre Member boundary, having an older mean age of 2469.1 ± 0.65 Ma (Fig. 14). However, the many in-situ brecciation textures encountered above 7a (see Figs. S3 and S4 in Lantink et al., 2019), as well as the large time difference between the U–Pb ages of the shales at 110 m and 130 m depth (~4 Myr), point to the likely occurrence of hiatuses in this upper part of the Kuruman IF; this may be related to the transition towards a more shallow-marine setting as represented by the granular IF facies of the overlying Griquatown IF. As such, it is possible that the number of ~1.2–1.3 Myr cycles above 6c was in reality larger. Indeed, the assumption of two additional 1.25 Myr cycles when counting the number of filtered ~16 m cycles (i.e., a total of seven) from shale 212 upwards yields a mean age of 2488.2 Ma for the shale in between 7a and 7b, which is identical to its mean U–Pb age.

7. Discussion

7.1 Difficulties in establishing the correlations

Our various correlation strategies and attempts as detailed in the preceding (Section 6) illustrate that establishing a cyclostratigraphic correlation between the Kuruman IF and Dales Gorge Member is far from straightforward. This is contrary to what one would expect given the likely astronomical origin of the main stratigraphic cycles involved their characteristic bundling pattern. In fact, we anticipated that finding the correct correlation based on pattern matching would not be a problem, given the relatively straightforward correlations of the cycles in the Kuruman IF and Dales Gorge Member within their individual basins. However, this proved not to be the case, as our initial preferred correlation based on pattern resemblance (option I) turned out to be incompatible with the results of high-precision U–Pb dating and the presence of additional ~5 m-scale alternations (3c–d), forming an extra ~16 m-scale bundle, in between 3b and 4a in the Kuruman IF. Given that the U–Pb ages are in almost perfect agreement with our Milankovitch hypothesis for these cycles in the Kuruman IF and Dales Gorge Member (Section 5.1), our confidence in these ages and cyclostratigraphic results is high, meaning that correlation option I (as a whole) is considered unlikely.

Yet also our second, ‘improved’ correlation, for which we combined the requirement of pattern resemblance with the U–Pb age constraints (option IIa), resulted in inconsistencies regarding the exact number of identified ~5 m cycles in the Kuruman IF and Dales Gorge Member. We then established a modified correlation of option II (option IIb) that largely eliminated these inconsistencies by focusing mainly on the number of (filtered) ~5 m and ~16 m cycles. However, this correlation seemed to make (much) less sense in terms of the expected overall similarity in the cycle pattern. Moreover, several other correlation options are conceivable that differ by one or two 405 kyr-related cycles from this option IIb, given the remaining uncertainty in the exact number of ~5 m cycles. We cannot even rule out the possibility of a combination of options IIa/b and option I for the upper part of the stratigraphy, where the geochronologic and cyclostratigraphic evidence allows for more flexibility and ambiguity.

These uncertainties raise the important question of *why* it is so much more difficult than expected to establish unequivocally the correlation between Kuruman IF and Dales Gorge Member, if we accept the hypothesis that the regular large-scale (> metre-thick) alternations in their stratigraphy are Milankovitch-driven. Below we discuss two possible, closely related reasons (Sections 7.1.1 and 7.1.2).

7.1.1 Difference in depositional environment and associated nonlinear response to the Milankovitch forcing

Whereas the Kuruman IF and Dales Gorge Member cycle patterns as expressed in the weathering profile can be traced individually over hundreds of kilometres within their respective sedimentary basins (Sections 4 and 5), we encountered serious problems when trying to correlate the two units based on this characteristic pattern. This observation essentially tells us that the local climate and/or depositional response to the astronomical forcing was apparently very different between the two regions, to the extent that it led to significant differences in stratigraphic expression.

Although the paleogeography of the Hamersley and Griqualand West Basins is believed to have been grossly identical (Fig. 2), we note that a distinguishing feature of the eccentricity-scale alternations in the Dales Gorge Member compared with their equivalents in the Kuruman IF, is the more indurated nature of the oxide facies 'BIF' intervals, and the occurrence of thicker stilpnomelane-rich carbonaceous shales within the softer 'S' intervals (Beukes, 1980; Trendall and Blockley, 1970). Based on cyclostratigraphic evidence from the Joffre Member of the Brockman IF, it was recently proposed that the main influence of the precession and eccentricity forcing on the Hamersley Basin environment occurred via, possibly monsoon-induced, changes in continental runoff and marine productivity, causing associated variations in organic carbon export, iron (oxyhydr)oxide precipitation and settling of fine-grained siliciclastics (Lantink et al., 2023).

By extension of this model, the depositional environment of the Dales Gorge Member could thus have been under a more 'direct' Milankovitch control – that is, being more strongly influenced by the variations in fluvial discharge and biological productivity – compared to the Kuruman IF. In contrast, the more mixed iron oxide-carbonate composition of the cycles in the Kuruman IF as implied by the more gradual changes in relief and gentler hill slopes (Fig. 3), could indicate a more remote position and/or attenuated response of the – inferred eccentricity-scale – lithological endmembers (i.e., 'shale' vs 'BIF'). However, we stress that the source location of the postulated runoff must have been relatively distal in any case, given the lack of evidence for a nearby delta system in the Hamersley Basin and very low detrital content of the BIF facies. Instead, a predominance of carbonate breccias and turbidites in several of the S bands in the Dales Gorge Member indicates that deposition occurred downslope of a carbonate platform (Krapež et al., 2003; Martin and Howard, 2023; Pickard et al., 2004) similar to the basinal facies of the Kuruman IF near Prieska (Fig. 2), while deposition in the central part of the Griqualand West Basin took place on top of a former ("drowned") platform (Beukes and Gutzmer, 2008; Beukes, 1980, 1987).

The important question remains whether and how these differences in depositional environment can be related to the observed differences in stratigraphic cycle *pattern* between the Kuruman IF and Dales Gorge Member. As demonstrated by the cyclostratigraphic analysis (Section 4), part of the fundamental difference in cycle pattern between the Kuruman IF and Dales Gorge Member weathering profiles can be attributed to the presence or absence of a number of enigmatic, very long-period cycles, namely a relatively strong ~23 m cycle in the Kuruman IF involved in the characteristic large-scale bundling, and a strong ~7 m and ~9 m cycle in the Dales Gorge Member involved in the characteristic merging of ~5 m-scale BIF-S alternations (Section 6.3 and Table 1). While the Milankovitch origin of the ~23 m cycle remains more elusive (Section 5.2), the wavelengths of the ~7 and ~9 m cycles suggest that they may represent combination tones (artefactual or real) of the interpreted dominant eccentricity cycles resulting from nonlinear interactions within the climate or depositional system (Section 5.3 and Table 1).

Accordingly, we can speculate that the presumed 'higher-productivity, runoff-influenced' environment of the Dales Gorge Member, although possibly under a more direct Milankovitch control, was also more susceptible to the associated nonlinear responses resulting in the development of (stronger) combination tones and thus fundamental differences in cycle pattern with respect to the Kuruman IF. For example, we can imagine that threshold and stochastic processes were involved with the transport and deposition of suspended river load or shelf sediments derived from continental drainage and associated delta- or shelf-slope instability (Postma et al., 1993; Weltje and de Boer, 1993), although the predominance of carbonate breccias and slumps and silicate hardgrounds at the base of the S bands suggests that this threshold behaviour may have been primarily related to sea level changes (Bekker et al., 2010; Krapež et al., 2003; Rasmussen et al., 2015).

Similarly, we have reason to suspect that the behaviour of the ‘ferric iron’ or oxide-facies BIF component of the system was particularly nonlinear. Specifically, the abrupt and asymmetric nature, i.e., rectangular or sawtooth shapes, of the BIF–S macroband alternations in the Dales Gorge Member (Figs. 3, 7 and 8) and of the Calamina cyclothem (see e.g. Fig. 9 in de Oliveira Rodriguez et al., 2019), invites speculation about differences in the (response) timescales of water-column iron (Fe^{2+}) oxidation vs replenishment (through upwelling or sea level change), and early diagenetic iron oxide reduction vs retention related to organic carbon export fluxes. In addition, we note intriguing similarities in spectral characteristics between the (ferric iron abundance) pattern of the Dales Gorge Member with the MS (i.e., magnetite abundance) record of the Kuruman IF, namely a relatively strong ~9 m (and ~11.5 m) cycle, and a much weaker ~23 m cycle than in the Fe/Mn and weathering profile records of the Kuruman IF (Figs. 5 and 6). These differences in cycle composition of the MS record seem to explain its anomalous bundling pattern of 2d–3a and 3b–3e (compared to 3ab and 3c–e in the Fe/Mn and weathering profile records; Fig. 5), which is consistent with their correlation to DB4–5 and DB6–8 in the Dales Gorge Member, respectively, according to option IIb (Fig. 14 and Section 6.3).

Conversely, we can speculate that the relatively strong ~23 m cycle and absence of a strong ~7 and ~9 m cycle in the Kuruman IF weathering profile and Fe/Mn pattern reflects a more sluggish, longer-term response to the Milankovitch forcing – resulting in preferential amplitude transfer to the longer-period (harmonic) cycles – that is more characteristic of the ‘carbonate facies’ component of the system compared to the ‘oxide facies’ and ‘shale facies’ components. Preliminary additional support for this interpretation is provided by the carbonate abundance record of the Dales Gorge Member, which exhibits similar spectral features to the Kuruman IF pattern, i.e., a relatively strong ~23 m cycle and absence of a ~7 m cycle (Fig. 8 and 9). However, we are well aware that making such (causal) connections between the different sedimentary components/settings and potential differences in the mode or extent of the nonlinear Milankovitch-induced response is (far too) premature, given the limited number of proxy records analysed so far. But most importantly, we do not yet know enough about the origin of the different cycles in the Kuruman and Brockman IF stratigraphy, or the functioning of the early Paleoproterozoic climate and BIF system in relation to astronomical forcing, to draw any conclusions at this time.

This brings us to our second proposed reason for why establishing a cyclostratigraphic correlation between the Kuruman IF and Dales Gorge Member proved to be so difficult, which is outlined below.

7.1.2 Our relative ignorance of the cycle patterns

A more general, overarching explanation for the problems with identifying the correlations has been our relative lack of knowledge about the cycles in the stratigraphy of the Kuruman IF and Dales Gorge Member. More specifically, there is still much uncertainty about the origin and composition of the cycle patterns from both an astronomical and geological perspective, such as which Milankovitch parameters were involved in the climate forcing, what their periods and amplitudes were, and how the cycles were eventually recorded in the stratigraphy. As a consequence, this leaves room for doubt about the (correct) cyclostratigraphic interpretation of the patterns and how to correlate them across basins.

A primary aspect of our ignorance regarding the interpretation of the cycle patterns pertains to a limited understanding of the responsible climatic and depositional processes underlying them. This lack of process understanding was already evident from our earlier discussion on proxy-dependent differences in cycle manifestation (Section 7.1.1). The problem is that the proxy records have been selected based on mainly empirical grounds (i.e., visual inspection of regular stratigraphic changes), rather than on an intrinsic understanding of their relationship with the astronomical forcing. In other words, we are unsure about what precisely the proxy variations reflect i.e. what is their climatic, environmental or possibly biological significance. As such, it is not clear which of the selected proxy records, or which of their spectral traits, provides a (more) reliable representation of the astronomical signal and is thus most suitable for establishing the correlations. A more general problem with using sedimentary proxies (as opposed to, e.g., isotope ratios) is that they may depend more on local depositional conditions than on regional or global climate signals and are more susceptible to distortion resulting from dilution and diagenetic effects (Herbert, 1994; von Dobeneck and Schmieder, 1999; Weedon, 2003; Westphal et al., 2004).

Then there is the question of how to link the results of the Kuruman IF and Dales Gorge Member to the recent precession-scale observations and associated climate model for the Joffre Member (Lantink et al., 2023). For example, we note that there is an offset or asymmetry between how the long eccentricity-related alternations are defined in the lithology – namely between iron oxide-facies ‘BIF’ and carbonate/shale-facies ‘S’ intervals – and regular alternations of chert -> iron oxide -> mudrock (-> iron oxide) at the precession scale (Lantink et al., 2023). Different lithological extremes (opposites) thus seem to define the cyclicity at the precession level compared to (very) long eccentricity. However, we do not yet understand how these transitions in lithological expression were translated, via nonlinear amplitude response, across Milankovitch timescales, and may have implications for our cyclostratigraphic interpretation of the sedimentary patterns.

This problem closely ties to the uncertainty about the so-called ‘phase relation’ between the Milankovitch forcing and stratigraphic variations in lithology. In Lantink et al. (2023), the carbonate-mudrock layers of precession-scale Knox cyclothems in the Joffre Member were linked to periods of increased monsoonal intensity during southern-hemisphere precession maxima; in line with this interpretation, the ‘S’ intervals in the Kuruman IF and Dales Gorge Member would thus be likely candidates for representing (long) eccentricity maxima. Given the larger precession amplitude and hence larger amplitude of the climate oscillations during intervals of maximum eccentricity, we would expect to find a stronger lithological imprint of the Milankovitch signal, i.e., one that is more characteristic, in these more shaley/carbonaceous intervals. However, during our search for the most plausible correlation based on pattern resemblance (Section 6.1 and 6.2), we have mainly focused on the characteristic pattern exhibited by the ‘BIF’ intervals. This strategy has partly a historical reason, as a characteristic cycle pattern was initially identified on the basis of the prominence of the BIF intervals as visible in the weathering profile of the Kuruman IF (Lantink et al., 2019). At the same time, we note that intervals of pronounced expression of the (precession-scale) Calamina cyclothem of the Dales Gorge Member, have so far only been identified in the BIF macrobands (Table 6 and 8 in Trendall and Blockley, 1970). This observation seems at odds with the prediction of largest precession amplitude during the S intervals interpreted as (very) long eccentricity maxima, thus posing a challenge to our lithological phase relationship hypothesis.

On a more fundamental level, the fragmentary or weak expression of the precession cycle as well as of short eccentricity in the stratigraphy of the Dales Gorge Member and Kuruman IF, leaves room for doubt about our first-order Milankovitch hypothesis of precession- and eccentricity-controlled (summer) insolation changes affecting monsoonal intensity. In particular, we have so far largely ignored the potential contribution of the obliquity cycle, and hence the possible manifestation of its longer-period amplitude modulators in the stratigraphy as well (Table 1). As mentioned in Section 5.1, our main reason for invoking a precession-eccentricity dominance on the deposition of the Kuruman IF and Dales Gorge Member, is the combined cyclostratigraphic and U–Pb evidence for a strong 405 kyr eccentricity imprint, which is the amplitude modulator of precession and not obliquity. However, this does not mean that obliquity may not also have exerted a significant control, knowing that additional obliquity signals are typically observed in Phanerozoic sediment sequences deposited around mid- and low latitudes during icehouse or coldhouse periods (e.g. de Vleeschouwer et al., 2017; Lourens et al., 1996; van der Laan et al., 2012). Moreover, model studies have shown that obliquity can also directly affect low-latitude climate systems such as the monsoon (Bosmans et al., 2015; Tuenter et al., 2003). A high-latitude climate, obliquity forcing scenario may be more in line with the hypothesis of Krapež et al. (2003) and Pickard et al. (2004), who ascribed the density current structures in the S intervals of the Dales Gorge Member to periods of eustatic sea level fall. However, attributing the S intervals to colder 'glacial' periods seems again more difficult to reconcile with their inferred phase relation to (very long-period) eccentricity maxima, and thus maxima in precession-driven summer insolation.

All uncertainties added together regarding the Milankovitch forcing – from the primary insolation changes to the (nonlinear) climatic and sedimentary feedbacks – thus leave us with a considerable degree of ambiguity about the astronomical origin (or otherwise) of individual large-scale (> metre-thick) cycles, their expression within the stratigraphy of the Kuruman IF and Dales Gorge Member, and consequently how to correlate their combined patterns of characteristic 'BIF-S' alternations and bundling. In particular, in several parts of the stratigraphy, ambiguity about the precise expression of the ~5 m cycle proved to be an important additional handicap for establishing a cyclostratigraphic framework, which should start from this key cycle that is thought to be related to the stable 405-kyr eccentricity cycle ($g_2 – g_5$) (Figs. 12-14). Specifically in the thicker S and BIF macroband intervals of the Dales Gorge Member, the exact number of ~5 m-scale alternations remains uncertain due to a locally weak expression compared to the more enigmatic, longer-period (or shorter-period) stratigraphic cycles, or other non-Milankovitch-related trends and distortions.

However, it is important to realise that the problems encountered with the correlation of the characteristic cycle patterns in the Kuruman IF and Dales Gorge Member did not only arise from the complexities of the geological response to and stratigraphic recording of the astronomical forcing; the correlations were further complicated by fundamental uncertainties in the dynamical properties of the (long-period) Milankovitch parameters themselves, due to chaotic diffusion within the solar system, and hence uncertainty in how the expected orbital interference patterns may have looked like during the early Paleoproterozoic. In particular, the uncertainty in the (stability of the) period of the ~16 m-scale, interpreted $g_4 – g_3$ eccentricity cycle, combined with the ambiguity in the number of ~5 m-scale, interpreted 405 kyr eccentricity cycles, gave room for different cyclostratigraphic interpretations and corresponding correlation options of the characteristic bundle patterns. For example, bundle DB13 to 15 is interpreted as a single ~16 m-scale cycle when correlated to 5bcd in the Kuruman according to option IIa (Fig. 13), which implies a shift in the period of $g_4 – g_3$ from ~1.3 Myr to ~1.6 Myr and back around this interval (1:4 ratio with the ~5 m cycle; Fig. 13). In contrast, DB13–15 is interpreted as a double ~16 m-scale cycle according to option IIb (Fig. 14), which implies a relatively stable $g_4 – g_3$ period of ~1.2–1.3 Myr for this interval and in the rest of the stratigraphy (1:3 ratio with the ~5 m cycle; Fig. 14).

7.2 Potential solutions

Our expectations for establishing a 405 kyr-cycle based framework and associated high-resolution astrochronology for the lower Paleoproterozoic in the Hamersley and Griqualand West Basins have been somewhat tempered, given the serious difficulties encountered during this study (Section 6). However, this does not necessarily mean that this goal cannot be reached, and significant progress may be made in the foreseeable future regarding our understanding of the various sources of uncertainty discussed above (Section 7.1.1).

First of all, a logical continuation of our study on regular large-scale alternations in the stratigraphy of the Kuruman IF and Dales Gorge Member, seems to shift the focus of research to the (search for possible) intermediate- to small-scale rhythms. In particular, a systematic or more targeted analysis of potential short eccentricity-, precession- and/or obliquity-related variability is expected to further our understanding of the primary Milankovitch-induced climatic and depositional processes, and their lithostratigraphic translation to the longer-period orbital-scale cyclicity. For example, the expression of obliquity might just have evaded our attention so far because its period becomes progressively closer to (and thus more difficult to distinguish from) that of precession when looking further back into the history of the Earth-Moon system (Berger and Loutre, 1994; Waltham, 2015; Farhat et al., 2022). In addition, we imagine that differences in lithological expression of the smaller-scale cycles between the different long-period orbital-scale extremes (i.e., in the 'BIF' vs 'S' intervals) and at their transitions, may provide further clues about the lithological phase relationships and differences in (nonlinear) sedimentary proxy expression. However, this approach critically hinges on the existence of such intervals in the stratigraphy of the Kuruman IF or Dales Gorge Member wherein the full hierarchy of Milankovitch cycles is sufficiently continuous and well recorded. A potentially easier starting point or more promising candidate might therefore be the Joffre Member of the Brockman IF, in which the imprint of precession and both its short and long eccentricity amplitude modulators appear to be well developed in certain intervals (Lantink et al., 2022; 2023), suggesting a more direct or less nonlinear response compared to the Dales Gorge Member and Kuruman IF.

In conjunction with more detailed cyclostratigraphic studies, the development of new (more climate-sensitive?) proxy records could provide alternative perspectives on the origin and composition of the characteristic cycle patterns in the Kuruman IF and Dales Gorge Member and how the correlation should be addressed. For example, previous chemostratigraphic studies have demonstrated the presence of primary and early diagenetic variations in the stable carbonate-carbon and iron isotope composition of these rocks (Heimann et al., 2010; Li et al., 2015; Tsikos et al., 2023), raising the question whether these proxies also track cyclicity at the Milankovitch-scale and can provide constraints on the various and/or varying processes underlying the observed changes in relative carbonate and (ferric) iron content at the long eccentricity-scale. In parallel with these efforts, the use of simple chemical (mass balance) or physical (toy) model simulations may help to further specify and test hypotheses for the observed cycle patterns in a more quantitative way. Such models may be particularly useful for exploring the effects of nonlinear behaviour arising from feedbacks within the climate system and/or stratigraphic distortion, as was done in the pioneering work on late Pleistocene glacial-interglacial cycles (e.g. models of Imbrie and Imbrie, 1980; Le Treut and Ghil, 1983; Short et al., 1991) and on Cretaceous carbonate cycles (e.g. models of Herbert, 1994; Ripepe and Fischer, 1991).

Regarding the fundamental uncertainties in orbital dynamics during the Precambrian, we suggest that the cyclostratigraphic interpretations and correlation of the patterns may benefit from comparison with a selection of orbital models showing different scenarios for (manifestations of) chaotic behaviour as formulated in Section 5 and Table 1. In other words, by serving as example 'target' curves, these solutions may inform us about how the characteristic interference patterns *might* have looked like when certain Milankovitch cycles had very different frequencies and/or amplitudes compared to the more recent past. Alternatively, a more systematic (statistical) assessment of specific occurrences of chaotic behaviour, based on large ensembles of astronomical solutions, may be more appropriate (e.g. Hoang et al., 2021). Specific questions that emerge from this study are: how likely is it that the period of $g_4 – g_3$ had a stable period of ~1.2-1.3 Myr for the entire interval of correlation i.e., for more than 10 Myrs? How much drift in the frequencies and/or amplitudes of $g_1 – g_5$ and $g_2 – g_1$ is possible and may affect the identification of $g_4 – g_3$? Which resonance state or ratio with $s_3 – s_4$ does a ~1.2-1.3 Myr period of the $g_4 – g_3$ cycle correspond to, and what would the corresponding interference patterns look like in case of a mixed precession and obliquity influence?

A final proposed though rather challenging strategy, is to generate more, and more precise, U–Pb TIMS ages. We note that some of the existing U–Pb ages have very small uncertainties, in particular, the 2σ uncertainty of the Klein Naute Shale, which is only ± 0.34 Myrs, while others have much larger uncertainties (> 1.5 Myrs). If possible, reducing the uncertainty in the U–Pb ages from the analysis of additional zircons would help to more precisely constrain specific correlation options, or a small subset of correlations. Thus far, the small size of the grains and large amount of chemical abrasion needed to remove the radiation-damaged parts unfortunately resulted in only tiny zircon fragments with low Pb concentrations for analysis. Importantly this strategy could also provide more insight into the origin of the sampled zircons, which is currently unknown. The potential hypotheses are: they originate from discrete tuff horizons that are for some reason only preserved within the shale rich horizons, or they represent sedimentary re-working of recently deposited ashes into the BIF source region (Krapež et al., 2003; Pickard, 2003; Trendall et al., 2004; Zi et al., 2021). In the latter case, the ages should be treated as maximum depositional ages that are presumed to be close to the sediment depositional age. If the grains were dominantly detrital, we would expect re-working of zircon from the older tuffs into the younger sediments and also older detrital grains. Our analysis of zircon from the lower part of DS9 and also DS1 contain some Archean zircon suggesting that there is a detrital component in these samples (Dataset S2).

7.3 Implications of the early Paleoproterozoic astrochronological framework

Despite the ongoing uncertainties in the correlations, we tentatively argue that our combined cyclostratigraphic and U–Pb dating efforts point much more strongly into the direction of correlation options IIa or IIb, than towards correlation I. Both sub-options of correlation II, or other (still unexplored) minor deviations of a single 405 kyr cycle, would all be consistent with a ‘near’-synchronous onset of the Kuruman IF and Dales Gorge Member, hence confirming the long-standing presumption (e.g. Beukes and Gutzmer, 2008; Button, 1976; Cheney, 1996; Martin et al., 1998; Nelson et al., 1999; Pickard, 2003; Trendall, 1968; Trendall et al., 2004).

At a more precise level, correlations IIa/b suggest a slightly earlier onset of BIF deposition in the Griqualand West Basin by at least one 405 kyr cycle compared to the Hamersley Basin, given the fact that BIF 1a of the Kuruman IF is correlated to CB5 of the top of the Colonial Chert Member of the Hamersley Group (Figs. 10-11); note that cycle 1a.0 of the Kuruman IF forms part of the Kliphuis Member chert (Fig. S2). While this one ~5 m cycle offset may not be correct, lithological observations from the southern Prieska area in the Griqualand West Basin reveal that the onset of BIF formation locally started at cycle 1b, and cycle 1a is still composed of ferruginous carbonate (see Fig. S4 in Lantink et al. (2019). This indicates that BIF deposition in the Prieska area also started one 405-kyr cycle later than in the central Ghaap plateau area, but at the same time as the Dales Gorge Member. In addition, prolonged BIF deposition at Prieska, where the Kuruman IF is much thicker, has been demonstrated by the cyclostratigraphic correlations of Lantink et al. (2019) (Fig. 2). Likewise, BIF deposition continued for much longer in the Hamersley Basin compared to in the central Ghaap plateau area of the Griqualand

West Basin, as represented by the ~350 m thick Joffre Member, the base of which loosely corresponds to 7a according to correlations IIa/b (Figs. 10-11). Thus correlations IIa/b seem to support the hypothesis that the Kuruman IF facies in the southern part of the Griqualand West Basin were deposited more proximal to the Dales Gorge Member (Cheney, 1996) and/or in a similarly deeper-marine (basinal) setting (Beukes and Gutzmer, 2008).

Intriguingly, correlations IIa/b and the constraints from the U–Pb dating are further consistent with suggestions of a genetic link between the impact spherule bed in the DS4 macroband of the Dales Gorge Member (Glikson and Allen, 2004; Hassler and Simonson, 2001) and a 1-cm-thick spherule layer identified at about 50 m above the base of the Kuruman IF (Glass and Simonson, 2012; Simonson et al., 2009). A stratigraphic distance of ~50 m above the base of the Kuruman IF roughly corresponds to cycles 2d–e, which is indeed correlated to DS4 or DB4 according to options IIa/b, supporting the hypothesis that the DS4 and Kuruman spherule layers are distal ejecta deposits of the same meteorite impact event. This event would have caused significant disruption of sedimentation proximal to the impact site, implying that deposition of especially the Dales Gorge Member may have been, or likely was, also affected to some extent (Hassler et al., 2019). However, given the lateral continuity of the metre-scale cycle patterns in the Dales Gorge Member and the continuation of a 1:3-3.5 bundle hierarchy at the interval of concern, we consider it unlikely that the impact obliterated an entire 405 kyr-related cycle, or multiple cycles, and thus forming an issue for the correlations. We further note that a second spherule-bearing interval in the Dales Gorge Member has been recently found in DS9 (Martin and Howard, 2023), which, as an alternative equivalent to the Kuruman spherule layer, would be consistent with correlation option I rather than option IIa/b. However, the interpretation of the spherules in DS9 as impact event still needs to be confirmed by geochemical evidence.

Finally, our preliminary astrochronology for the Kuruman IF and Dales Gorge Member may cast new perspectives on the timing and timescales of incipient oxygenation ‘transients’ recorded in the underlying strata of the Griqualand West and Hamersley Basins. Specifically, geochemical evidence was found for an atmospheric ‘whiff of oxygen’ in the S1 unit of the Mount McRae Shale in Western Australia (Anbar et al., 2007) some ~30 m below the Colonial Chert Member. Based on a multi-sample Re/Os age of 2501 ± 8 Ma, this event is simultaneously thought to coincide with the Archean-Proterozoic chronometric boundary, currently established at 2.5 Ga. According to correlations IIa/b, the base of the Colonial Chert Member is equivalent to the well-dated Klein Naute Shale as developed in the central Griqualand West Basin, i.e. having an age of 2484.6 ± 0.34 Ma (Figs. 13 and 14). A downward extrapolation from this level using the sedimentation rates established for the Kuruman and Brockman

IF – an assumption that is not unreasonable given the continuation of a ~16 m cycle in the Gamohaan Formation (Figs. 5, 13 and 14) – would thus suggest that the whiff of oxygen of Anbar et al. (2007) is in fact significantly younger (i.e., ca 2886 to 2489 Ma). This conclusion is of course premature, and further cyclostratigraphic testing combined with high-precision U–Pb dating is needed to also explore possible synchroneity with a putative oceanic 'oxygen oasis' identified in the Naute Shale (Kendall et al., 2010) – the South African counterpart of the Mount McRae Shale in the basinal facies of the Griqualand West Basin (Beukes and Gutzmer, 2008). Such future downward extension of the astrochronologic framework can thus help us to distinguish between more locally manifested redox phenomena, or larger-scale oxygenation transients in the lead-up to the GOE, including the potential role of multi-million year Milankovitch forcing (Boulila, 2012; Lantink et al. 2023); the latter scenario might also render these intervals as suitable candidates for a chronostratigraphic redefinition of the Archean-Proterozoic boundary (Martin and Howard, 2023).

8. Conclusions

The primary aim of this study has been to establish a 405 kyr cycle-based framework for the early Paleoproterozoic Kuruman IF of South Africa and Dales Gorge Member of the Brockman IF in Western Australia. Achieving this goal seemed realistic at first given the evidence from cyclostratigraphic analysis and TIMS U–Pb dating for a 405-kyr eccentricity origin for the prominent ~5 cycle, and a strong ~1.3 Myr cycle possibly related to $g_4 - g_3$, identified in both stratigraphic units. However, we subsequently encountered significant problems when trying to determine a correlation based on matching their characteristic cycle patterns, and the final correlation remains unsolved to date. In part, the difficulty in correlating appears to stem from a difference in expression and amplitude of certain cycles (i.e., a ~7 m/590 kyr, ~9 m/700 kyr and ~23 m/1.8 Myr cycle) whose origins remain enigmatic, but which may be related to a difference in depositional environment. But more generally, these issues illustrate our current lack of understanding of the (nonlinear and likely complex) response of the early Proterozoic climate and BIF system to the astronomical forcing, as well as the fundamental uncertainty about the astronomical forcing itself, i.e. solar system dynamical behaviour at that time.

Nevertheless, our correlation efforts have provided a much more precise estimate of the absolute and relative timing of Kuruman IF and Dales Gorge Member BIF deposition than was previously available. This illustrates the potential strength of the integrated (cyclo)stratigraphic approach in enabling more precise reconstructions of the sedimentary and paleogeographic histories of the

Griqualand West and Hamersley Basins. Possible strategies to further constrain the correlations and gain more insight into the origin of the cycle patterns include a systematic analysis of sub-405 kyr-scale variability (i.e. precession-, short eccentricity-, and possible obliquity-related patterns), further improving of the U–Pb geochronology, searching for other (more) climate-sensitive proxies, comparison with astronomical example solutions and the use of climatic and geochemical model simulations.

Acknowledgements

This research was funded by the Dutch National Science Foundation grant NWO ALWOP.190 (FJH, PRDM, MLL); Swiss National Science Foundation grant 200021_169086 (JHFLD); Dr. Schurmannfonds grants 2017-126, 2018-136 and 2019-145 (FJH, PRDM, MLL) and the Heising-Simons Foundation grant 133-AAJ2896 (MLL). We thank Keith Saunders and Allan Bennet from Wireline Alliance for the downhole geophysical logging; Michael Wawrick and Lena Hancock from the GSWA for the Hylogger data extraction from cores 47A and SGP001; Gregory Jack for arranging of the drone flying and fieldwork logistics together with the GSWA; Marcel van Maarssenveen, Jakob Steiner and Timothy Baars for their advice on the GPS measurements and photogrammetric modelling; and Nam Hoang, Federico Mogavero and Jacques Laskar for their expertise and discussions on chaotic solar system evolution. Our special thanks go to the late Rineke Gieles for her dedicated help with the XRF core scanning and who sadly passed away in 2020; and to Prof. Nic Beukes, for his guidance in the UUBH-1 drilling project and who sadly passed away in 2023.

References

Anbar, A. D., Duan, Y., Lyons, T. W., Arnold, G. L., Kendall, B., Garvin, J., & Buick, R. (2007). A Whiff of Oxygen Before the Great Oxidation Event? *Science*, *317*(5846), 1903–1906.

Batenburg, S. J., Sprovieri, M., Gale, A. S., Hilgen, F. J., Hüsing, S., Laskar, J., Liebrand, D., Lirer, F., Orue-Etxebarria, X., Pelosi, N., & Smit, J. (2012). Cyclostratigraphy and astronomical tuning of the Late Maastrichtian at Zumaia (Basque country, Northern Spain). *Earth and Planetary Science Letters*, *359–360*, 264–278.

Bekker, A., Holland, H. D., Wang, P. L., Rumble, D., Stein, H. J., Hannah, J. L., Coetzee, L. L., & Beukes, N. J. (2004). Dating the rise of atmospheric oxygen. *Nature*, *427*(6970), 117–120.

Bekker, Andrey, Slack, J. F., Planavsky, N., Krapež, B., Hofmann, A., Konhauser, K. O., & Rouxel, O. J. (2010). Iron formation: The sedimentary product of a complex interplay among mantle, tectonic, oceanic, and biospheric processes. *Economic Geology*, *105*(3), 467–508.

Berger, A., & Loutre, M. F. (1994). Astronomical forcing through geological time. In P. L. De Boer & D. G.

Smith (Eds.), *Orbital forcing and cyclic sequences* (pp. 15–24). Blackwell Scientific Publications Oxford.

Beukes, N.J., & Gutzmer, J. (2008). Origin and paleoenvironmental significance of major iron formations at the Archean-Paleoproterozoic boundary. *Society of Economic Geologists Reviews*, *15*(August 2016), 5–47.

Beukes, N. J. (1978). *Die Karbonaatgesteentes en Ysterformasies van die Ghaap-groep van die Transvaal-supergroep in Noord-Kaapland*. PhD Thesis.

Beukes, N. J. (1980). Lithofacies and stratigraphy of the Kuruman and Griquatown iron-formations, northern Cape Province, South Africa. *Transactions of the Geological Society of South Africa*, *83*, 69–86.

Beukes, N. J. (1983). Chapter 4. Palaeoenvironmental setting of iron-formations in the depositional basin of the Transvaal Supergroup, South Africa. In *Iron-Formation Facts and Problems* (Issue 6, pp. 131–198). Developments in Precambrian Geology.

Beukes, N. J. (1987). Facies relations, depositional environments and diagenesis in a major Early Proterozoic stromatolitic carbonate platform to basinal sequence, Campbellrand Subgroup, Transvaal Supergroup, Southern Africa. *Sedimentary Geology*, *54*(1–2), 179–546.

Bloemsma, M. R. (2015). *Development of a Modelling Framework for Core Data Integration Using XRF Scanning*. PhD Thesis.

Bosmans, J. H. C., Drijfhout, S. S., Tuenter, E., Hilgen, F. J., & Lourens, L. J. (2015). Response of the North African summer monsoon to precession and obliquity forcings in the EC - Earth GCM. *Climate Dynamics*, *44*, 279–297.

Boulila, S., Galbrun, B., Laskar, J., & Pälike, H. (2012). A ~9 myr cycle in Cenozoic δ 13C record and long-term orbital eccentricity modulation: Is there a link? *Earth and Planetary Science Letters*, *317–318*, 273–281.

Button, A. (1976). *Transvaal and Hamersley Basins: Review of basin development and mineral deposits*.

Charbonnier, G., Boulila, S., Spangenberg, J. E., Vermeulen, J., & Galbrun, B. (2023). Astrochronology of the Aptian stage and evidence for the chaotic orbital motion of Mercury. *Earth and Planetary Science Letters*, *610*, 118104.

Cheney, E. S. (1996). Sequence stratigraphy and plate tectonic significance of the Transvaal succession of southern Africa and its equivalent in Western Australia. *Precambrian Research*, *79*, 3–24.

Cowan, D., & Cooper, G. (2003). Wavelet analysis of detailed drillhole magnetic susceptibility data, Brockman Iron Formation, Hamersley Basin, Western Australia. *Exploration Geophysics*, *34*(2), 63-68.

Crowley, T. J., Kim, K., Mengel, J. G., Short, D. A., Crowley, T. J., Kim, K., & Mengel, J. G. (1992). Modeling 100,000-Year Climate Fluctuations in Pre-Pleistocene Time Series. *Science*, *255*(5045), 705–707.

Da Silva, A. C., Hladil, J., Chadimova, L., Slavik, L., Hilgen, F. J., Bábek, O., & Dekkers, M. J. (2016). Refining the Early Devonian time scale using Milankovitch cyclicity in Lochkovian–Pragian sediments (Prague Synform, Czech Republic). *Earth and Planetary Science Letters*, *55*, 125–139.

de Kock, M. O., Evans, D. A. D., & Beukes, N. J. (2009). Validating the existence of Vaalbara in the Neoarchean. *Precambrian Research*, *174*(1–2), 145–154.

de Oliveira Carvalho Rodrigues, P., Hinnov, L. A., & Franco, D. R. (2019). A new appraisal of depositional cyclicity in the Neoarchean- Paleoproterozoic Dales Gorge Member (Brockman Iron Formation, Australia). *Precambrian Research*, *328*, 27–47.

De Vleeschouwer, D., Da Silva, A. C., Sinnesael, M., Chen, D., Day, J. E., Whalen, M. T., Guo, Z., & Claeys, P. (2017). Timing and pacing of the Late Devonian mass extinction event regulated by eccentricity and obliquity. *Nature Communications*, *8*(1), 1–11.

Fang, Q., Wu, H., Hinnov, L. A., Jing, X., Wang, X., & Jiang, Q. (2015). Geologic evidence for chaotic behavior of the planets and its constraints on the third-order eustatic sequences at the end of the Late Paleozoic Ice Age. *Palaeogeography, Palaeoclimatology, Palaeoecology*, *440*, 848–859.

Farhat, M., Auclair-Desrotour, P., Boué, G., & Laskar, J. (2022). The resonant tidal evolution of the Earth-Moon distance. *Astronomy & Astrophysics*, *665*, L1.

Glass, B. P., & Simonson, B. M. (2012). Distal impact ejecta layers: Spherules and more. *Elements*, *8*(1), 43–48.

Glikson, A., & Allen, C. (2004). Iridium anomalies and fractionated siderophile element patterns in impact ejecta, Brockman Iron Formation, Hamersley Basin, Western Australia: Evidence for a major asteroid impact in simatic crustal regions of the early Proterozoic earth. *Earth and Planetary Science Letters*, *220*(3–4), 247–264.

Gradstein, F. M., Ogg, J. G., Schmitz, M. D., & Ogg, G. M. (2020). *The Geologic Time Scale 2020*.

Gumsley, A. P., Chamberlain, K. R., Bleeker, W., Söderlund, U., de Kock, M. O., Larsson, E. R., & Bekker, A. (2017). Timing and tempo of the Great Oxidation Event. *Proceedings of the National Academy of Sciences*, *114*(8), 1811–1816.

Hancock, E. A., & Huntington, J. F. (2010). The GSWA NVCL HyLogger: rapid mineralogical analysis for characterizing mineral and petroleum core. In *Geological Survey of Western Australia*.

Harmsworth, R. A., Kneeshaw, M., Morris, R. C., Robinson, C. J., & Shrivastava, P. K. (1990). BIF-Derived Iron Ores of the Hamersley Province. *Geology of the Mineral Deposits of Australia and New Guinea*, *642*, 617–642.

Haslett, J., & Parnell, A. C. (2008). A simple monotone process with application to radiocarbon-dated depth chronologies. *Journal of the Royal Statistical Society: Series C (Applied Statistics)*, *57*(4), 399–418.

Hassler, S. W., & Simonson, B. M. (2001). The sedimentary record of extraterrestrial impacts in deep-shelf environments: Evidence from the early Precambrian. *Journal of Geology*, *109*(1), 1–19.

Hassler, S., Biller, S., & Simonson, B. M. (2019). Petrography and sedimentology of the~ 2490 Ma DS 4 impact spherule layer revisited, Brockman Iron Formation (Hamersley Group, Western Australia). *Meteoritics & Planetary Science*, *54*(10), 2241-2253.

Hays, J. D., Imbrie, J., & Shackleton, N. J. (1976). Variations in the earth’s orbit: Pacemaker of the ice ages. *Science*, *194*(4270), 1121–1132.

Heimann, A., Johnson, C. M., Beard, B. L., Valley, J. W., Roden, E. E., Spicuzza, M. J., & Beukes, N. J. (2010). Fe, C, and O isotope compositions of banded iron formation carbonates demonstrate a major role for dissimilatory iron reduction in ~2.5Ga marine environments. *Earth and Planetary Science Letters*, *294*(1–2), 8–18.

Hennekam, R., Sweere, T., Tjallingii, R., de Lange, G. J., & Reichart, G. J. (2019). Trace metal analysis of sediment cores using a novel X-ray fluorescence core scanning method. *Quaternary International*, *514*, 55–67.

Herbert, T. D. (1994). Reading orbital signals distorted by sedimentation: models and examples. In P. L. De Boer & D. G. Smith (Eds.), *Orbital forcing and cyclic sequences* (pp. 483–507).

Hilgen, F. J. (1991). Extension of the astronomically calibrated (polarity) time scale to the Miocene/Pliocene boundary. *Earth and Planetary Science Letters*, *107*(2), 349–368.

Hilgen, F., Zeeden, C., & Laskar, J. (2020). Paleoclimate records reveal elusive ~200-kyr eccentricity cycle for the first time. *Global and Planetary Change*, *194*, 103296.

Hinnov, L. A. (2018). Cyclostratigraphy and astrochronology in 2018. In *Stratigraphy & Timescales* (Vol. 3, pp. 1–80).

Hinnov, L. A., & Hilgen, F. J. (2012). Cyclostratigraphy and astrochronology. In *The Geologic Time Scale 2012* (pp. 63–83).

Hoang, N. H., Mogavero, F., & Laskar, J. (2021). Chaotic diffusion of the fundamental frequencies in the Solar System. *Astronomy and Astrophysics*, *654*, A156.

Holland, H. D. (2002). Volcanic gases, black smokers, and the great oxidation event. *Geochimica et Cosmochimica Acta*, *66*(21), 3811–3826.

Huang C. (2018). Astronomical time scale for the Mesozoic. In *Stratigraphy & Timescales* (pp. 81–150).

Huang, Chunju, Tong, J., Hinnov, L., & Chen, Z. Q. (2011). Did the great dying of life take 700 k.y.? Evidence from global astronomical correlation of the Permian-Triassic boundary interval. *Geology*, *39*(8), 779–782.

Huybers, P. (2009). Pleistocene glacial variability as a chaotic response to obliquity forcing. *Climate of the Past*, *5*(3), 481-488.

Huybers, P., & Wunsch, C. (2005). Obliquity pacing of the late Pleistocene glacial terminations. *Nature*, *434*(7032), 491-494.

Ikeda, M., & Tada, R. (2014). A 70 million year astronomical time scale for the deep-sea bedded chert sequence (Inuyama, Japan): Implications for Triassic-Jurassic geochronology. *Earth and Planetary Science Letters*, *399*, 30–43.

Imbrie, J., & Imbrie, J. Z. (1980). Modeling the climatic response to orbital variations. *Science*, *207*(4434), 943-953.

Imbrie, J., Berger, A., Boyle, E. A., Clemens, S. C., Duffy, A., Howard, W. R., Kukla, G., Kutzbach, J., Martinson, D. G., Mcintyre, A., Mix, A. C., Morley, J. J., Peterson, L. C., Pisias, N. G., Prell, W. L., Raymo, M. E., Shackleton, N. J., & Lemaitre, G. (1993). On the structure and origin of major glaciation cycles 2. The 100,000-year cycle. *Paleoceanography and Paleoclimatology*, *8*(6), 699–735.

Imbrie, J., Hays, J. D., Martinson, D. G., Mclntyre, A., Mix, A. C., Morley, J. J., Pisias, N. G., Prell and, W. L., & Shackleton, N. J. (1984). The orbital theory of pleistocene climate: support from a revised chronology of the marine O180 record. In *Milankovitch and Climate* (pp. 269–305).

Kendall, B., Reinhard, C. T., Lyons, T. W., Kaufman, A. J., Poulton, S. W., & Anbar, A. D. (2010). Pervasive oxygenation along late Archaean ocean margins. *Nature Geoscience*, *3*(9), 647–652.

Knoll, A. H., & Beukes, N. J. (2009). Introduction: Initial investigations of a Neoarchean shelf margin-basin transition (Transvaal Supergroup, South Africa). *Precambrian Research*, *169*(1–4), 1–14.

Konhauser, K. O., Planavsky, N. J., Hardisty, D. S., Robbins, L. J., Warchola, T. J., Haugaard, R., Lalonde, S. V., Partin, C. A., Oonk, P. B. H., Tsikos, H., Lyons, T. W., Bekker, A., & Johnson, C. M. (2017). Iron formations: A global record of Neoarchaean to Palaeoproterozoic environmental history. *Earth-Science Reviews*, *172*, 140–177.

Krapež, B., Barley, M. E., & Pickard, A. L. (2003). Hydrothermal and resedimented origins of the precursor sediments to banded iron formation: Sedimentological evidence from the Early Palaeoproterozoic Brockman Supersequence of Western Australia. *Sedimentology*, *50*(5), 979–1011.

Lantink, M. L., Davies, J. H. F. L., Mason, P. R. D., Schaltegger, U., & Hilgen, F. J. (2019). Climate control on banded iron formations linked to orbital eccentricity. *Nature Geoscience*, *12*(5), 369–374.

Lantink, M. L., Davies, J. H., Ovtcharova, M., & Hilgen, F. J. (2022). Milankovitch cycles in banded iron formations constrain the Earth–Moon system 2.46 billion years ago. *Proceedings of the National Academy of Sciences*, *119*(40), e2117146119.

Lantink, M. L., Lenstra, W. K., Davies, J. H., Hennekam, R., Martin, D. M., Mason, P. R., ... & Hilgen, F. J. (2023). Precessional pacing of early Proterozoic redox cycles. *Earth and Planetary Science Letters*, *610*, 118117.

Laskar, J. (1990). The chaotic motion of the solar system: A numerical estimate of the size of the chaotic zones. *Icarus*, *88*(2), 266–291.

Laskar, J. (2020). Astrochronology. In *Geologic Time Scale 2020*.

Laskar, J., Fienga, A., Gastineau, M., & Manche, H. (2011). La2010: A new orbital solution for the long term motion of the Earth. *Astronomy and Astrophysics*, *532*, A89.

Laskar, J., Robutel, P., Joutel, F., Gastineau, M., Correia, a. C. M., & Levrard, B. (2004). A long-term numerical solution for the insolation quantities of the Earth. *Astronomy and Astrophysics*, *428*(1), 261–285.

Laskar, Jacques. (1993). Orbital, precessional, and insolation quantities for the Earth from-20 Myr to+ 10 Myr. *Astronomy and Astrophysics*, *270*, 522–533.

Le Treut, H., & Ghil, M. (1983). Orbital forcing, climate interactions, and glaciation cycles. *Journal of Geophysical Research: Oceans*, *88*(C9), 5167–5190.

Li, W., Beard, B. L., & Johnson, C. M. (2015). Biologically recycled continental iron is a major component in banded iron formations. *Proceedings of the National Academy of Sciences*, *112*(27), 8193-8198.

Li, M., Hinnov, L., & Kump, L. (2019). Acycle: Time-series analysis software for paleoclimate research and education. *Computers and Geosciences*, *127*(September 2018), 12–22.

Lomb, N. R. (1976). Least-squares frequency analysis of unequally spaced data. *Astrophysics and Space Science*, *39*(2), 447–462.

Lourens, L. J., Antonarakou, A., Hilgen, F. J., Hoof, A. A. M. Van, & Zachariasse, W. J. (1996). Evaluation of the Plio-Pleistocene astronomical timescale. *Paleoceanography*, *11*(4), 391–413.

Ma, C., Meyers, S. R., & Sageman, B. B. (2017). Theory of chaotic orbital variations confirmed by Cretaceous geological evidence. *Nature*, *542*(7642), 468–470.

Marino, M., Maiorano, P., Lirer, F., & Pelosi, N. (2009). Response of calcareous nannofossil assemblages to paleoenvironmental changes through the mid-Pleistocene revolution at Site 1090 (Southern Ocean). *Palaeogeography, Palaeoclimatology, Palaeoecology*, *280*(3–4), 333–349.

Martin, D. M., Clendenin, C. W., Krapež, B., & McNaughton, N. J. (1998). Tectonic and geochronological constraints on late Archaean and Palaeoproterozoic stratigraphic correlation within and between the Kaapvaal and Pilbara Cratons. *Journal of the Geological Society*, *155*(2), 311-322.

Martin, D McB and Howard, HM 2023, 6IAS: Out with the old, in with the new — a traverse across the Archean–Proterozoic boundary in the Mount Bruce Supergroup: Geological Survey of Western Australia, Record 2023/2, 58p.

Martinez, M., & Dera, G. (2015). Orbital pacing of carbon fluxes by a ~9-My eccentricity cycle during the Mesozoic. *Proceedings of the National Academy of Sciences*, *112*(41), 12604–12609.

Meyers, S. R. (2012). Seeing red in cyclic stratigraphy: Spectral noise estimation for astrochronology.

Paleoceanography, *27*(3), 1–12.

Meyers, S. R. (2014). *An R package for astrochronology. Available at cran.rproject.org/web/packages/astrochron/index.html*.

Nelson, D. R., Trendall, A. F., & Altermann, W. (1999). Chronological correlations between the Pilbara and Kaapvaal cratons. *Precambrian Research*, *97*(3–4), 165–189.

Olsen, P. E., & Kent, D. V. (1999). Long-period Milankovitch cycles from the Late Triassic and Early Jurassic of eastern North America and their implications for the calibration of the Early Mesozoic time-scale and the long-term behaviour of the planets. *Philosophical Transactions of the Royal Society A: Mathematical, Physical and Engineering Sciences*, *357*(1757), 1761–1786.

Olsen, Paul E., Laskar, J., Kent, D. V., Kinney, S. T., Reynolds, D. J., Sha, J., & Whiteside, J. H. (2019). Mapping solar system chaos with the geological orrery. *Proceedings of the National Academy of Sciences of the United States of America*, *166*(22), 10664–10673.

Oonk, P. B., Tsikos, H., Mason, P. R., Henkel, S., Staubwasser, M., Fryer, L., ... & Williams, H. M. (2017). Fraction-specific controls on the trace element distribution in iron formations: Implications for trace metal stable isotope proxies. *Chemical Geology*, *474*, 17-32.

Pickard, A. L. (2003). SHRIMP U–Pb zircon ages for the Palaeoproterozoic Kuruman Iron Formation, Northern Cape Province, South Africa: Evidence for simultaneous BIF deposition on Kaapvaal and Pilbara Cratons. *Precambrian Research*, *125*(3–4), 275–315.

Pickard, April L., Barley, M. E., & Krapež, B. (2004). Deep-marine depositional setting of banded iron formation: Sedimentological evidence from interbedded clastic sedimentary rocks in the early Palaeoproterozoic Dales Gorge Member of Western Australia. *Sedimentary Geology*, *170*(1–2), 37–92.

Postma, G., Hilgen, F. J., & Zachariasse, W. J. (1993). Precession-punctuated growth of a late Miocene submarine-fan lobe on Gavdos (Greece). *Terra Nova*, *5*(5), 438–444.

Rasmussen, B., Krapež, B., & Muhling, J. R. (2015). Seafloor silicification and hardground development during deposition of 2.5 Ga banded iron formations. *Geology*, *43*(3), 235–238.

Raymo, M. E., & Nisancioglu, K. (2003). The 41 kyr world: Milankovitch's other unsolved mystery. *Paleoceanography*, *18*(1), 1–6.

Ripepe, M., & Fischer, A. G. (1991). Stratigraphic rhythms synthesized from orbital variations. *Kansas Geological Survey Bulletin*, *233*, 335–344.

Ruddiman, W. F., Raymo, M. E., Martinson, D. G., & Backman, J. (1989). Pleistocene evolution: northern hemisphere ice sheets and North Atlantic Ocean. *Paleoceanography*, *4*(4), 353–412.

Scargle, J. D. (1982). Studies in astronomical time series analysis. II-Statistical aspects of spectral analysis of unevenly spaced data. *The Astrophysical Journal*, *263*, 835–853.

Sexton, P. F., Norris, R. D., Wilson, P. A., Pälike, H., Westerhold, T., Röhl, U., Bolton, C. T., & Gibbs, S.

(2011). Eocene global warming events driven by ventilation of oceanic dissolved organic carbon. *Nature*, *471*(7338), 349–353.

Short, D. A., Mengel, J. G., Crowley, T. J., Hyde, W. T., & North, G. R. (1991). Filtering of Milankovitch cycles by Earth’s geography. *Quaternary Research*, *35*(2), 157–173.

Simonson, B. M., Sumner, D. Y., Beukes, N. J., Johnson, S., & Gutzmer, J. (2009). Correlating multiple Neoarchean-Paleoproterozoic impact spherule layers between South Africa and Western Australia. *Precambrian Research*, *169*(1–4), 100–111.

Sinnesael, M., McLaughlin, P. I., Desrochers, A., Mauviel, A., Weirdt, J. De, Claeys, P., & Vandenbroucke, T. R. A. (2021). Precession-driven climate cycles and time scale prior to the Hirnantian glacial maximum. *Geology*, *49*(11), 1295–1300.

Sprovieri, M., Sabatino, N., Pelosi, N., Batenburg, S. J., Coccioni, R., Iavarone, M., & Mazzola, S. (2013). Late cretaceous orbitally-paced carbon isotope stratigraphy from the bottaccione gorge (Italy). *Palaeogeography, Palaeoclimatology, Palaeoecology*, *379–380*, 81–94.

Thomson, D. J. (1982). Spectrum Estimation and Harmonic Analysis. *Proceedings of the IEEE*, *70*(9), 1055–1096.

Trendall, A. F. (1968). Three Great Basins of Precambrian Banded Iron Formation Deposition: A Systematic Comparison. *Geological Society of America Bulletin*, *79*(11), 1527–1544.

Trendall, A. F., & Blockley, J. B. (1970). *The iron formations of the Precambrian Hamersley Group, Western Australia with special reference to the associated crocidolite* (Vol. 119). Geological Survey of Western Australia.

Trendall, A. F., & Blockley, J. G. (1968). Stratigraphy of the Dales Gorge Member of the Brockman Iron Formation in the Precambrian Hamersley Group of Western Australia. In *Geological Survey of Western Australia Annual Report for 1967* (pp. 48–53).

Trendall, A. F., Compston, W., Nelson, D. R., De Laeter, J. R., & Bennett, V. C. (2004). SHRIMP zircon ages constraining the depositional chronology of the Hamersley Group, Western Australia. *Australian Journal of Earth Sciences*, *51*(5), 621–644.

Tsikos, H., Siahi, M., Rafuza, S., Mhlanga, X. R., Oonk, P. B. H., Papadopoulos, V., ... & Lyons, T. W. (2022). Carbon isotope stratigraphy of Precambrian iron formations and possible significance for the early biological pump. *Gondwana Research*, *109*, 416-428.

Tuenter, E., Weber, S. L., Hilgen, F. J., & Lourens, L. J. (2003). The response of the African summer monsoon to remote and local forcing due to precession and obliquity. *Global and Planetary Change*, *36*(4), 219–235.

van der Laan, E., Hilgen, F. J., Lourens, L. J., de Kaenel, E., Gaboardi, S., & Iaccarino, S. (2012). Astronomical forcing of Northwest African climate and glacial history during the late Messinian (6.5-5.5 ma). *Palaeogeography, Palaeoclimatology, Palaeoecology*, *313–314*, 107–126.

von Dobeneck, T., & Schmieder, F. (1999). Using Rock Magnetic Proxy Records for Orbital Tuning and Extended Time Series Analyses into the Super- and Sub-Milankovitch Bands. In *Use of Proxies in Paleoceanography: Examples from the South Atlantic* (pp. 601–633).

Waltham, D. (2015). Milankovitch Period Uncertainties and Their Impact On Cyclostratigraphy. *Journal of Sedimentary Research*, *85*(8), 990–998.

Weedon, G. P. (2003). Practical considerations. In *Time-series analysis and cyclostratigraphy: examining stratigraphic records of environmental cycles* (pp. 129 - 160).

Weltje, G., & De Boer, P. L. (1993). Astronomically induced paleoclimatic oscillations reflected in Pliocene turbidite deposits on Corfu (Greece): Implications for the interpretation of higher order cyclicity in ancient turbidite systems. *Geology*, *21*(4), 307–310.

Weltje, G. J., Bloemsma, M. R., Tjallingii, R., Heslop, D., Röhl, U., & Croudace, I. W. (2015). Prediction of geochemical composition from XRF core scanner data: a new multivariate approach including automatic selection of calibration samples and quantification of uncertainties. In *Micro-XRF studies of sediment cores* (pp. 507–534).

Westerhold, A. T., Marwan, N., Drury, A. J., Liebrand, D., Agnini, C., Anagnostou, E., Barnet, J. S. K., Bohaty, S. M., De, D., Florindo, F., Frederichs, T., Hodell, D. A., Holbourn, A. E., Kroon, D., Lauretano, V., Littler, K., Lourens, L. J., & Lyle, M. (2020). An astronomically dated record of Earth ' s climate and its predictability over the last 66 Million Years. *Science*, *369*(6509), 1383–1387.

Westphal, H., Böhm, F., & Bornholdt, S. (2004). Orbital frequencies in the carbonate sedimentary record: Distorted by diagenesis? *Facies*, *50*(1), 3–11.

Wingate, MTD, Fielding, IOH, Lu, Y and Martin, DMcB 2021a, 225758: tuffaceous volcanic rock, Wittenoom Gorge; Geochronology Record 1812: Geological Survey of Western Australia, 4p.

Wingate, MTD, Fielding, IOH, Lu, Y and Martin, DMcB 2021b, 225756: volcaniclastic rock, Wittenoom Gorge; Geochronology Record 1810: Geological Survey of Western Australia, 6p.

Wu, H., Zhang, S., Hinnov, L. A., Jiang, G., Feng, Q., Li, H., & Yang, T. (2013). Time-calibrated Milankovitch cycles for the late Permian. *Nature Communications*, *4*, 2452.

Zachos, J. C., McCarren, H., Murphy, B., Röhl, U., & Westerhold, T. (2010). Tempo and scale of late Paleocene and early Eocene carbon isotope cycles: Implications for the origin of hyperthermals. *Earth and Planetary Science Letters*, *299*(1–2), 242–249.

Zeebe, R. E. (2017). Numerical Solutions for The Orbital Motion of The Solar System Over The Past 100 Myr: Limits and New Results. *ArXiv*, *154*(5), 193.

Zeebe, R. E., & Lourens, L. J. (2019). Solar System chaos and the Paleocene–Eocene boundary age constrained by geology and astronomy. *Science*, *365*(6456), 926–929.

Zhou, M., Wu, H., Hinnov, L. A., Fang, Q., Zhang, S., Yang, T., & Shi, M. (2022). Empirical Reconstruction of Earth-Moon and Solar System Dynamical Parameters for the Past 2.5 Billion Years From Cyclostratigraphy. *Geophysical Research Letters*, *49*(16), e2022GL098304.

Zi, J.-W., Sheppard, S., Muhling, J. R., & Rasmussen, B. (2021). Refining the Paleoproterozoic tectonothermal history of the Penokean Orogen: New U–Pb age constraints from the Pembine-Wausau terrane, Wisconsin, USA. *GSA Bulletin*, *July*, 1–15.

Figures

Figure 1. Geological map of the Griqualand West basin (South Africa) and Hamersley basin (NW Australia) and the locations of the studied sections and drill-cores of the Kuruman and Brockman Iron Formations, respectively.

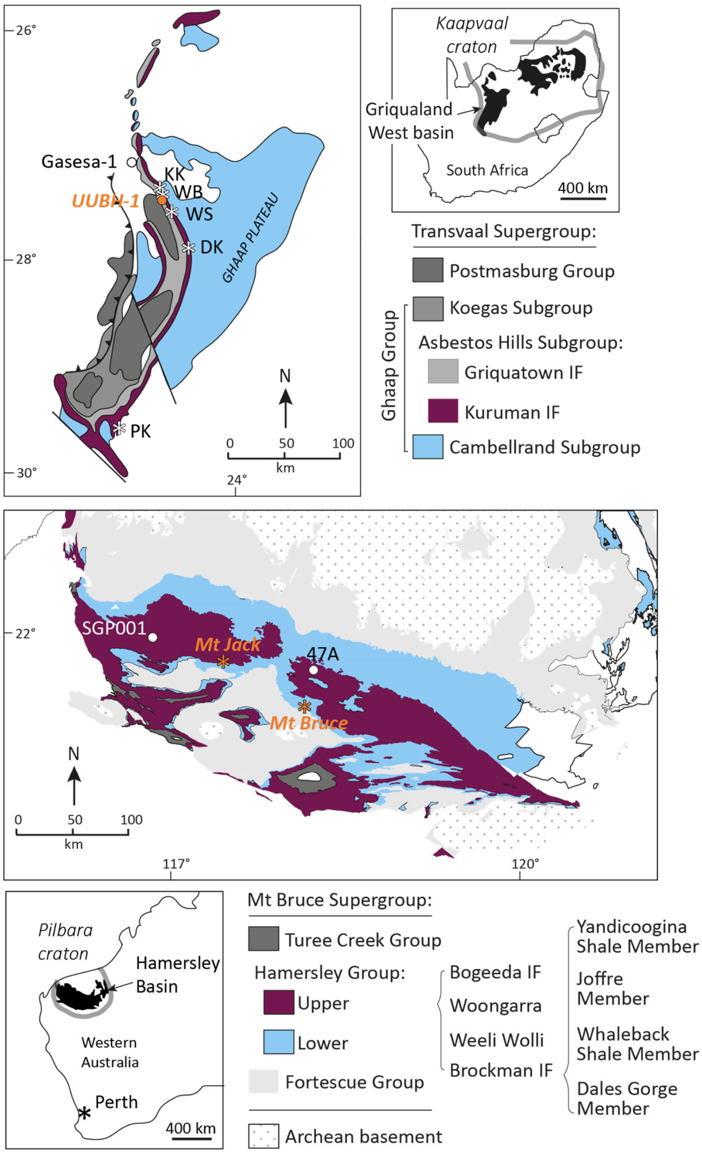

Figure 2. Schematic cross-section of the Ghaap Group on the Kaapvaal craton (left) and Hamersley Group on the Pilbara craton (right), showing their broadly correlative succession of lithofacies. Purple bands mark the stratigraphic intervals of the Kuruman and Dales Gorge Member BIFs that are the focus of this study. Note that the correlation of the Kuruman IF between the central Kuruman area and southern Prieska area is based on the cyclostratigraphic observations of Lantink et al. (2019) and is in disagreement with Beukes' (1980; 1983) correlations of macro- and megacycles, which imply a much higher depositional rate in the south. Figure adapted from Beukes and Gutzmer (2008).

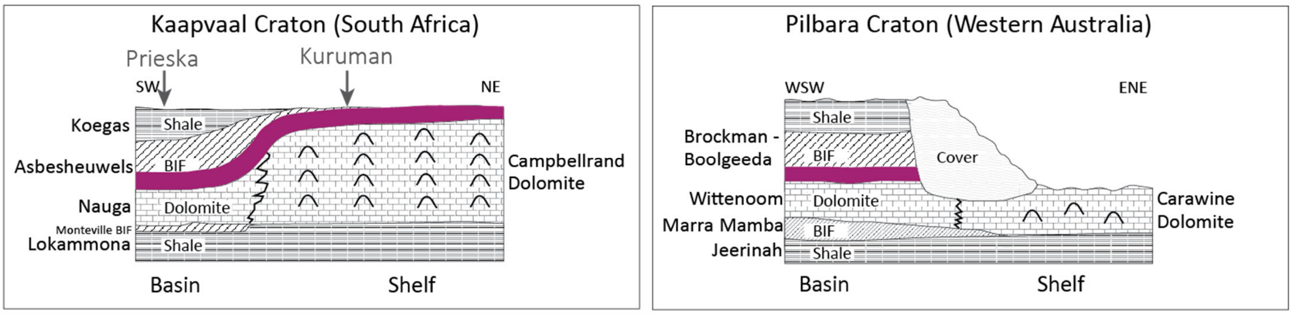

Figure 3. Regular metre-scale alternations and bundling in the weathering profile of the Kuruman IF at section Whitebank (**A**) and in the Dales Gorge Member near section Mount Jack (**B**). White labels in the image of the Kuruman IF denote the characteristic prominent BIF intervals as defined in Lantink et al. (2019). For the Dales Gorge Member, the thicker S macrobands of the BIF–S macroband pattern of Trendall and Blockley (1970) are indicated.

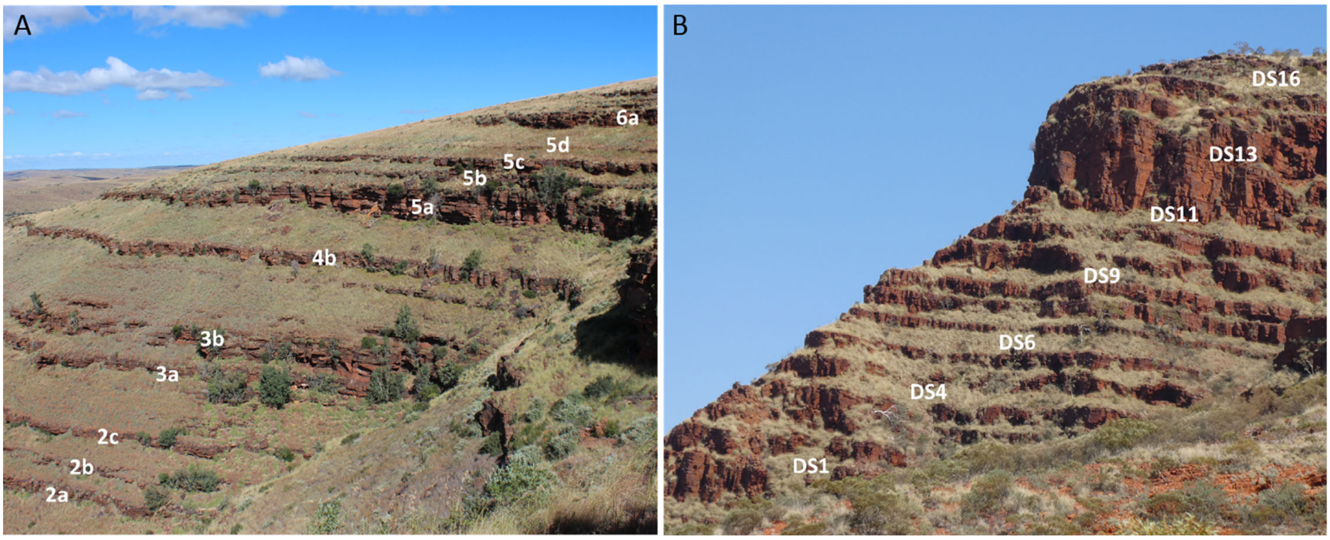

Figure 4 *(next page).* Examples of photogrammetry models constructed for the Dales Gorge Member field sections using an UAV. (**A**) Textured 2.5D mesh of section Mt Jack East with the position of the GCP markers indicated by the blue flags. Marker 4 is positioned in the lower part of DB0 and marker 3 is placed at the base of DB16. (**B**) Dense point cloud of section Mt Bruce East, slightly rotated with respect to the original orientation to correct for stratigraphic dip. The purple dots in the yellow box indicate manually selected boundaries between successive high-relief 'BIF' and lower-relief 'S' intervals that were used for measuring layer thickness and creating a stratigraphic log. The lowermost dot marks the base of DB4 and the uppermost dot marks the top of WB1. Coloured intervals (blue to green to red gradient) indicate the sections from which 'verticality' scalar values were extracted and averaged out horizontally to create a representative verticality record.

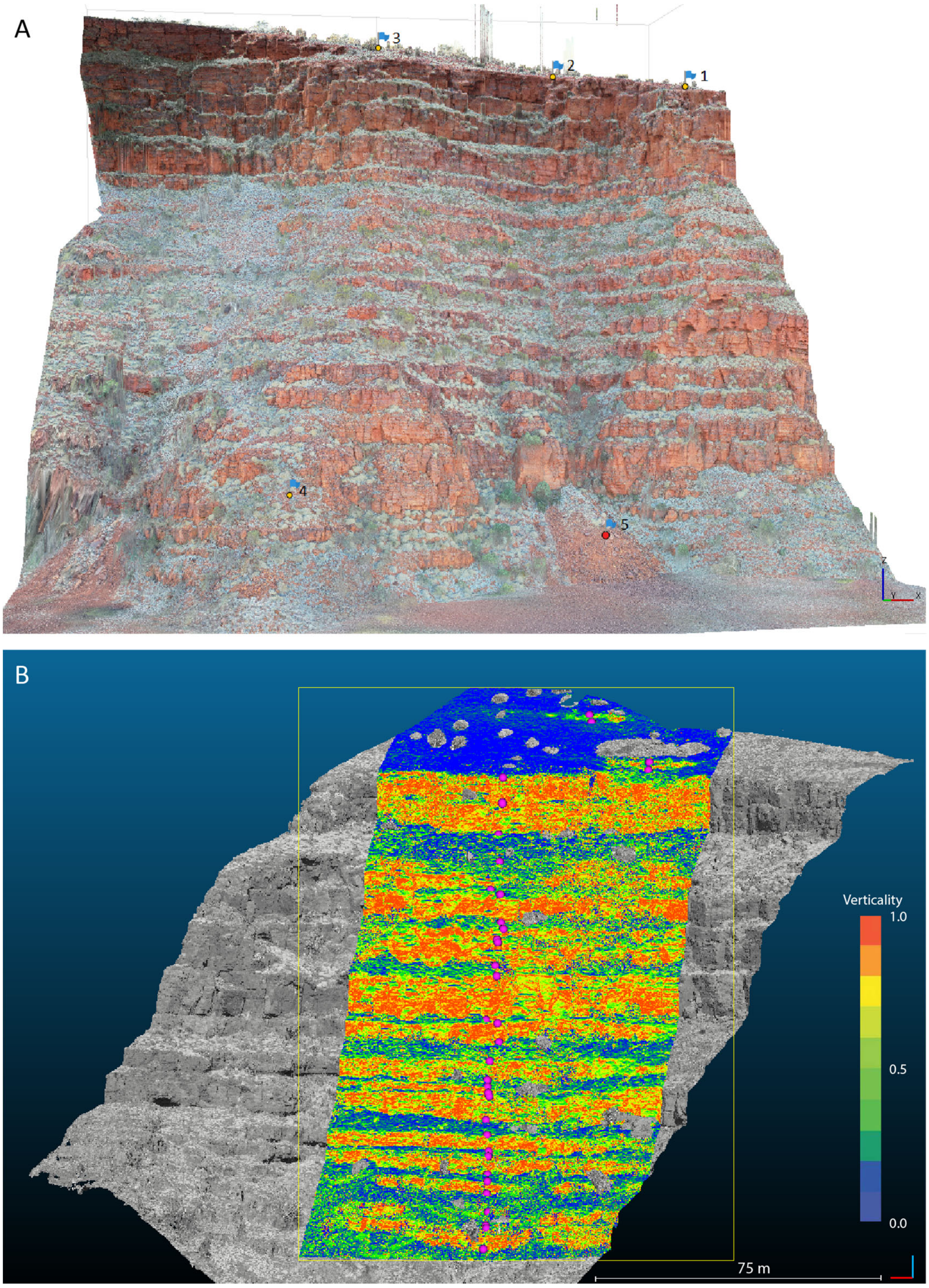
A
3
2
1
4
5
z
y
x
B
Verticality
1.0
0.5
0.0
75 m

Figure 5 *(next page).* Stratigraphic panel and TIMS U-Pb ages for the Kuruman and upper Gamohaan Formations showing the correlation of the characteristic cycle pattern as schematically logged in field sections Whitebank (WB) and Woodstock (WS) by Lantink et al. (2019) to the higher-resolution Fe/Mn and magnetic susceptibility (MS) records of core UUBH-1 from this study. Black lines for the MS and log(Fe/Mn) records indicate in a 75-point moving average of the original records (in grey) and blue curves on the right represent the output of Gaussian bandpass filtering. Horizontal black lines and corresponding cycle numbers on the left of the panel mark the 'BIF' intervals of individual ~5 m-scale alternations, represented by maxima in the relief and/or core proxies; thicker black lines indicate the correlation of the more pronounced BIF intervals included in the original cycle numbering of Lantink et al. (2019). Orange '+' symbols mark the intervals where an additional ~16 m-scale bundle is recognised relative to Lantink et al. (2019), as reflected by an additional maximum in the 0.055 m^{-1} ± 0.025 filtered log(Fe/Mn) signal. Note that there is a ~1.3 m thick interval of core loss above 2c. 'K.N.S.' = Klein Naute Shale.

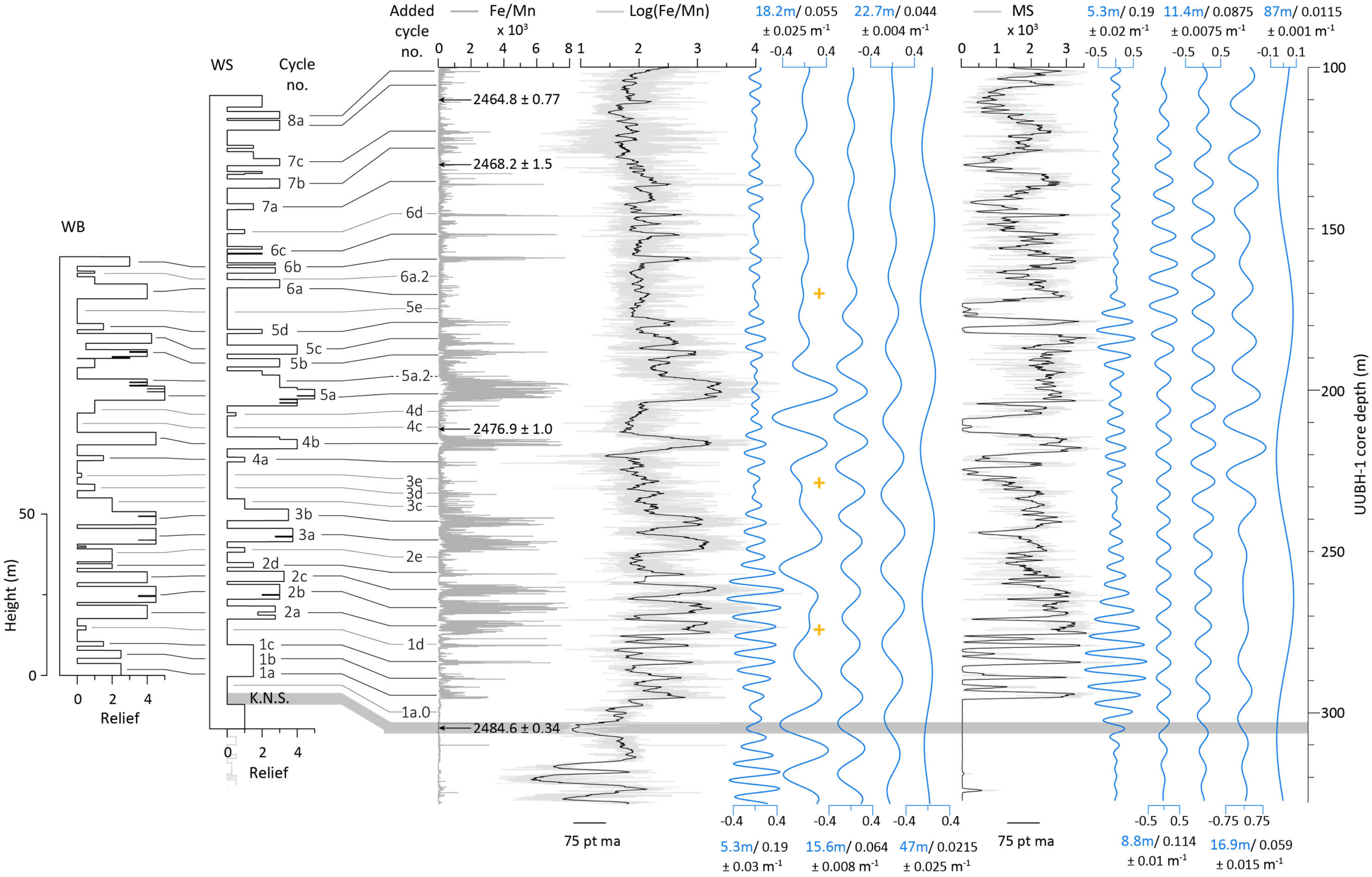
WB
WS
Cycle no.
Added cycle no.
Height (m)
50
0
0 2 4
Relief
0 2 4
Relief
K.N.S.
8a
7c
7b
7a
6d
6c
6b
6a.2
6a
5e
5d
5c
5b
5a.2
5a
4d
4c
4b
4a
3e
3d
3c
3b
3a
2e
2d
2c
2b
2a
1d
1c
1b
1a
1a.0
Fe/Mn x 10³
0 2 4 6 8
2464.8 ± 0.77
2468.2 ± 1.5
2476.9 ± 1.0
2484.6 ± 0.34
Log(Fe/Mn)
1 2 3 4
75 pt ma
18.2m/ 0.055 ± 0.025 m⁻¹
-0.4 0.4
22.7m/ 0.044 ± 0.004 m⁻¹
-0.4 0.4
5.3m/ 0.19 ± 0.03 m⁻¹
-0.4 0.4
15.6m/ 0.064 ± 0.008 m⁻¹
-0.4 0.4
47m/ 0.0215 ± 0.025 m⁻¹
-0.4 0.4
+
+
+
MS x 10³
0 1 2 3
75 pt ma
5.3m/ 0.19 ± 0.02 m⁻¹
-0.5 0.5
11.4m/ 0.0875 ± 0.0075 m⁻¹
-0.5 0.5
87m/ 0.0115 ± 0.001 m⁻¹
-0.1 0.1
8.8m/ 0.114 ± 0.01 m⁻¹
-0.5 0.5
16.9m/ 0.059 ± 0.015 m⁻¹
-0.75 0.75
UUBH-1 core depth (m)
100
150
200
250
300

Figure 6. Spectral analysis results for the Kuruman Iron Formation. (**A**) Lomb-Scargle power spectra of LOWESS detrended log(Fe/Mn) and magnetic susceptibility depth records. Peak labels of prominent spectral peaks are indicated in metres. (**B**) MTM power spectra of the records in (**A**) after applying a 0.1 m interpolation, with LOWSPEC background estimation and harmonic F-test results (in red). Peak labels in black represent significant spectral peaks according to the requirements of Meyers (2012), i.e., satisfying both the 90% LOWSPEC confidence level and 90% harmonic F-test confidence level; for the peak label in light grey the latter is not the case.

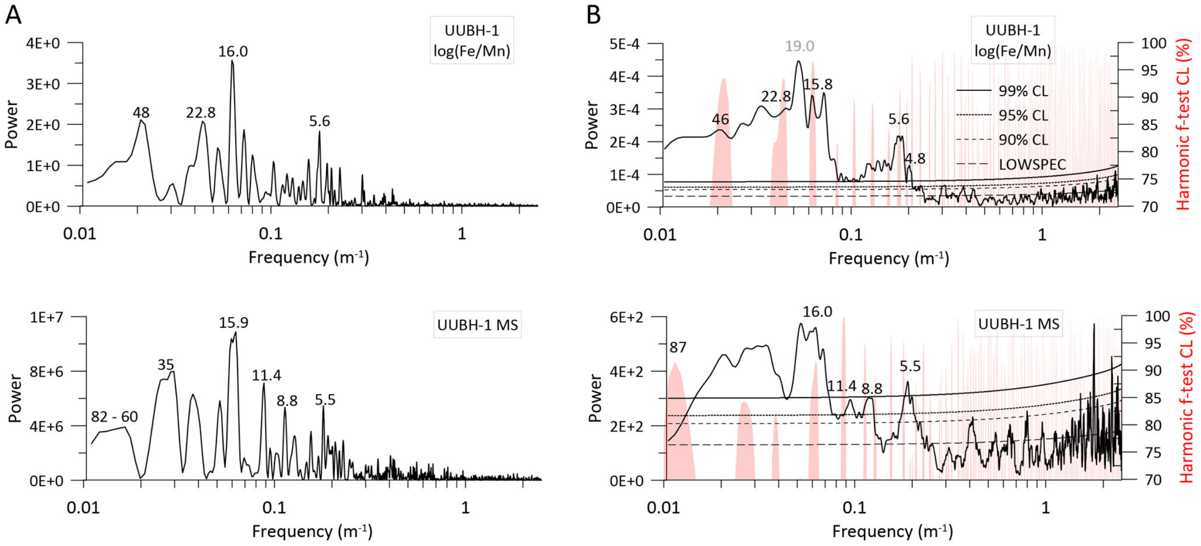

Figure 7 *(next page)*. *Composite* relief logs and verticality profiles for the Mt Bruce and Mt Jack sections with corresponding bandpass filters in blue. Indicated on the left of the schematic columns are the S macroband numbers of the characteristic BIF-S macroband alternations of the Dales Gorge Member, the underlying Colonial Chert Member and overlying Whaleback Shale Member, according to the nomenclature of Morris (1983); Harmsworth et al. (1990).

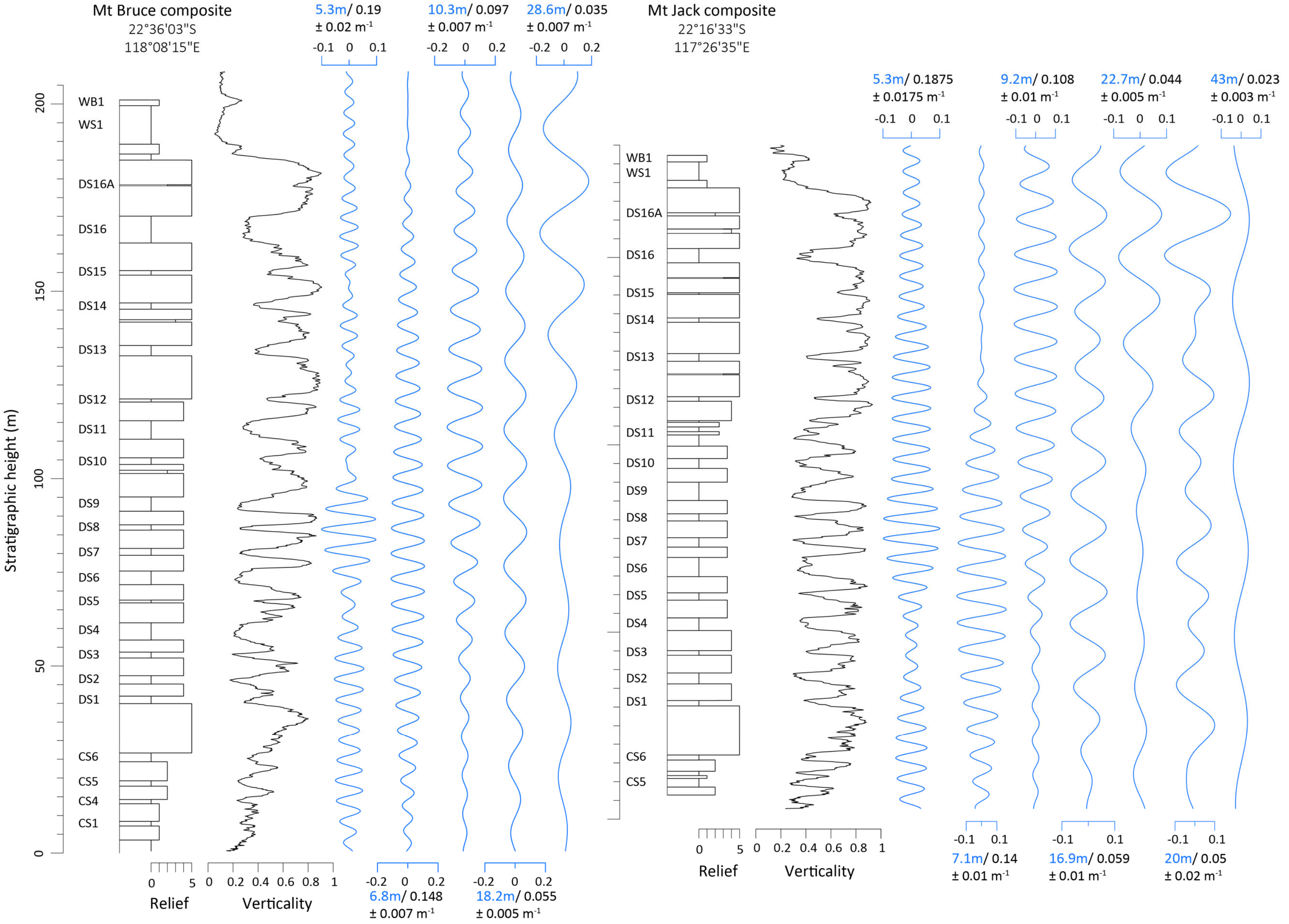
Mt Bruce composite
22°36'03"S
118°08'15"E
5.3m/ 0.19
± 0.02 m-1
-0.1 0 0.1
10.3m/ 0.097
± 0.007 m-1
-0.2 0 0.2
28.6m/ 0.035
± 0.007 m-1
-0.2 0 0.2
Stratigraphic height (m)
0
50
100
150
200
WB1
WS1
DS16A
DS16
DS15
DS14
DS13
DS12
DS11
DS10
DS9
DS8
DS7
DS6
DS5
DS4
DS3
DS2
DS1
CS6
CS5
CS4
CS1
0 5
Relief
0 0.2 0.4 0.6 0.8 1
Verticality
-0.2 0 0.2
6.8m/ 0.148
± 0.007 m-1
-0.2 0 0.2
18.2m/ 0.055
± 0.005 m-1
Mt Jack composite
22°16'33"S
117°26'35"E
5.3m/ 0.1875
± 0.0175 m-1
-0.1 0 0.1
9.2m/ 0.108
± 0.01 m-1
-0.1 0 0.1
22.7m/ 0.044
± 0.005 m-1
-0.1 0 0.1
43m/ 0.023
± 0.003 m-1
-0.1 0 0.1
WB1
WS1
DS16A
DS16
DS15
DS14
DS13
DS12
DS11
DS10
DS9
DS8
DS7
DS6
DS5
DS4
DS3
DS2
DS1
CS6
CS5
0 5
Relief
0 0.2 0.4 0.6 0.8 1
Verticality
-0.1 0.1
7.1m/ 0.14
± 0.01 m-1
-0.1 0.1
16.9m/ 0.059
± 0.01 m-1
-0.1 0.1
20m/ 0.05
± 0.02 m-1

Figure 8. Hylogger ferric oxide and carbonate abundance records from cores 47A and SGP001 and TIMS U–Pb ages. Results of Gaussian bandpass filtering (in blue) and a 75-point and 125-point moving average (in black) are given for the log(ferric oxide) and log(carbonate) records, respectively. The positions of the S macroband numbers are indicated on the left.

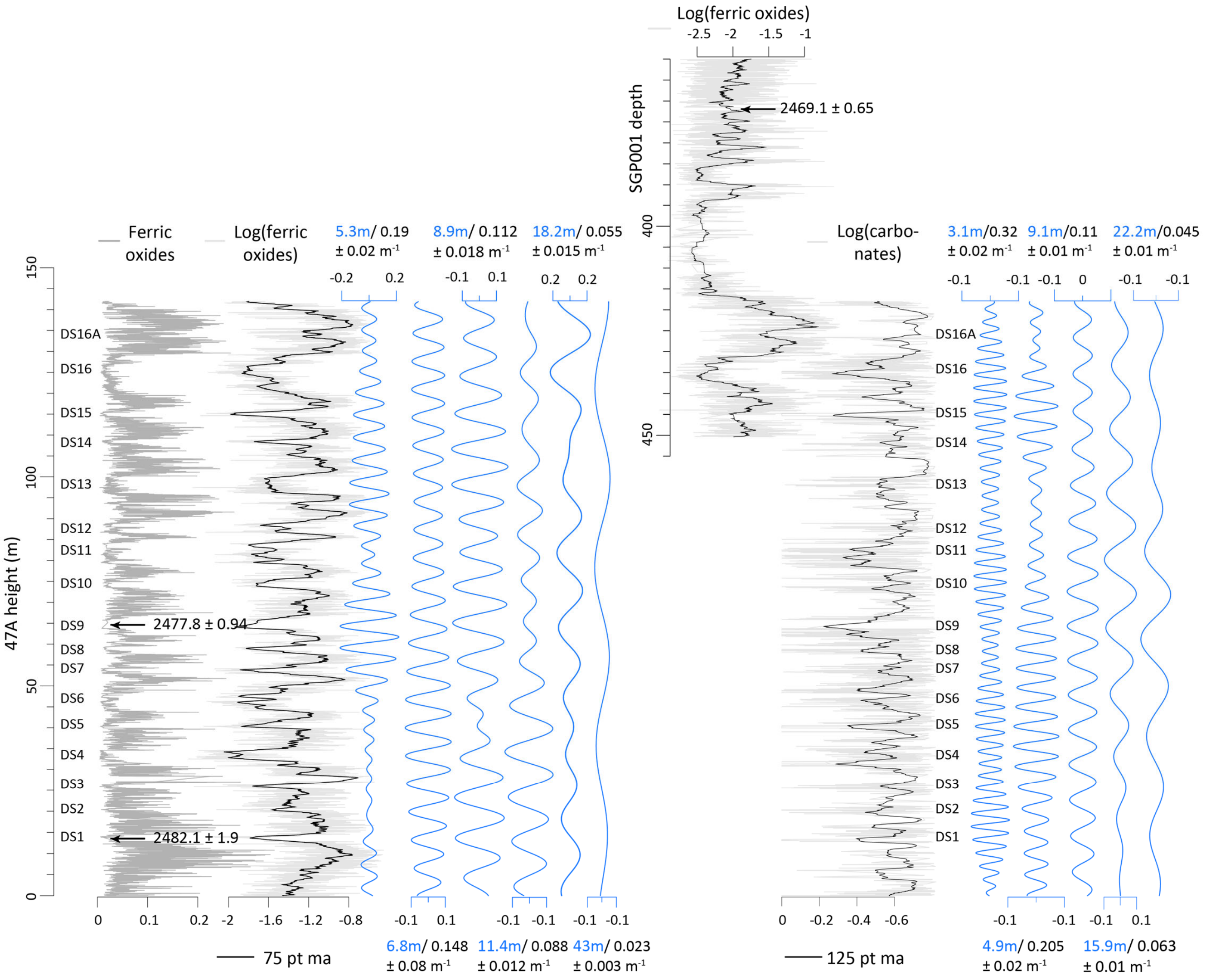

Figure 9. Spectral analysis results for the Dales Gorge Member. (**A**) Lomb-Scargle power spectra of LOWESS detrended verticality profiles (Mt Bruce and Mt Jack) and core 47A Hylogger depth records. Peak labels of prominent spectral peaks are indicated in metres. (**B**) MTM (3 2π) power spectra of the records in (**A**) after applying a 0.1 m interpolation, with LOWSPEC background estimation and harmonic F-test results (in red). The spectrum of the log(ferric oxide) record was made with a time-bandwidth product of 2 instead of 3. Peak labels in black represent significant spectral peaks according to the requirements of Meyers (2012), i.e., satisfying both the 90% LOWSPEC confidence level and 90% harmonic F-test confidence level; for peak labels in light grey the latter is not the case.

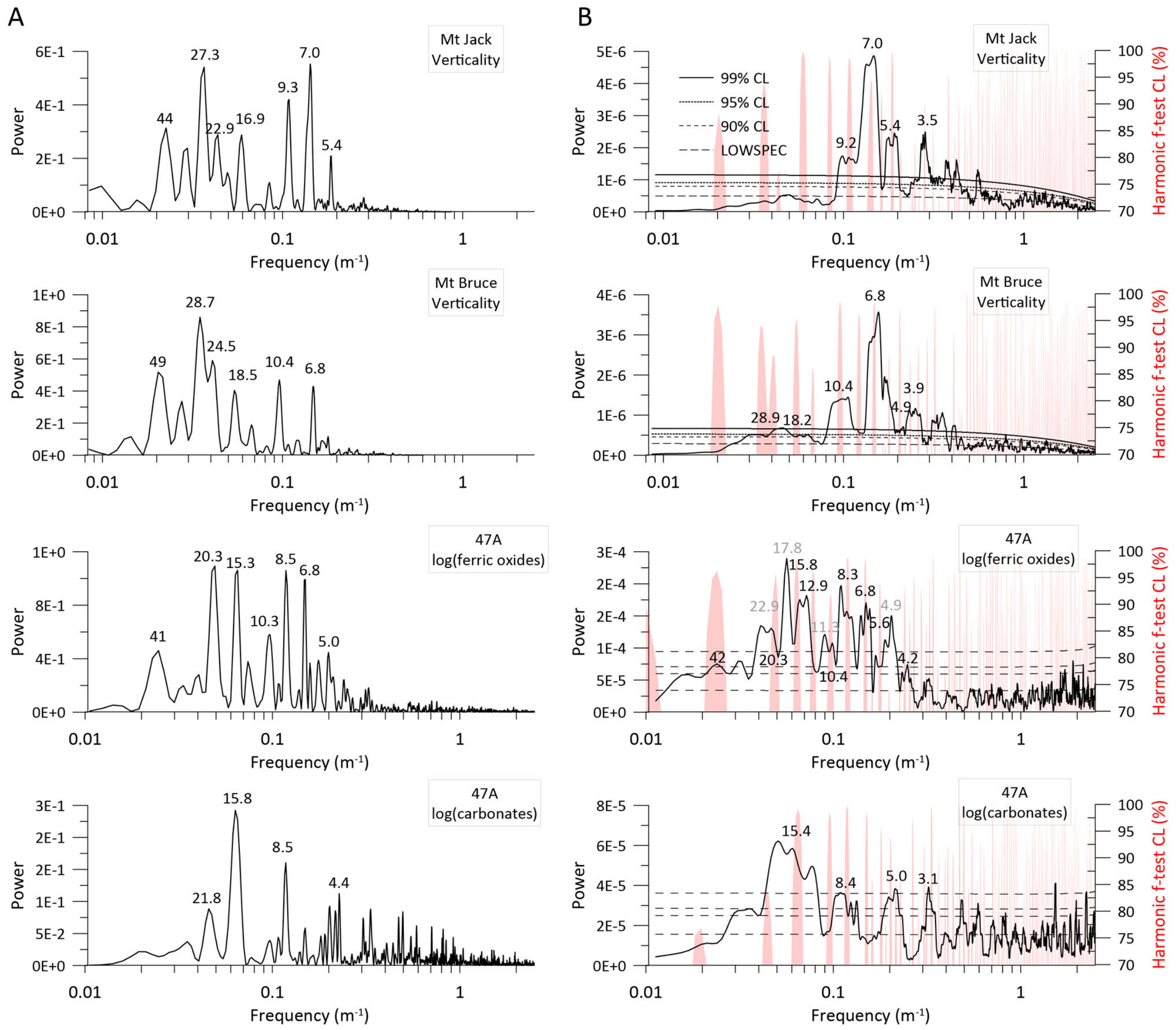

Figure 10. Concordia diagrams showing the concordant high-precision U–Pb TIMS results and the calculated ages for DS1 and DS9 (Dales Gorge Member) and shales 212 m and 110 m (Kuruman Formation). The grey band represents the uncertainty on the Concordia curve due to the decay constant uncertainties. The ellipses represent the U–Pb isotopic data and 2σ uncertainty for individual chemically abraded zircon fragments. MSWD: mean square of the weighted deviates.

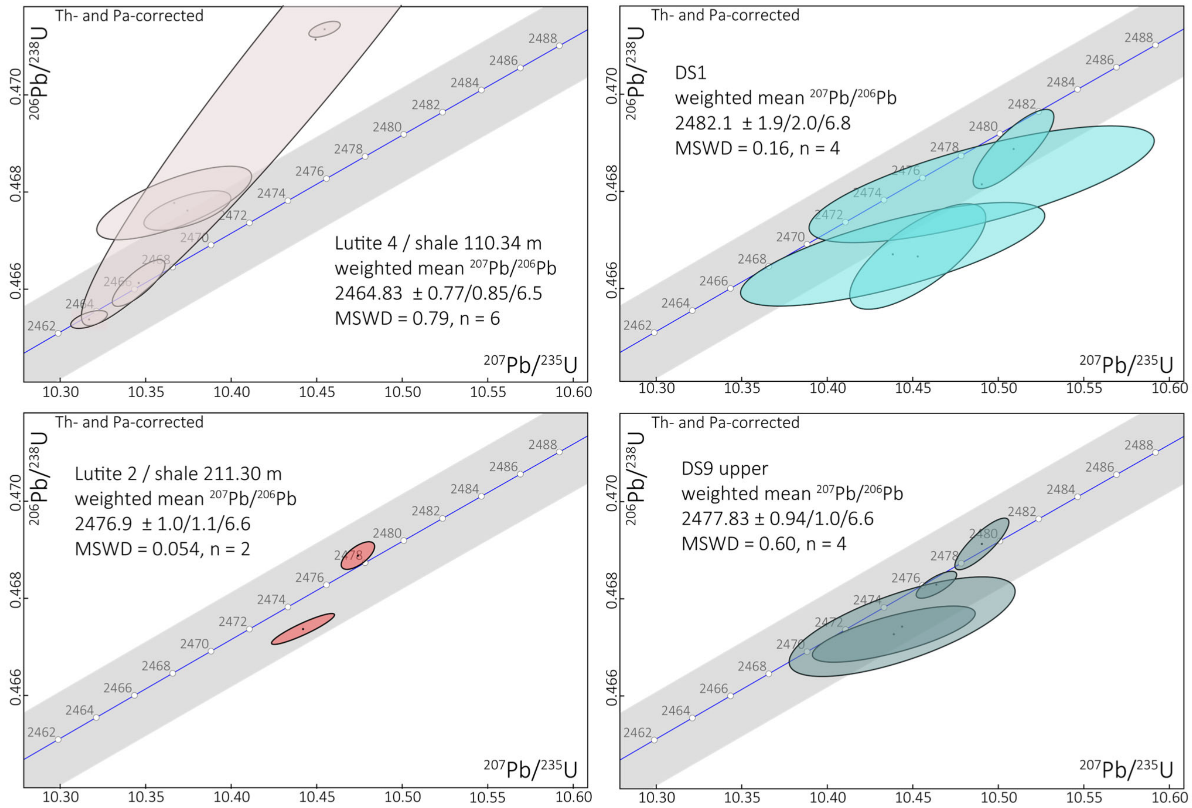

Figure 11. Bchron depositional rate model for the lower Brockman IF (left) based on the high-precision U–Pb ages from DS1, DS9 of the Dales Gorge Member and shale 371 from core DD98 of Lantink et al. (2022), and updated depositional rate model for the Kuruman IF (right) based on the improved ages of the shales at 212 m and 110 m depth in core UUBH-1. The red dotted lines indicate 97.5% confidence intervals.

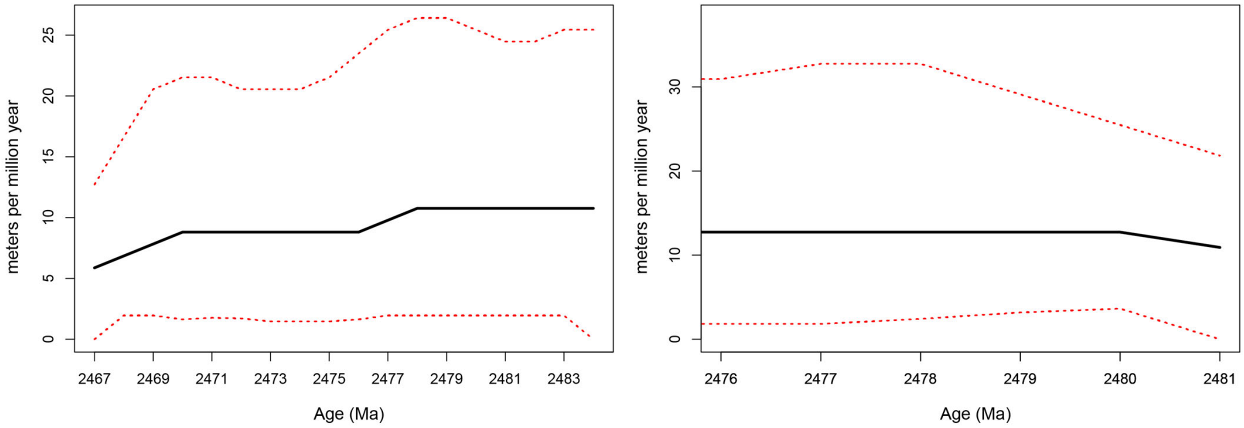

Table 1. Time calibrated period, relative strength and proposed astronomical origin (or otherwise) of the different cycles identified in the stratigraphy of the Kuruman IF and Dales Gorge Member.

Dales Gorge Member			Kuruman Formation					
L-S /MTM peak (m)	Period (kyr) assuming 4.9m = 405 kyr	Strength	L-S/ MTM peak (m)	Period (kyr) assuming 5.1m = 405 kyr	Strength	Possible origin	Laskar et al. 2004 [-15 +5 Myr] mean period (kyr)	Laskar et al. 2004 amplitude b'k x 10^4
3.1	262	+			-	$(g_2 - g_5) + (g_1 - g_5)$ and/or semi-7 m cycle ?	285	
4.9	405	+	4.8-5.6	381-445	++	$g_2 - g_5$	405	107
6.8	562	++			-	$(g_2 - g_5) - (g_4 - g_3)$ (?)	486 / 593*	20
8.3	686	++	8.8	699	+/-	$g_2 - g_1$ (?) and/or semi-16 m cycle ?	688	18
10.4 11.3 12.9	860 934 1066	+/- - -	11.4	905	+/-	double 405 kyr, $g_1 - g_5$ or thin 16 m cycle ??	967	28
15.8	1306	++	15.9	1263	++	$g_4 - g_3$ (?), or $s_3 - s_4$??, or $g_1 - g_5$???	2369	30
20.3 21.8 (22.9)	1678 1802 (1892)	+/-	22.8	1811	+	double 11.5 m cycle or $g_4 - g_3$??		
42	3471	+/-	46	3653	+	16 and 23 m diff. tone ?		

*assuming $g_4 – g_3$ has a period of 1.3 Myr.

Figure 12 *(next page)*. Correlation option I for the Kuruman IF and Dales Gorge Member. Initial correlation that is based on resemblance in characteristic weathering profile patterns only. Black connecting lines indicate the correlation of ~5 m-scale ‘BIF’ intervals and/or interpreted 405 kyr cycles (dotted lines where this is uncertain), with thicker lines marking the more prominent BIFs that form the basis of the correlation. Note that this correlation implies the presence of three condensed 405 kyr-related cycles in DS11. It is also in disagreement with the TIMS U-Pb ages of DS9 and the shale below 4c in the Kuruman IF, whose maximum age difference is less than 3 Myr, while, according to the cyclostratigraphic interpretation, there are at least eight 405 kyr-related cycles, i.e. more than 3 Myrs in between these two shale levels (see red arrow). *Inferred age of the shale below 2e in the Kuruman IF that is correlated to DS9 in the Dales Gorge Member, based on adding 8 x 405 kyr to the age of the shale below 4c in the Kuruman IF.

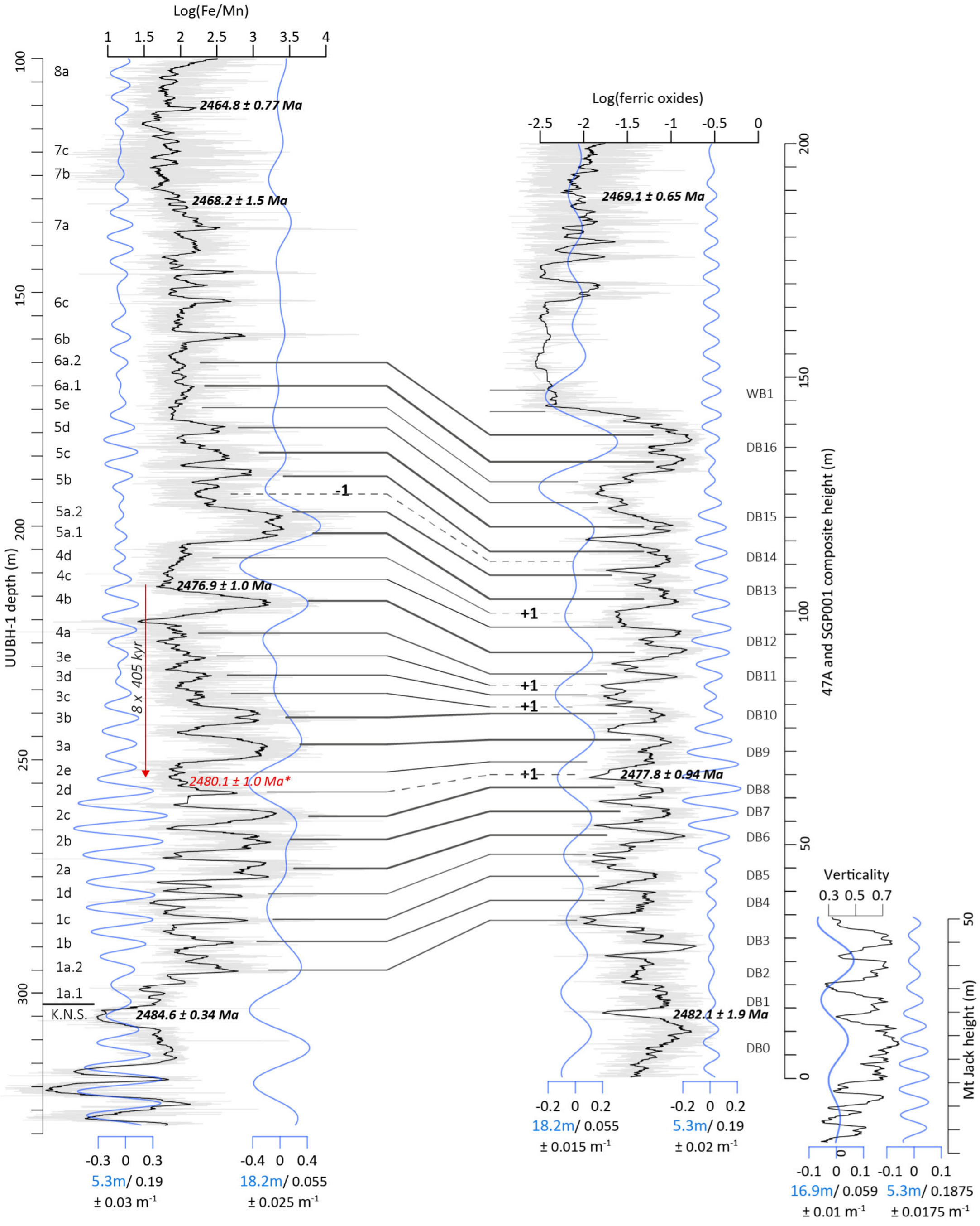
Log(Fe/Mn)
1 1.5 2 2.5 3 3.5 4
UUBH-1 depth (m)
100
150
200
250
300
8a
7c
7b
7a
6c
6b
6a.2
6a.1
5e
5d
5c
5b
5a.2
5a.1
4d
4c
4b
4a
3e
3d
3c
3b
3a
2e
2d
2c
2b
2a
1d
1c
1b
1a.2
1a.1
K.N.S.
2464.8 ± 0.77 Ma
2468.2 ± 1.5 Ma
2476.9 ± 1.0 Ma
8 x 405 kyr
2480.1 ± 1.0 Ma*
2484.6 ± 0.34 Ma
-1
+1
+1
+1
+1
-0.3 0 0.3
5.3m/ 0.19
± 0.03 m-1
-0.4 0 0.4
18.2m/ 0.055
± 0.025 m-1
Log(ferric oxides)
-2.5 -2 -1.5 -1 -0.5 0
2469.1 ± 0.65 Ma
2477.8 ± 0.94 Ma
2482.1 ± 1.9 Ma
WB1
DB16
DB15
DB14
DB13
DB12
DB11
DB10
DB9
DB8
DB7
DB6
DB5
DB4
DB3
DB2
DB1
DB0
47A and SGP001 composite height (m)
200
150
100
50
0
-0.2 0 0.2
18.2m/ 0.055
± 0.015 m-1
-0.2 0 0.2
5.3m/ 0.19
± 0.02 m-1
Verticality
0.3 0.5 0.7
Mt Jack height (m)
50
0
-0.1 0 0.1
16.9m/ 0.059
± 0.01 m-1
-0.1 0 0.1
5.3m/ 0.1875
± 0.0175 m-1

Figure 13 *(next page)*. Correlation option IIa for the Kuruman IF and Dales Gorge Member. Second correlation based on both similarity in characteristic cycle pattern (as expressed in both outcrop and core proxy data) and consistency with the U-Pb ages. Black connecting lines indicate the correlations of observed ~5 m-scale BIF intervals and/or interpreted 405 kyr cycles (dotted lines where this is uncertain). Thick lines mark the more prominent BIFs of each interpreted ~16 m-scale bundle (broad ~18 m filter outputs shown). Note that this correlation implies the presence of two condensed 405 kyr-related cycles in DS4, one in between 4a and 4b and one in between 4b and 4c. It also implies that the top of DB15 to DS16 represents a single 405 kyr cycle.

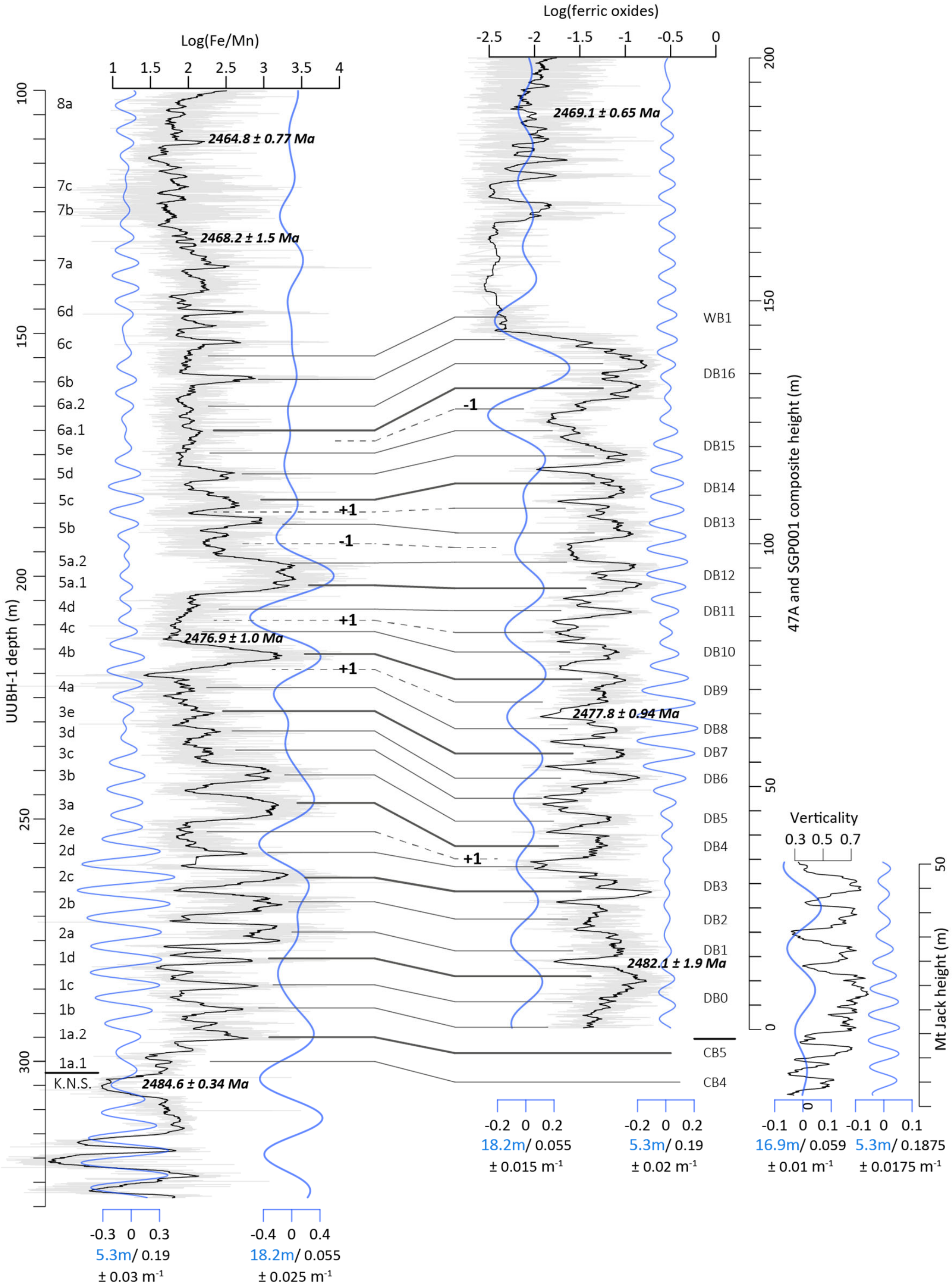
Log(Fe/Mn)
1 1.5 2 2.5 3 3.5 4
UUBH-1 depth (m)
100
150
200
250
300
8a
7c
7b
7a
6d
6c
6b
6a.2
6a.1
5e
5d
5c
5b
5a.2
5a.1
4d
4c
4b
4a
3e
3d
3c
3b
3a
2e
2d
2c
2b
2a
1d
1c
1b
1a.2
1a.1
K.N.S.
2464.8 ± 0.77 Ma
2468.2 ± 1.5 Ma
2476.9 ± 1.0 Ma
2484.6 ± 0.34 Ma
+1
-1
+1
+1
-1
+1
-0.3 0 0.3
5.3m/ 0.19
± 0.03 m⁻¹
-0.4 0 0.4
18.2m/ 0.055
± 0.025 m⁻¹
Log(ferric oxides)
-2.5 -2 -1.5 -1 -0.5 0
2469.1 ± 0.65 Ma
2477.8 ± 0.94 Ma
2482.1 ± 1.9 Ma
WB1
DB16
DB15
DB14
DB13
DB12
DB11
DB10
DB9
DB8
DB7
DB6
DB5
DB4
DB3
DB2
DB1
DB0
CB5
CB4
47A and SGP001 composite height (m)
200
150
100
50
0
-0.2 0 0.2
18.2m/ 0.055
± 0.015 m⁻¹
-0.2 0 0.2
5.3m/ 0.19
± 0.02 m⁻¹
Verticality
0.3 0.5 0.7
Mt Jack height (m)
50
0
-0.1 0 0.1
16.9m/ 0.059
± 0.01 m⁻¹
-0.1 0 0.1
5.3m/ 0.1875
± 0.0175 m⁻¹

Figure 14 *(next page)*. Correlation option IIb for the Kuruman IF and Dales Gorge Member. Modified correlation II that is most consistent with the ~5 m and ~16 m filtering. Black connecting lines indicate the correlation of observed ~5 m-scale BIF intervals and/or interpreted 405 kyr cycles (dotted lines where this is uncertain). Thick horizontal lines indicate the correlations of ~5 m-scale BIF intervals that occur near or closest to maxima in the (filtered) ~16 m cycle in the Kuruman IF and/or Dales Gorge Member (narrow ~16 m bandpass filter outputs shown). Compared to option IIa, in this option IIb the Dales Gorge Member is shifted downwards relative to the Kuruman IF by one (filtered) ~5 m cycle in the interval 2e-4c and 5b, and by one (filtered) ~16 m cycle (two ~5 m cycles) in the interval DB13–16.

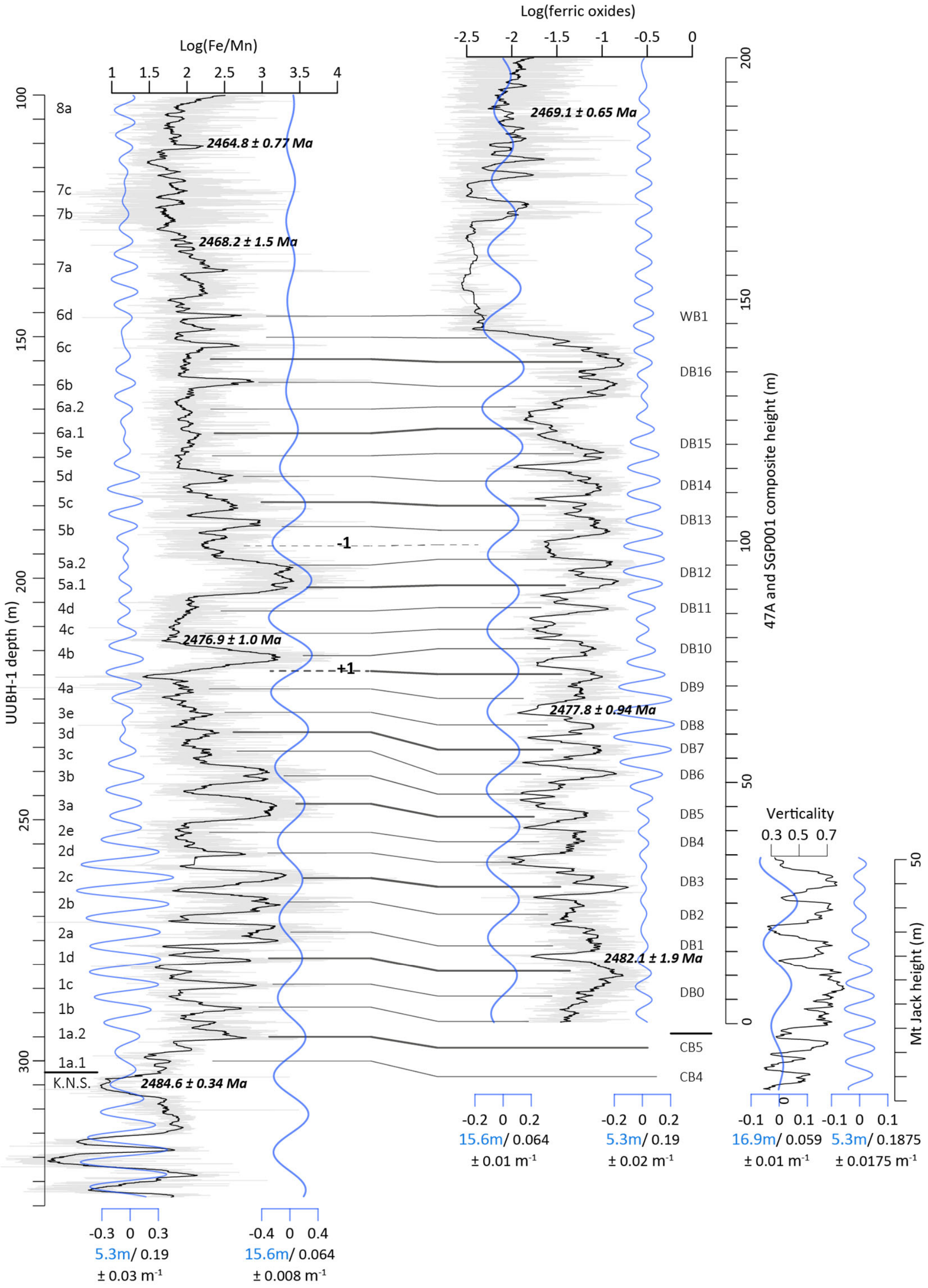
Log(Fe/Mn)
1 1.5 2 2.5 3 3.5 4
UUBH-1 depth (m)
100 150 200 250 300
8a
7c
7b
7a
6d
6c
6b
6a.2
6a.1
5e
5d
5c
5b
5a.2
5a.1
4d
4c
4b
4a
3e
3d
3c
3b
3a
2e
2d
2c
2b
2a
1d
1c
1b
1a.2
1a.1
K.N.S.
2464.8 ± 0.77 Ma
2468.2 ± 1.5 Ma
2476.9 ± 1.0 Ma
2484.6 ± 0.34 Ma
-1
+1
-0.3 0 0.3
5.3m/ 0.19
± 0.03 m-1
-0.4 0 0.4
15.6m/ 0.064
± 0.008 m-1
Log(ferric oxides)
-2.5 -2 -1.5 -1 -0.5 0
2469.1 ± 0.65 Ma
2477.8 ± 0.94 Ma
2482.1 ± 1.9 Ma
WB1
DB16
DB15
DB14
DB13
DB12
DB11
DB10
DB9
DB8
DB7
DB6
DB5
DB4
DB3
DB2
DB1
DB0
CB5
CB4
47A and SGP001 composite height (m)
0 50 100 150 200
-0.2 0 0.2
15.6m/ 0.064
± 0.01 m-1
-0.2 0 0.2
5.3m/ 0.19
± 0.02 m-1
Verticality
0.3 0.5 0.7
Mt Jack height (m)
0 50
-0.1 0 0.1
16.9m/ 0.059
± 0.01 m-1
-0.1 0 0.1
5.3m/ 0.1875
± 0.0175 m-1

Supplementary Information for

Towards an astrochronological framework for the lower Paleoproterozoic Kuruman and Brockman Iron Formations

Margriet L. Lantink[1,2]*, Joshua H. F. L. Davies[3,4], Rick Hennekam[5], David McB. Martin[6], Paul R. D. Mason[1], Gert-Jan Reichart[1,5], and Frederik J. Hilgen[1]

[1] Department of Earth Sciences, Utrecht University, the Netherlands
[2] Department of Geoscience, University of Wisconsin-Madison, WI, Unites States
[3] Sciences de la Terre et de l'atmosphère, Université du Québec à Montréal, QC, Canada
[4] Department of Earth Sciences, University of Geneva, Switzerland
[5] Department of Ocean Systems, Royal Netherlands Institute of Sea Research (NIOZ), the Netherlands
[6] Department of Mines, Industry Regulation and Safety, Geological Survey of Western Australia, Perth, WA, Australia

*Corresponding author. Email: lantink@wisc.edu

This file includes:

Supplementary Figures S1-9
References

Supplementary Figures

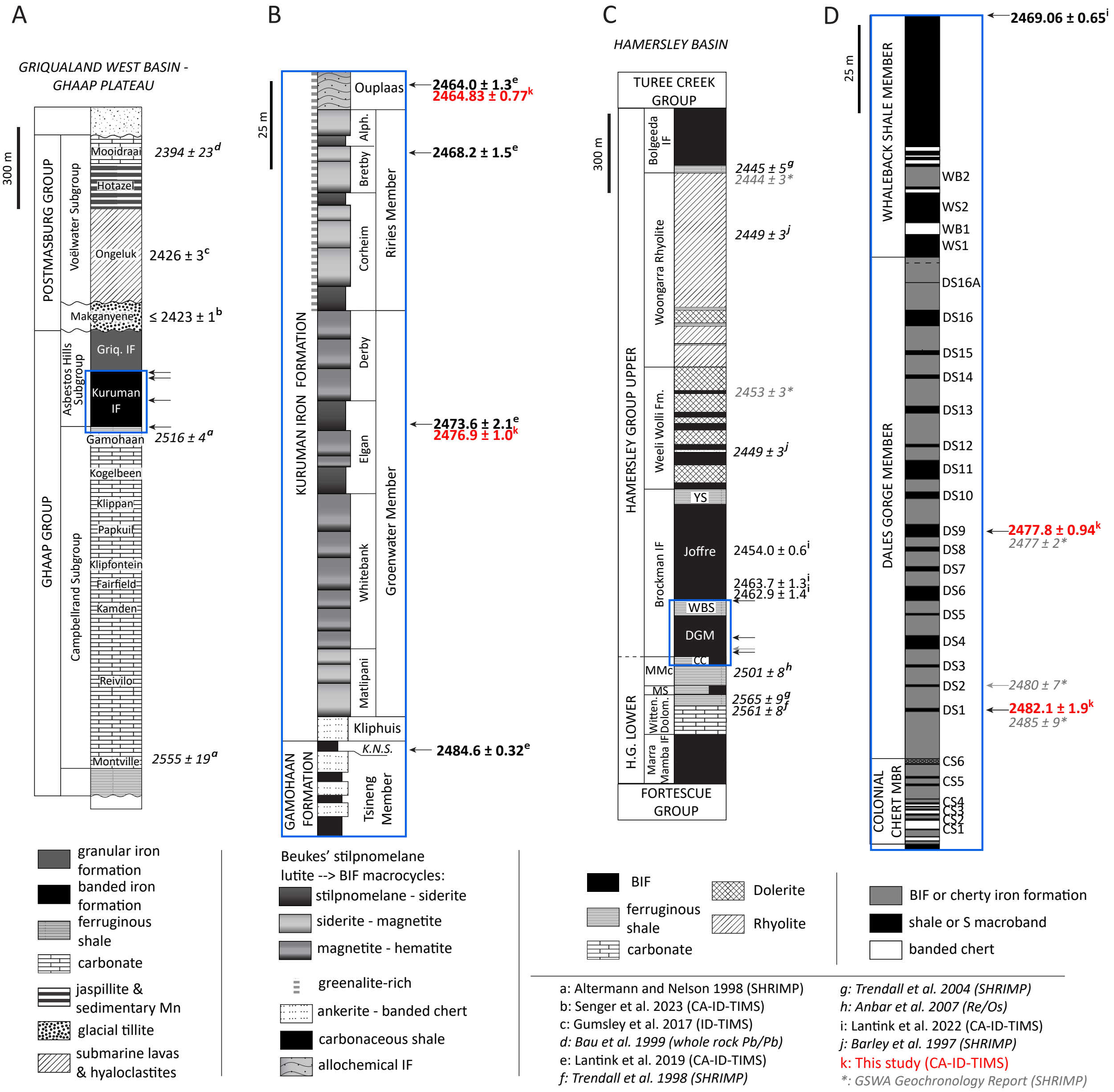

Figure S1. Stratigraphy and geochronology of the Transvaal Supergroup in the Griqualand West Basin and Mount Bruce Supergroup in the Hamersley Basin. (**A**) Schematic column for the Ghaap carbonate platform area adapted from Fig. 2 in Beukes (1987) and Fig. 2 in Pickard (2003). Arrows indicate the positions of the ages of lutites 1–4 shown in **B**. (**B**) Zoom-in on the Kuruman IF and upper Gamohaan Formation showing the classical stilpnomelane lutite --> BIF macrocycles and members as identified by Beukes in the old core WB98 from Whitebank. Adapted from Fig. 5 in Beukes (1980) and Fig. 4 in Beukes (1983). (**C**) Schematic column for Mount Bruce Supergroup after Trendall and Blockley (1970). MS = Mount Sylvia Formation, MMc = Mt McRae Shale. Arrows indicate the positions of the ages shown in **D**. (**D**) Zoom-in on the stratigraphy of Colonial Chert, Dales Gorge and Whaleback Shale Members representative for the Wittenoom area based on Trendall and Blockley (1970) p. 37, 73 and 87. Shale macrobands are labelled according to the later established formal nomenclature as presented in Harmsworth et al. (1990). All ages are reported in 2σ. References for the GSWA reports are Wingate et al., 2018 (Weeli Wolli), Wingate et al., 2020 (Woongarra Rhyolite), Wingate et al., 2021a (DS1), Wingate et al., 2021b (DS9) and Wingate et al., 2021c (DS2).

Table S1. Instrument settings of the XRF core scanner.

Tube voltage (kV)	Current (μA)	Time analysed (s)	Filter	Elements (atomic number)
10	200	15	none	Mg (12) - (Mn (25)
30	150	15	Pb-thin	Fe (26) - U (92)
50	1,000	45	Cu	Ba (56)

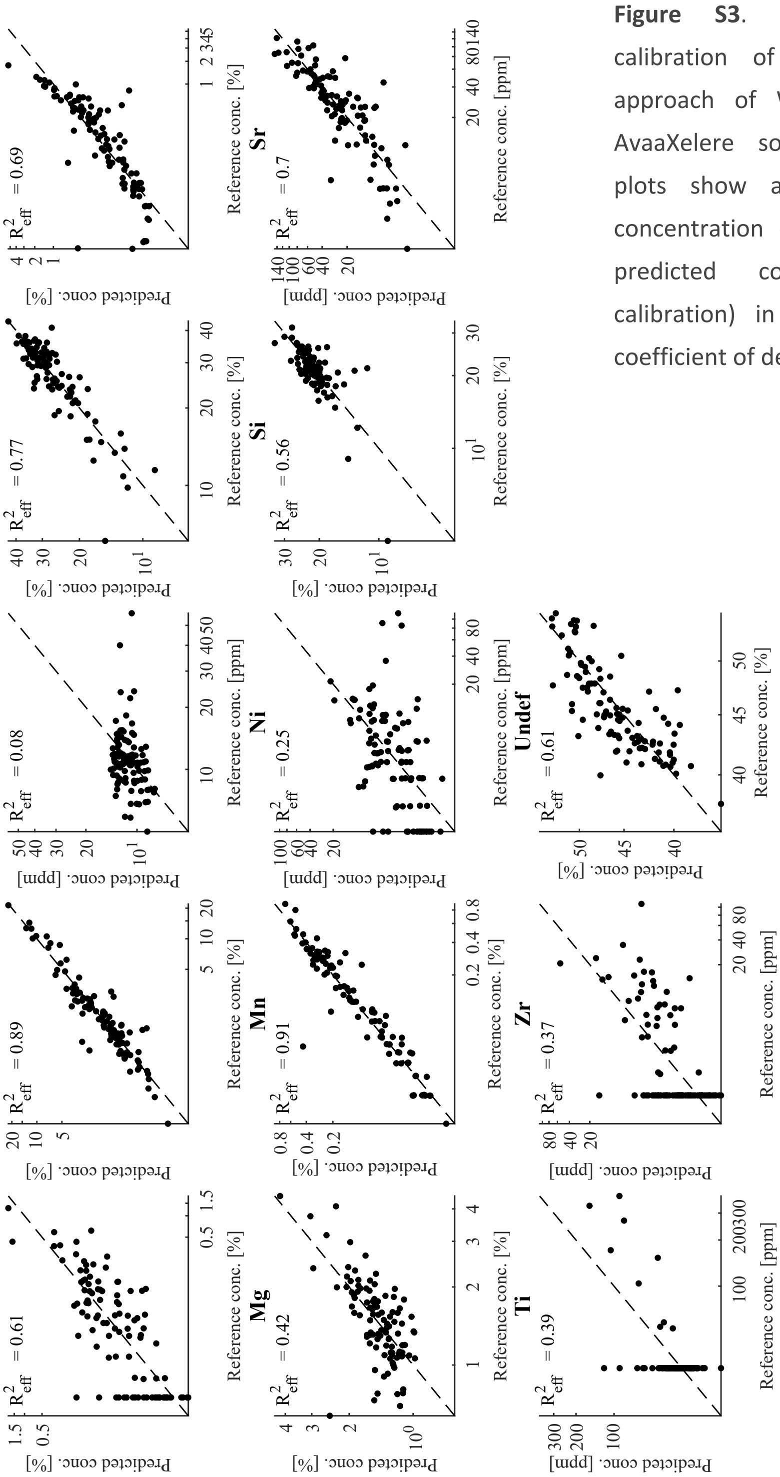

Figure S3. Results of multivariate log-ratio calibration of the XRF data following the approach of Weltje et al. (2015) and using the AvaaXelere software of Bloemsma (2015). X-Y plots show a comparison between the measured concentration of the reference samples and their predicted concentration (according to the calibration) in weight % with linear regression coefficient of determination (R^2) values.

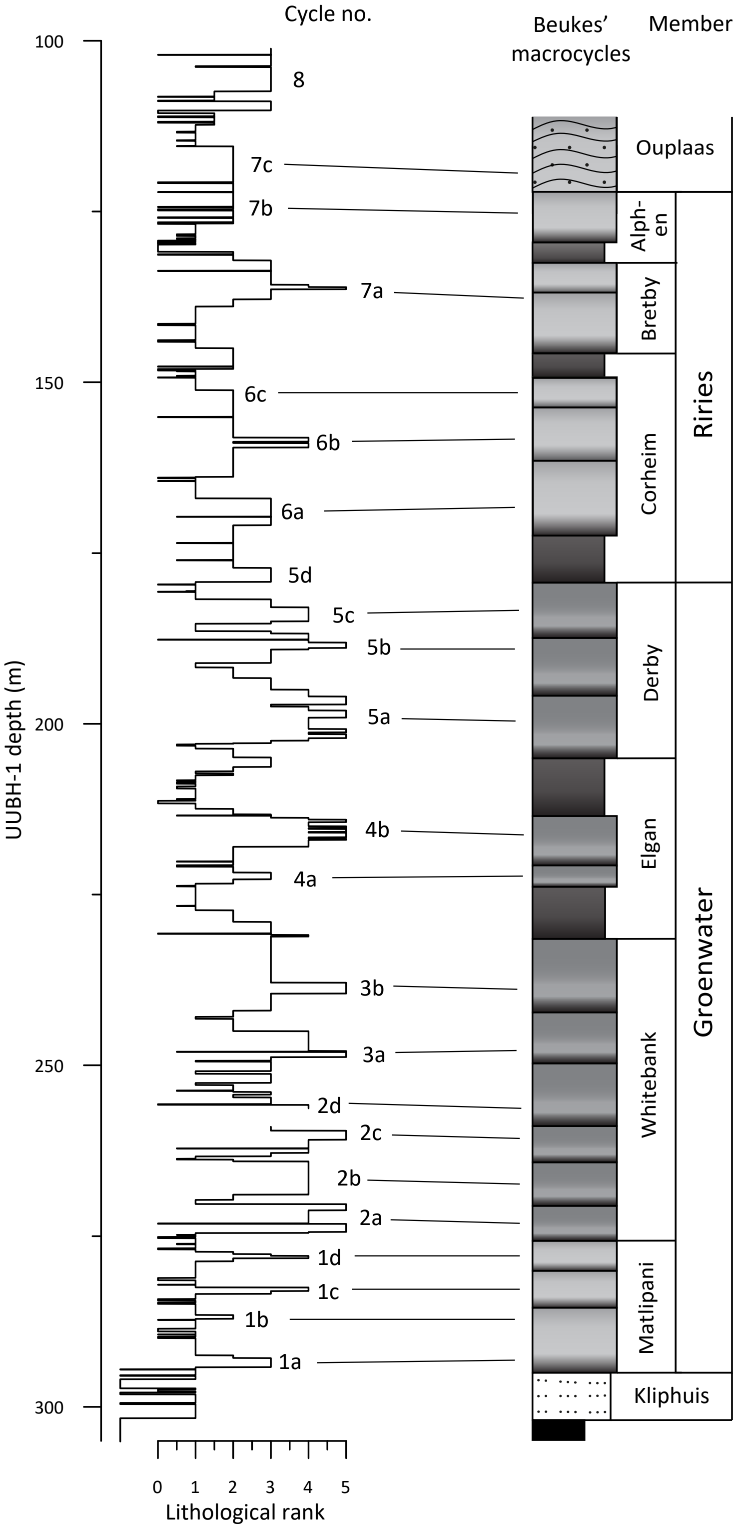

Figure S3. Lithological rank series of the UUBH-1 core revealing the characteristic cycles of Lantink et al. (2019) (left) and comparison to Beukes' macrocycles and the traditional members (right) observed in the old core WB98 from Whitebank (modified after Beukes, 1980; 1983). Colours and symbols are the same as in Fig. S1.

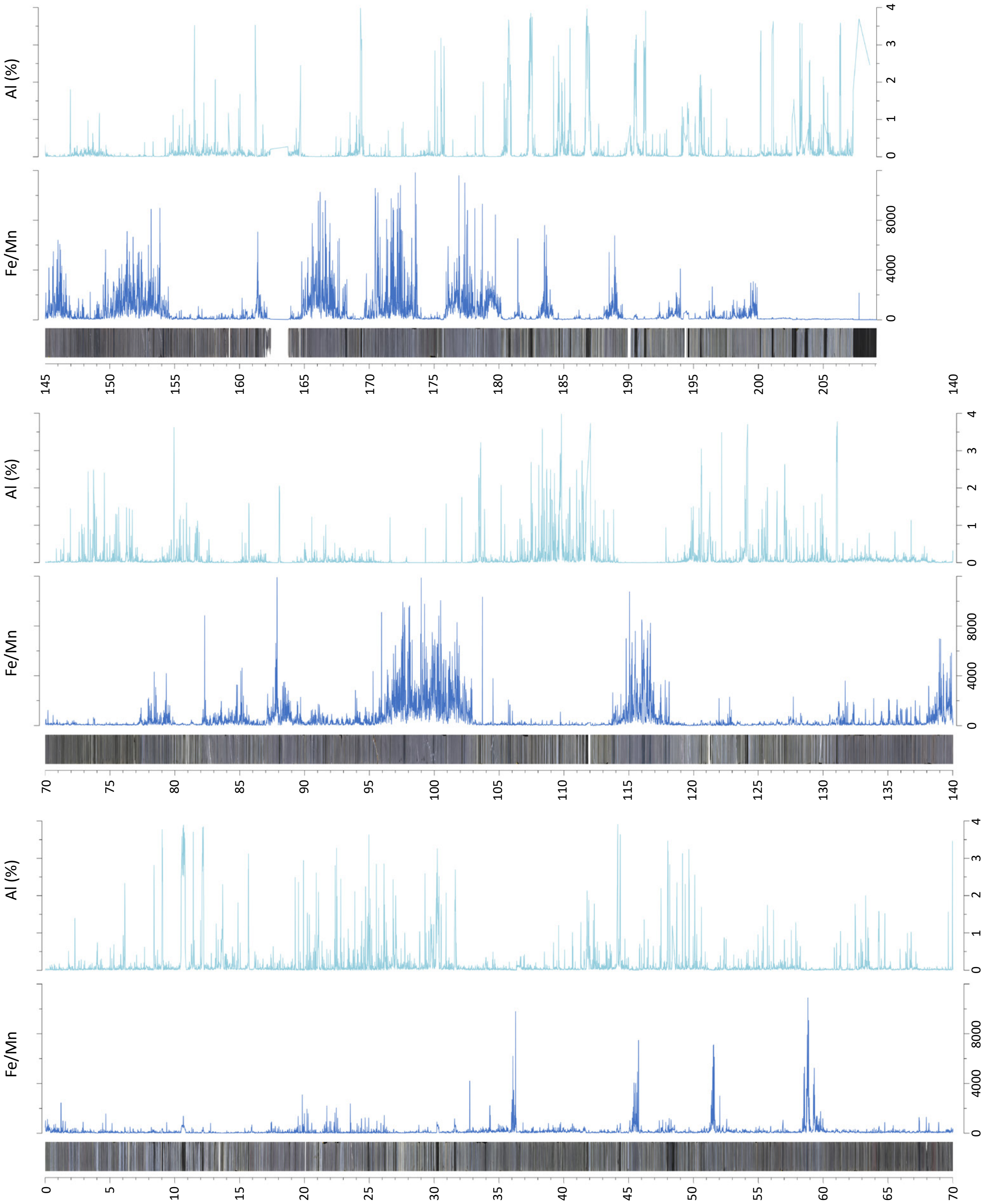

Figure S4. XRF core scanning and photo composite of UUBH-1 for the depth interval that includes the Kuruman Formation (100–302 m). Calibrated Fe/Mn and Al (wt %) records are shown.

Figure S5. Construction of UAV-derived photogrammetry models for the Dales Gorge Member field sections at Mt Bruce and Mt Jack and extraction of stratigraphic data.

<u>Mt Bruce West</u>

Textured 2.5D mesh with GCP marker positions constructed in Agisoft Metashape:

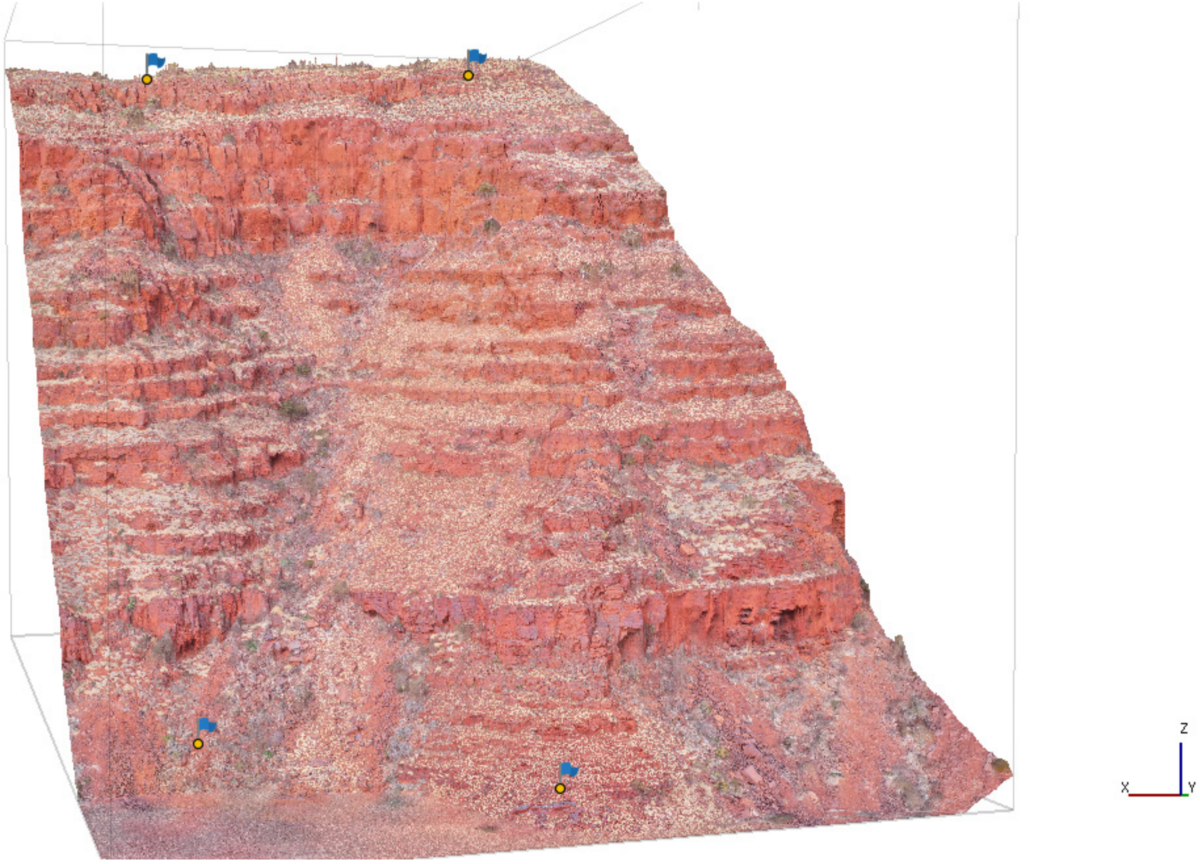

GCP positions and error (in metres):

GCP	X/Longitude	Y/Latitude	Z/Altitude	X_model	Y_model	Z_model	X_error	Y_error	Z_error
1	118.136749	-22.601359	1102.6066	118.13675	-22.601358	1102.472446	0.11	0.08	-0.13
2	118.135667	-22.601266	1105.564	118.135665	-22.601266	1105.607911	-0.14	0.02	0.04
3	118.136721	-22.599511	912.0408	118.136724	-22.599512	912.134382	0.28	-0.18	0.09
4	118.136032	-22.599088	909.7827	118.13603	-22.599087	909.77934	-0.25	0.08	0.00

Next page: dip corrected point cloud in CloudCompare (~8°/25° determined by visual fitting of a plane with the stratigraphic layers). Yellow boxes indicate selected points used for manual logging (point picking upper and lower boundary of layers: purple dots) and extraction of semi-quantitative ‘verticality’ scalar values (colour scale):

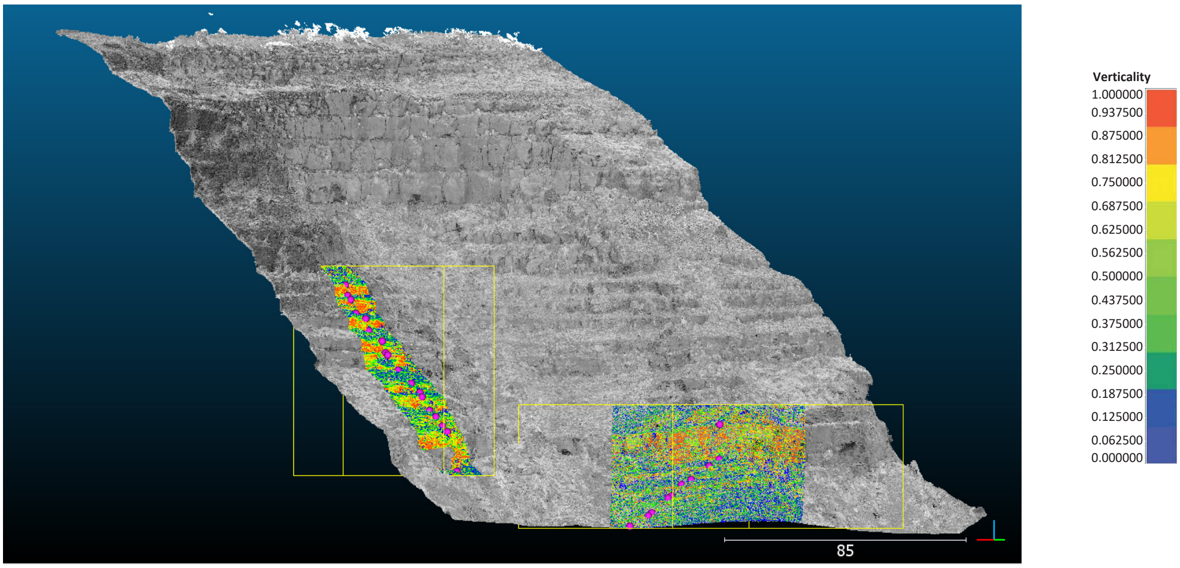

Lower section. Counter dip correction of 6°/205:

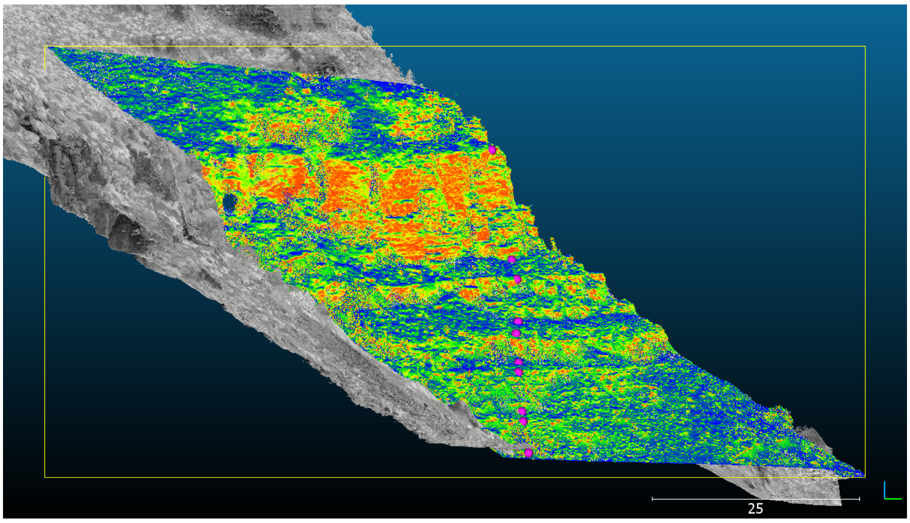

Upper section:

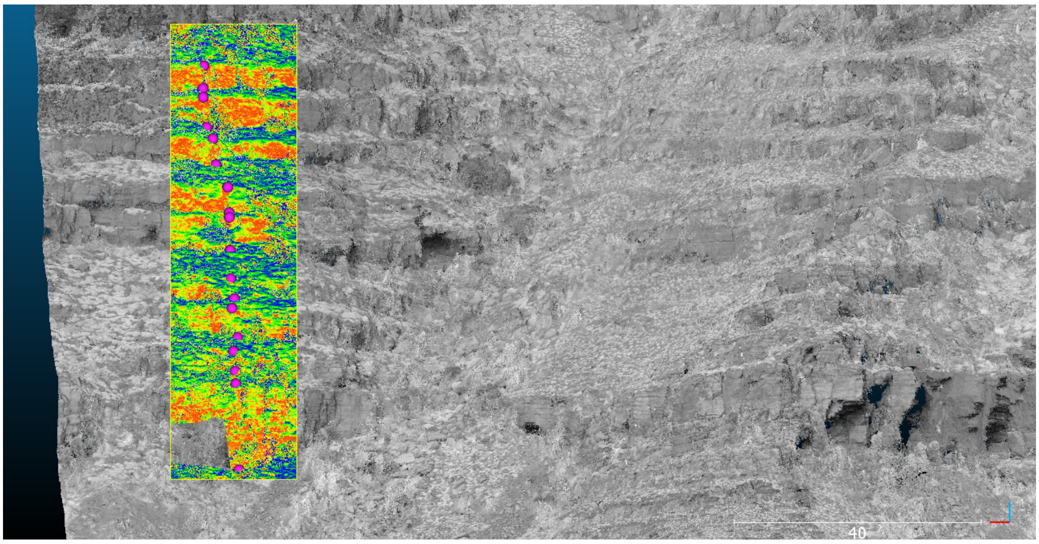

Mt Bruce East

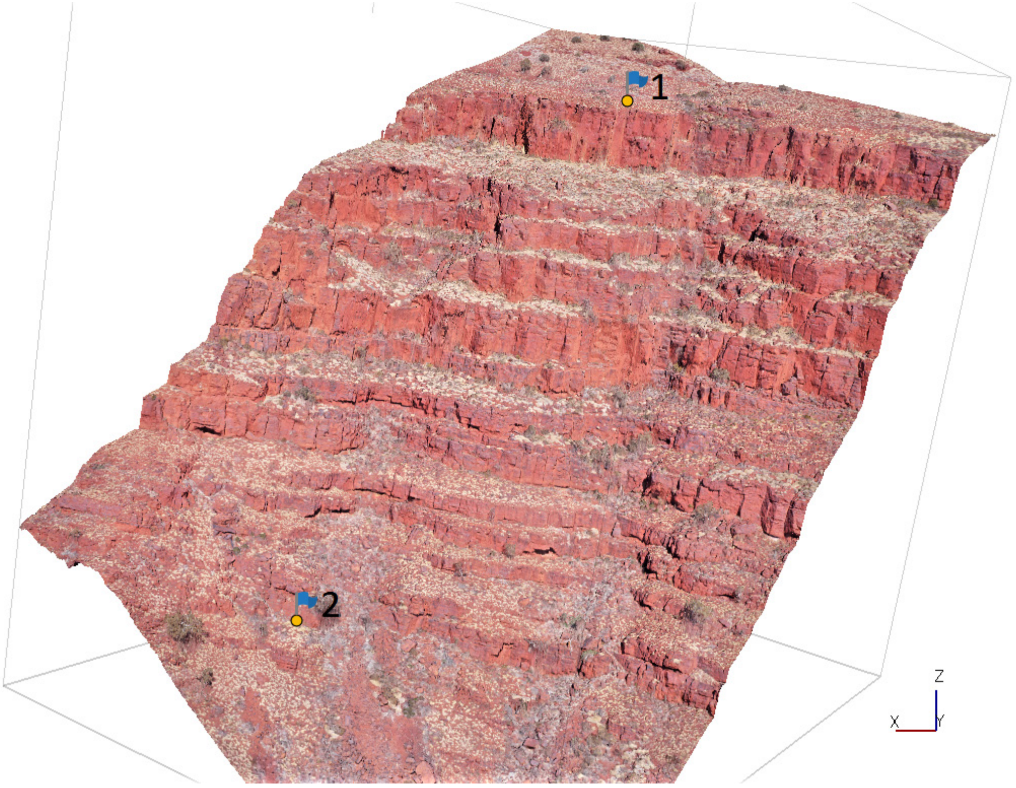

GCP	X/Longitude	Y/Latitude	Z/Altitude	X_model	Y_model	Z_model	X_error	Y_error	Z_error
1	118.1391	-22.602	1094.169	118.1391	-22.602	1094.283	0.22334	-0.02986	0.114268
2	118.14	-22.6012	963.9399	118.14	-22.6012	963.9461	0.032086	0.01303	0.0062

12.5°/330° dip corrected:

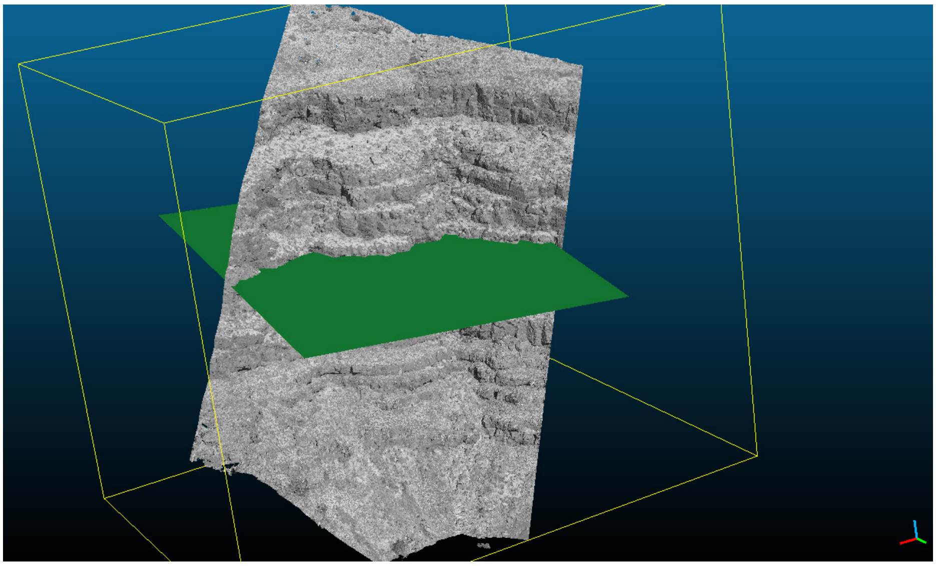

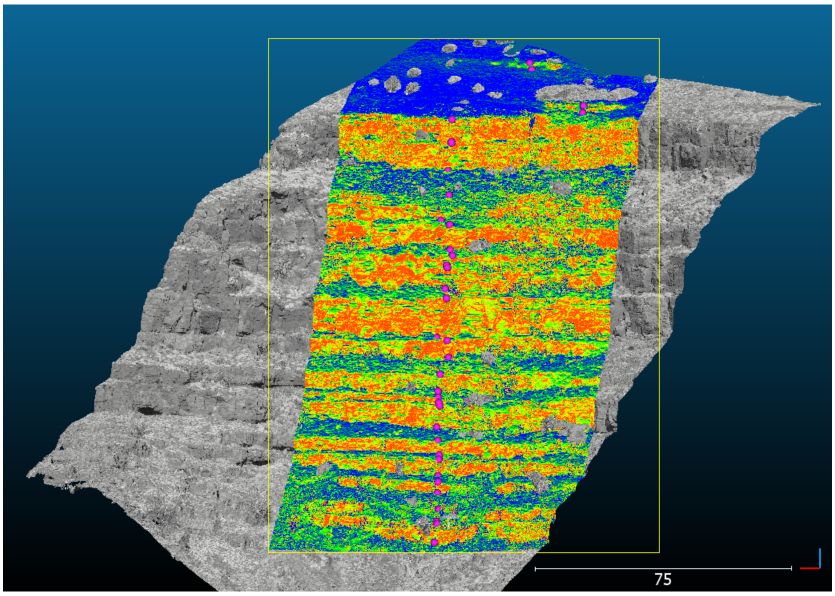

Mt Jack East

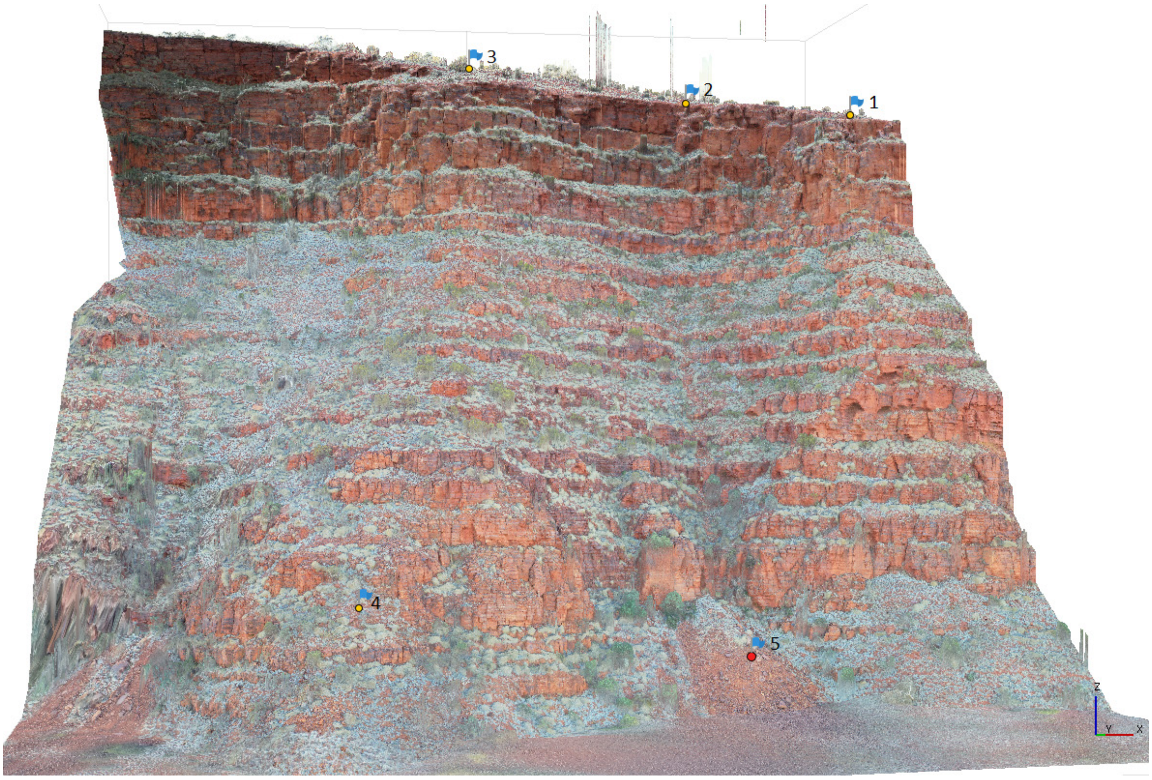

GCP	X/Longitude	Y/Latitude	Z/Altitude	X_model	Y_model	Z_model	X_error	Y_error	Z_error
1	117.4434	-22.2754	935.0897	117.4434	-22.2754	935.0912	0.006	0.009	0.002
2	117.443	-22.2753	941.2268	117.443	-22.2753	941.2386	0.011	0.003	0.012
3	117.4424	-22.2753	953.4025	117.4424	-22.2753	953.3886	-0.004	-0.007	-0.014
4	117.4426	-22.2767	827.867	117.4426	-22.2767	827.8555	0.007	-0.006	-0.012
5	117.4433	-22.2763	814.997	117.4433	-22.2763	815.0091	-0.020	0.001	0.012

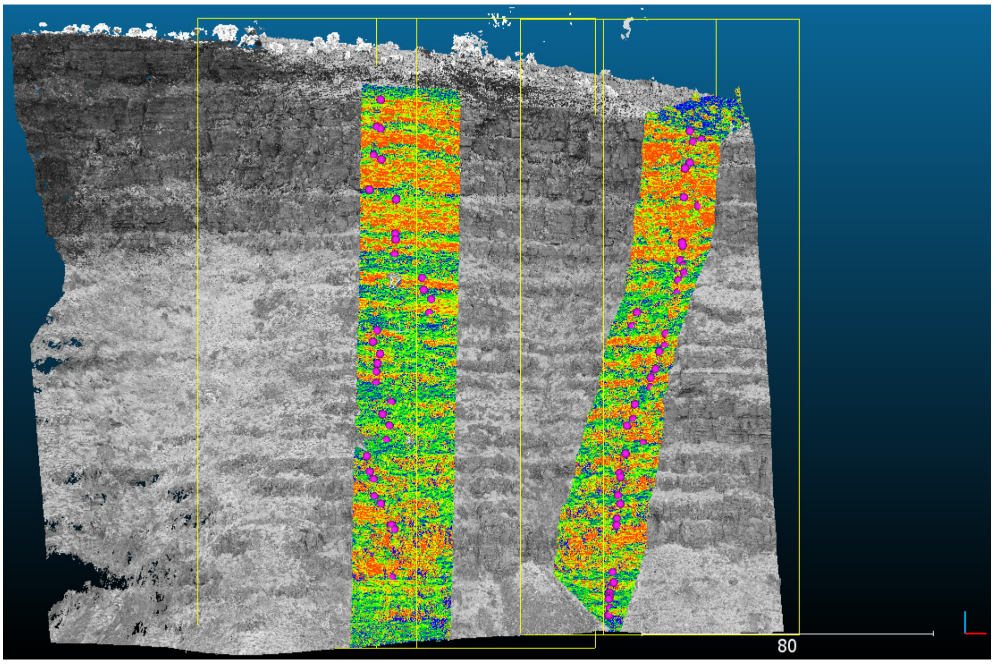

Mt Jack West

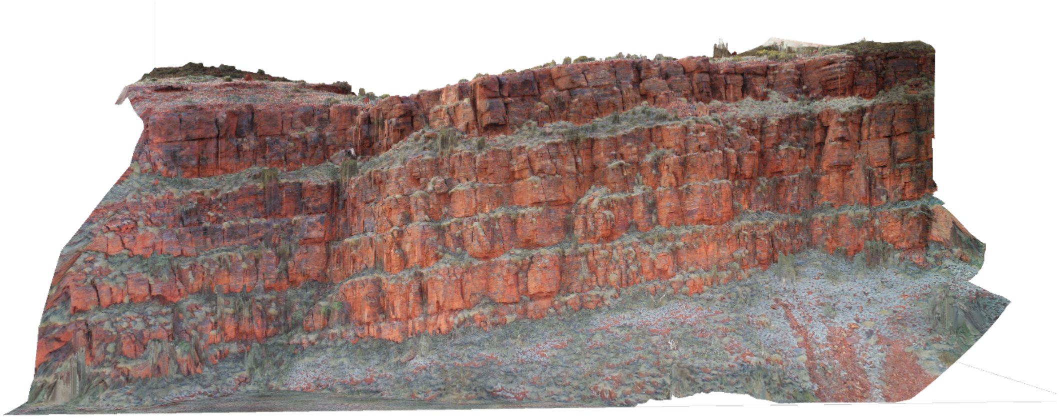

8°/275°dip corrected:

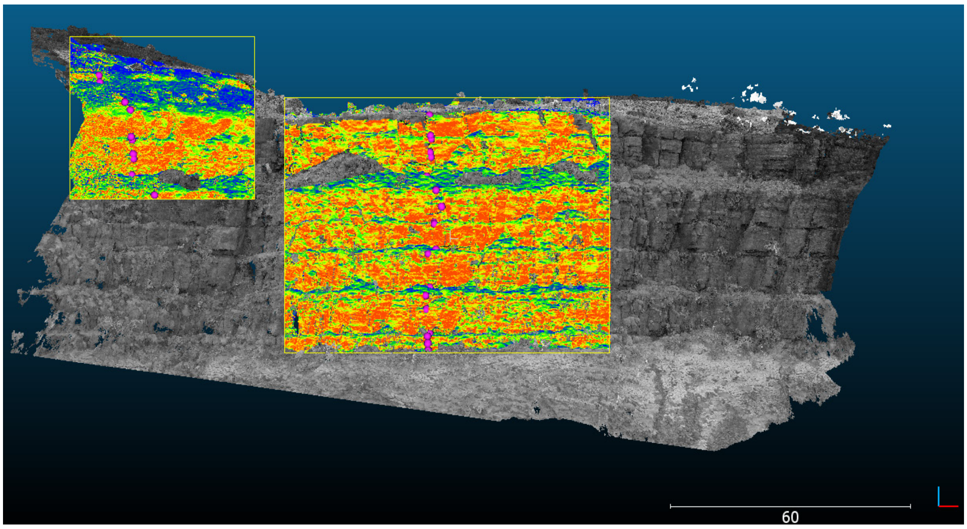

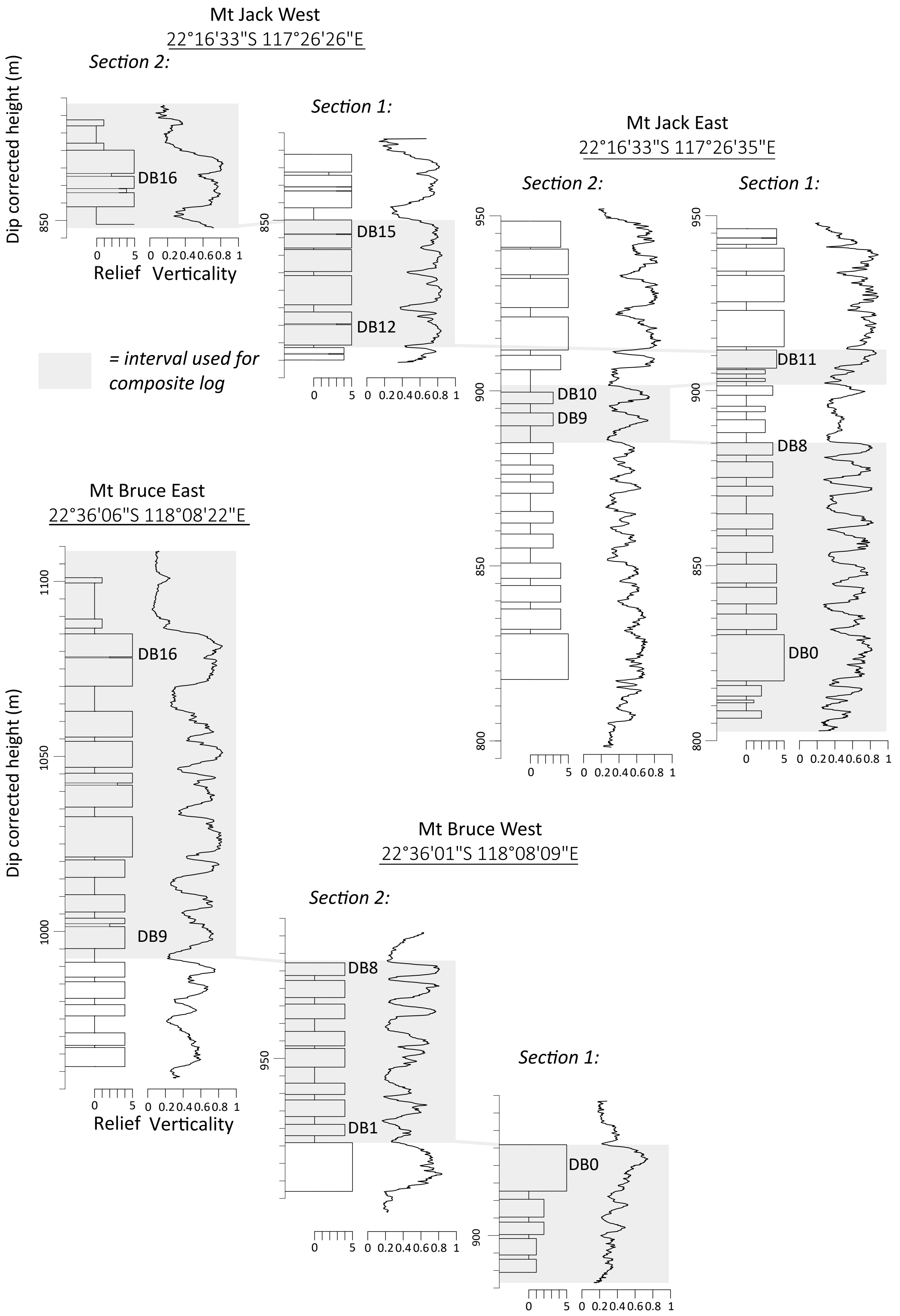

Figure S6. Compilation of the Mt Bruce and Mt Jack composite logs and verticality profiles obtained from the different subsections.

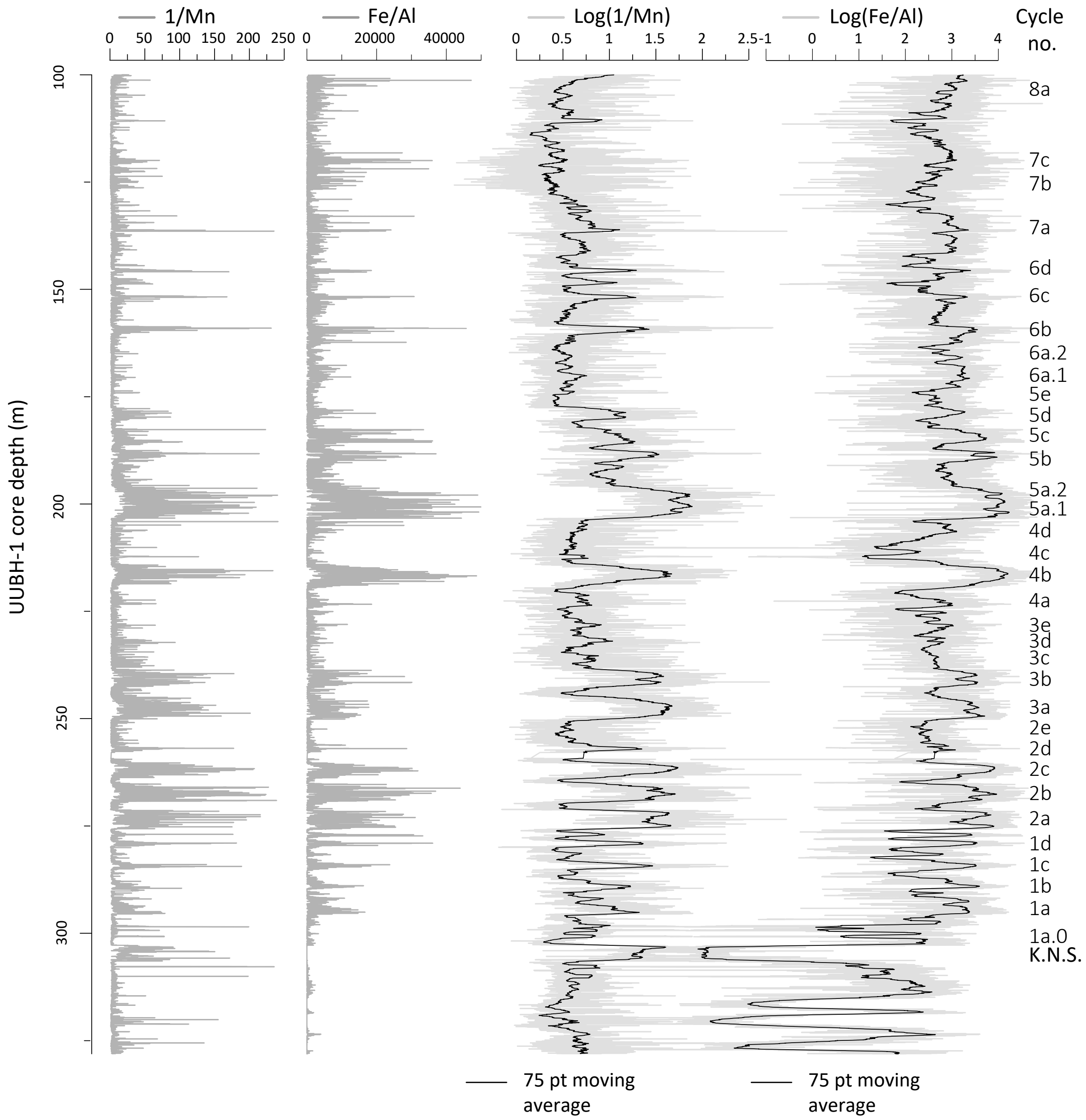

Figure S7. The 1/Mn and Fe/Al records of core UUBH-1 with updated cycle numbers of the Kuruman IF indicated. Note that the pattern of regular metre-scale alternations between iron oxide-rich and iron carbonate/shale-rich facies is virtually identical to the expression in the Fe/Mn record.

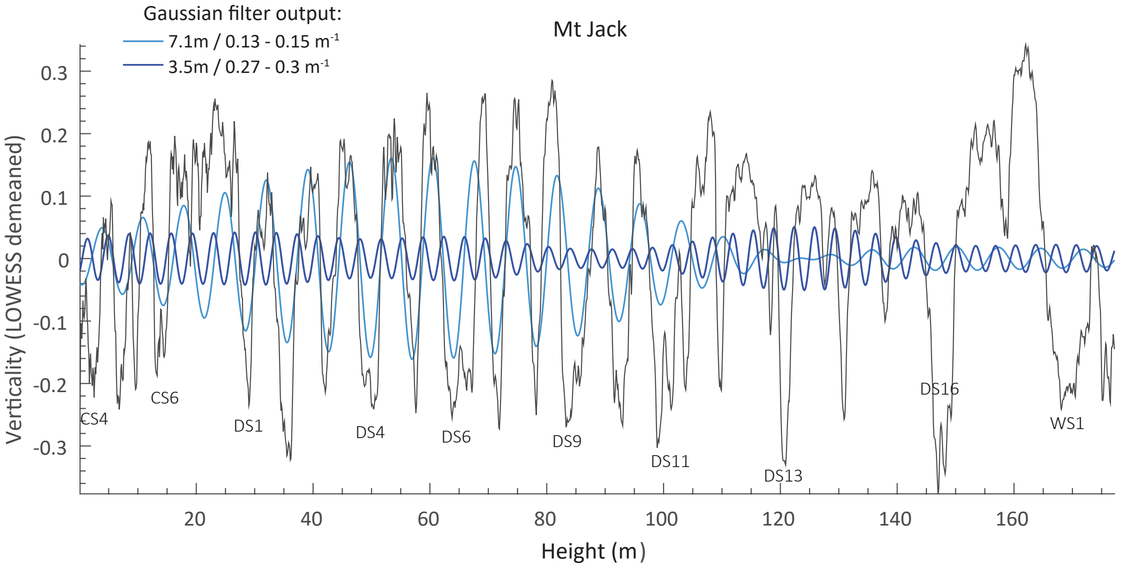

Figure S8. Comparison of the ~3.5 m and ~7 m filtered cycles in the Mt Jack verticality record. In most parts of the record, exactly two filtered ~3.5 m cycles occur per single filtered ~7 m cycle. The maxima of the filtered ~3.5m cycle coincide with the edges of the BIF intervals, while the minima correspond to the thinner S intervals. These filtering relationships suggests that the ~3.5 m cycle is (at least partly) a harmonic of the 7 m cycle, resulting from the blocky shape of the BIF-S alternations and the larger proportional thickness of the BIF intervals relative to the S intervals. Note, however, that the filtered ~3.5 m cycle also picks up faint splitting features visible in several of the thicker BIF macrobands, particularly seen in the upper half of the Dales Gorge Member, as well as the additional verticality maximum in between CB4 and CB5 of the Colonial Chert Member.

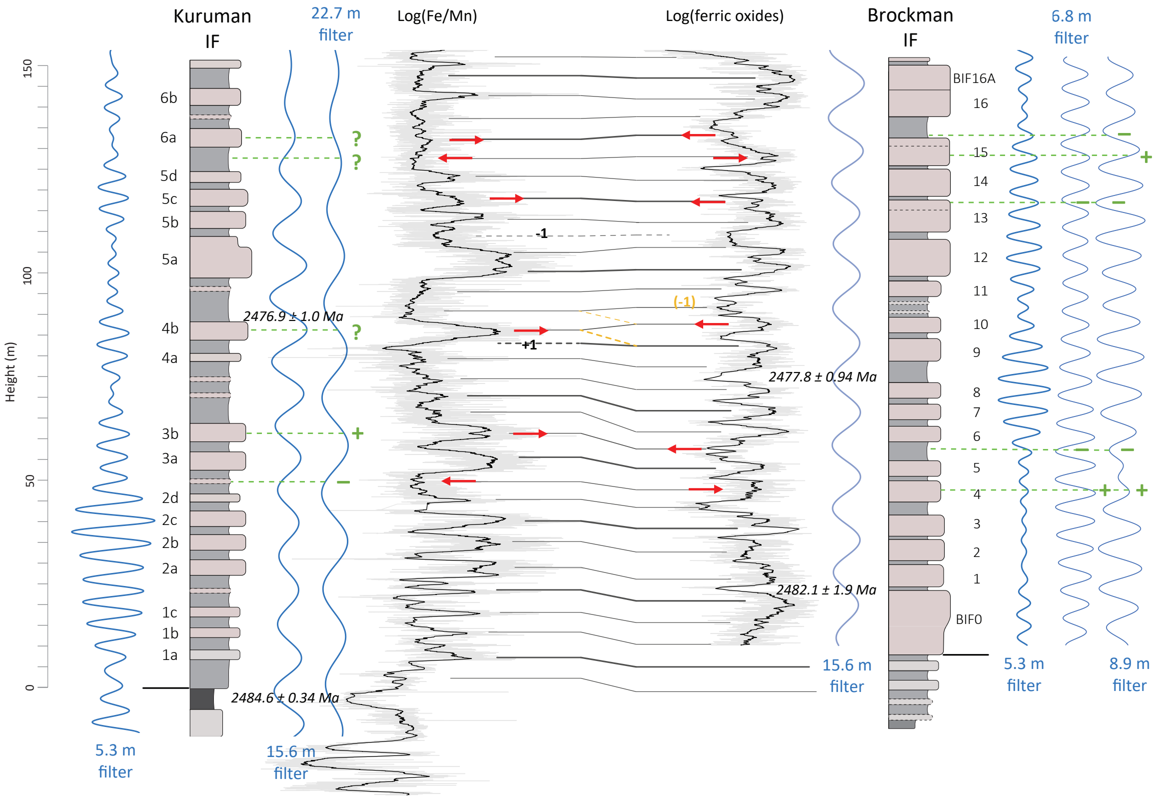

Figure S9. Discrepancies in characteristic cycle pattern between the Kuruman IF and Dales Gorge Member according to correlation option IIb and possible explanations. Idealised stratigraphic columns are shown of the characteristic 'BIF' vs 'carbonate-shale' alternations as expressed in the outcrop weathering profiles of both stratigraphic units, in addition to the Fe/Mn record of the UUBH-1 core and ferric oxide abundance record of the 47A core with corresponding bandpass filtered curves as previously shown in Figs. 5, 8 and 14 of the main article. Red arrows pointing to the right (left) indicate relatively prominent (weak) 'BIF' intervals that are correlated to relatively weak (prominent) 'BIF' intervals at the ~5 m scale in their stratigraphic counterpart. Green horizontal lines with '+' or '-' symbols indicate intervals where the difference in stratigraphic expression might be explained by a maximum or mininum of the stronger ~23 m cycle in the Kuruman IF and/or a maximum/minimum of the stronger ~7 m and 9 m cycles in the Dales Gorge Member. '?' symbols point to intervals in the Kuruman IF where the difference in expression with the equivalent ~5 m-scale BIF in the Dales Gorge Member does not appear to be explained by the 23 m cycle.

References

Altermann, W., & Nelson, D. R. (1998). Sedimentation rates, basin analysis and regional correlations of three Neoarchaean and Palaeoproterozoic sub-basins of the Kaapvaal craton as inferred from precise U–Pb zircon ages from volcaniclastic sediments. Sedimentary Geology, 120(1-4), 225-256.

Barley, M. E., Pickard, A. L., & Sylvester, P. J. (1997). Emplacement of a large igneous province as a possible cause of banded iron formation 2.45 billion years ago. Nature, 385(6611), 55-58.

Bau, M., Romer, R. L., Lüders, V., & Beukes, N. J. (1999). Pb, O, and C isotopes in silicified Mooidraai dolomite (Transvaal Supergroup, South Africa): implications for the composition of Paleoproterozoic seawater and ‘dating’the increase of oxygen in the Precambrian atmosphere. Earth and Planetary Science Letters, 174(1-2), 43-57.

Senger, M. H., Davies, J. H. F. L., Ovtcharova, M., Beukes, N., Gumsley, A., Gaynor, S. P., ... & Schaltegger, U. (2023). Improving the chronostratigraphic framework of the Transvaal Supergroup (South Africa) through in-situ and high-precision U-Pb geochronology. Precambrian Research, 392, 107070.

Trendall, A. F., Nelson, D. R., De Laeter, J. R., & Hassler, S. W. (1998). Precise zircon U-Pb ages from the Marra Mamba Iron Formation and Wittenoom Formation, Hamersley Group, Western Australia. Australian Journal of Earth Sciences, 45(1), 137-142.

Wingate, MTD, Lu, Y, Kirkland, CL and Johnson, SP 2018, 195892: rhyodacite, Woongarra Pool; Geochronology Record 1453: Geological Survey of Western Australia, 4p.

Wingate, MTD, Lu, Y and Martin, DMcB 2020, 225735: tuffaceous siltstone, Yallangi Bore; Geochronology Record 1683: Geological Survey of Western Australia, 5p.

Wingate, MTD, Fielding, IOH, Lu, Y and Martin, DMcB 2021c, 225760: tuffaceous volcanic rock, Wittenoom Gorge; Geochronology Record 1813: Geological Survey of Western Australia, 4p.